Aircraft Tail-Specific Performance Modeling for Fuel Efficient Flight Operations in the Cruise Phase

Master of Science Thesis

Frans Vossen

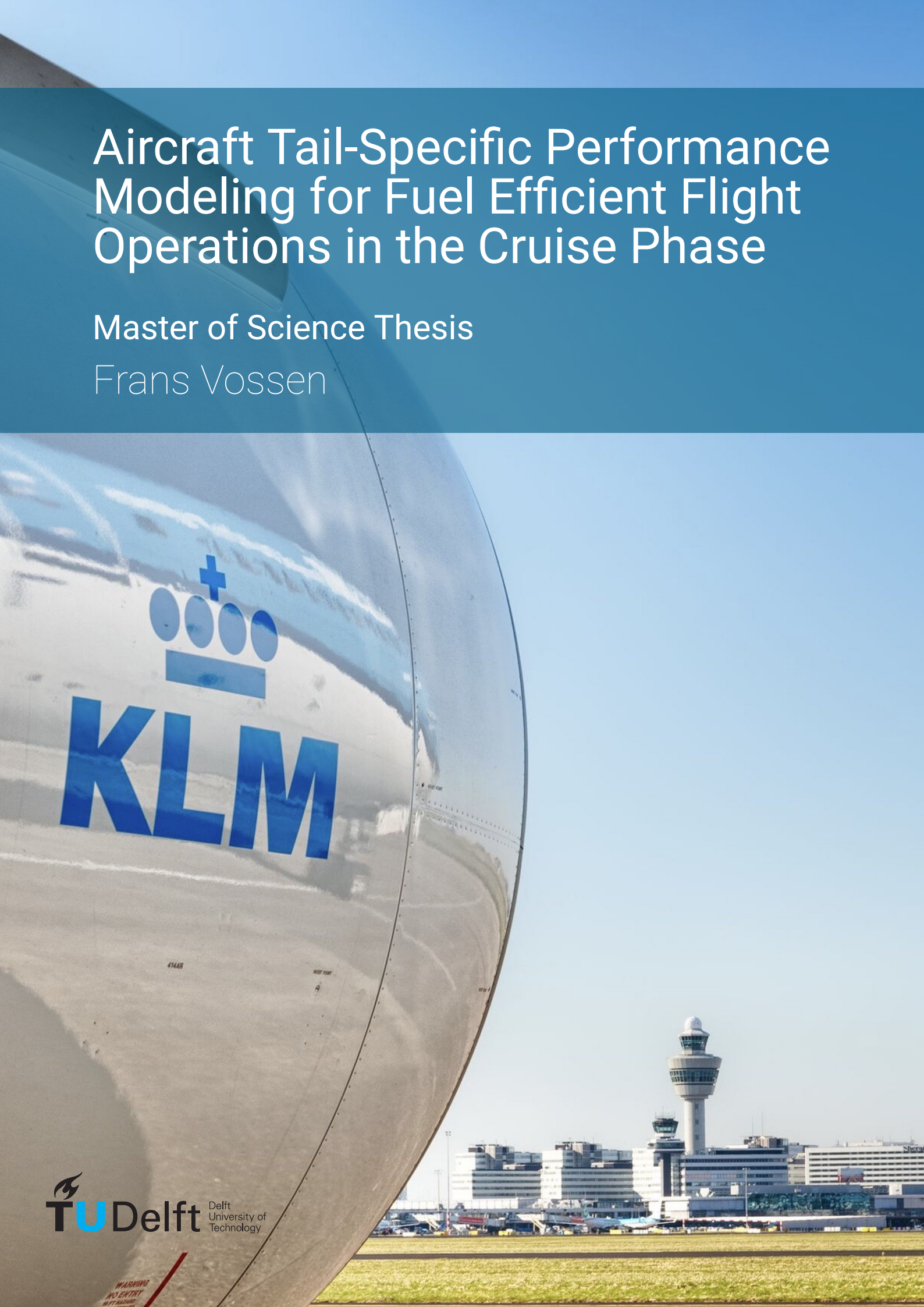

TU Delft Delft University of Technology

Aircraft Tail-Specific Performance Modeling for Fuel Efficient Flight Operations in the Cruise Phase

by

Frans Vossen

to obtain the degree of Master of Science
at the Delft University of Technology,
to be defended publicly on the 24th of October 2023.

Student number:	4666631	
Project duration:	July 2022 – October 2023	
Thesis committee:	Dr.ir B.F. Lopes Dos Santos	Delft University of Technology
	Dr. J. Sun	Delft University of Technology
	Dr.ir. M.J. Ribeiro	Delft University of Technology
	Dr.ir. M.F.M. Hoogreef	Delft University of Technology
	Ir. J. de Wilde	KLM Royal Dutch Airlines
	Ir. C. Evertse	KLM Royal Dutch Airlines
	F. Huisman	KLM Royal Dutch Airlines

An electronic version of this thesis is available at http://repository.tudelft.nl/.

TU Delft

Acknowledgements

This report marks the end of my educational career at Delft University of Technology. From starting my Bachelor of Aerospace Engineering in 2017 to finishing my Master now in 2023, this journey has been an intense and pleasant ride.

Having been given the opportunity to perform both my internship and thesis at KLM Royal Dutch Airlines, has really helped me to develop myself on both a personal and professional level. It was not until the start of my internship that I began to see the true potential of my education. Having been able to capture a glimpse of the job opportunities here, has provided me with new goals to strive for and motivation to make it happen. This would not have been possible without the help and support of both my supervisors Christiaan Evertse and Jasper de Wilde. I also want to thank Frans Huisman for inviting me to the team and for the many contractual extensions.

My thesis would not have been possible without the support of Junzi Sun from TU Delft. Our many and often not-so-short meetings really made the difference and kept me motivated to maximize my potential. I would also like to thank Bruno Santos and Marta Ribeiro for their support in the progress sessions.

Last but certainly not least, I want to express my gratitude to my family and friends for their constant support during my time at TU Delft. They were always there for me and gave me the chance to relax and recharge from my often demanding studies.

Frans Vossen
Delft, October 2023

Contents

List of Figures

List of Tables

Nomenclature

Abbreviations

AoA	Angle of Attack
AOBT	Actual On-Block Time
ARIMA	Autoregression Integrated Moving Average
ARMA	AutoRegression Moving Average
ATA	Actual Time of Arrival
ATC	Air Traffic Control
BADA	Base of Aircraft Data
CART	Classification and Regression Trees
CAS	Calibrated Airspeed
CDA	Continuous Descent Approach
CFD	Computational Fluid Dynamics
CG	Center of Gravity
CI	Cost Index
CORSIA	Carbon Offsetting and Reduction Scheme for International Aviation
DAE	Differential Algebraic Equations
DCI	Dynamic Cost Index
DOC	Direct Operating Costs
ECON	Economical Flight
EGT	Exhaust Gas Temperature
EPR	Engine Pressure Ratio
GTP	Global Temperature Potential
GWP	Global Warming Potential
HLD	High Lift Devices
ICAO	International Civil Aviation Organization
ISA	International Standard Atmosphere
LG	Legendre-Gauss
LGL	Legendre-Gauss-Lobatto
LGPM	Lengdre-Gauss-Pseudospectral Method
LGR	Legendre-Gauss-Radau

LHV	Lower Heating Value
LRC	Long Range Cruise
MILP	Mixed Integer Linear Programming
ML	Machine Learning
MLW	Maximum Landing Weight
MOO	Multi-Objective Optimization
MPO	Multi-Phase Optimization
MPTO	Multi-Phase Trajectory Optimization
MRC	Maximum Range Cruise
MSL	Mean sea-level
MTOW	Maximum Take-Off Weight
NLP	Non-Linear Program
NOC	Non-Optimal Control
OC	Optimal Control
OEW	Operating Empty Weight
PDB	Performance Database
QAR	Quick Access Recorder
RF	Random Forests
RK	Runge-Kutta
RM	Revenue Management
RTA	Required Time of Arrival
SAR	Specific Air Range
SGR	Specific Ground Range
SID	Standard Instrument Departure
SOBT	Scheduled On-Block Time
SOO	Single-Objective Optimization
SPO	Single-Phase Optimization
SPTO	Single-Phase Trajectory Optimization
SR	Specific Range
SSE	Sum of Square Errors
STA	Scheduled Time of Arrival
SVR	Support Vector Regression
TAS	True Airspeed
TBO	Trajectory-Based Operations

TIT	Turbine Inlet Temperature
ToC	Top of Climb
ToD	Top of Descent
TOP	Trajectory Optimization Problem
TSFC	Thrust Specific Fuel Consumption
ULD	Unit Load Devices
WFP	Waiting For Passengers

Symbols

v_g	Ground speed	m/s
α	Angle of attack	deg
δ	Pressure ratio related to MSL	–
δ_f	Flap deflection	deg
δ_{HL}	High lift devices position	deg
δ_{LG}	Landing gear position	deg
δ_{SB}	Speed brakes position	deg
γ	Flight path angle	deg
γ_a	Ratio of specific heat for air	–
λ	By-pass ratio	–
$\mathcal{C}$	Set of numerical discretization points	
$\mathcal{K}$	Set of path discretization points	
μ	Aircraft bank angle	deg
$\boldsymbol{p}$	System parameters	
$\boldsymbol{u}$	Control parameters	
$\boldsymbol{x}$	State parameters	
ψ	Aircraft heading	deg
ρ	Air density	kg/m^3
θ	Temperature ratio related to MSL	–
A	Wing aspect ratio	–
a_0	Speed of sound at sea-level	m/s
c	Numerical discretization point	
C_F	Fuel coefficient	–
C_L	Lift coefficient	–
C_T	Thrust specific fuel consumption	N/Ns
C_{fuel}	Fuel cost	EUR/kg

C_{time}	Average time cost	EUR/min
C_{D_0}	Zero lift drag coefficient	–
C_{D_i}	Lift induced drag coefficient	–
$C_{T,c}$	Corrected TSFC	kg/Ns
C_{Th}	Thrust coefficient	–
D	Aircraft drag	N
e	Oswald factor	–
f_{CO_2}	CO_2 emission rate	kg/s
f_{CO}	CO emission rate	kg/s
f_{H_2O}	H_2O emission rate	kg/s
f_{HC}	HC emission rate	kg/s
f_{NO_X}	NO_X emission rate	kg/s
f_{SO_X}	SO_X emission rate	kg/s
f_{soot}	Soot emission rate	kg/s
ff	Fuel flow	kg/s
ff_c	Corrected fuel flow	kg/s
g	Gravitational acceleration	m/s^2
h	Altitude	m
k	Path discretization point	
L	Aircraft lift	N
M	Mach number	–
m	Aircraft mass	kg
N_1	Fan/low pressure spool rotation speed	–
N_2	core/high pressure spool rotation speed	–
P	Polynomial degree	
p	Air pressure	Pa
R	Gas constant	J/kgK
S	Wing surface area	m^2
s	Along path distance	m
SR	Specific range	nm/kg
T	Aircraft thrust	N
T_c	Corrected thrust	N
T_h	Temperature at altitude h	K
v	Airspeed	m/s

V_{MO}	Maximum Operating Speed	m/s
vs	Vertical speed	m/s
w	Wind speed	m/s
W_{MTOW}	Maximum take-off weight	N
x	Lateral position	m
y	Longitudinal position	m

Introduction

Aviation has always had a great interest in operational efficiency. From the start of the Jet Age in the 1950s aviation has undergone many transformations. This journey took off with aircraft designs becoming more aerodynamic, fuel-efficient, and capable of carrying more payload over longer distances. The digital age followed around the 1980s, in which technologies emerged providing pilots with more information and insights. The introduction of the Flight Management System (FMS) provided pilots with enhanced capabilities in Avionics, navigational systems, and communication technologies, improving flight safety and efficiency. The last evolution in technology that we are currently in, is the era driven by Data Analytics and Artificial Intelligence (AI). These technologies are optimizing operations, enhancing safety, and improving environmental sustainability, with new capabilities that cannot be offered by the systems in the aircraft.

The purpose of this thesis is to investigate methods of data science and Machine Learning (ML) that can provide pilots with optimized data-driven solutions. The research focuses on a specific type of operation: the economy cruise. This operation is characterized by a cost index from which the aircraft determines optimal cruise speeds that balance between fuel and time costs. Within this domain, this research focuses on the relationship between cost index, cruise speed, and fuel consumption to achieve fuel-efficient flight.

To determine optimal cruise speeds from the cost index, the aircraft requires fuel consumption estimates at different speeds under current flight conditions. The FMS uses generic performance data that describes the average performance of a newly delivered aircraft/engine combination. Given that each aircraft has a unique performance that changes over time, an aircraft/tail-specific performance model is developed from big data and ML methods. This model is used to compare the supposedly optimum MRC speeds determined by the aircraft, to the true optimal speeds determined by the model for each tail individually.

To translate deviations in MRC speeds during flight to overall benefits, simulations are performed. These simulations evaluate practical cost index strategies on network-wide and flight-specific levels, to determine savings in both fuel and time by flying the tail-specific speeds.

The objective of this thesis can be summarized into investigating how fuel-efficient flight operations can be analyzed such that:

1. benefits from improvements in aircraft tail-specific performance can be quantified;
2. savings can be validated and explained on a per-flight basis;
3. strategies can be evaluated on a network-wide scale without performing costly experiments.

The research has been conducted in collaboration with KLM Royal Dutch Airlines. This provides a unique opportunity to relate scientific research with practical applicability. This has resulted in the consideration of many operational limitations to arrive at solutions that fit real-life operations while using the latest technologies in Machine Learning and Data Science. KLM Royal Dutch Airlines provided me with valuable guidance on this journey and delivered large amounts of in-flight data to develop this new methodology. At the same time, Delft University of Technology helped me greatly with implementing and identifying suitable technologies from scientific research, to arrive at the best of both worlds.

This thesis report is organized into two parts. Each part provides an independent piece of the research with some areas of overlap. Part I provides the scientific paper, showing the final methodology and focus of this thesis, while Part II shows the literature study that was conducted during the first three months.

I

Scientific Paper

Delft University of Technology, Aerospace Engineering (2023), 1–30
MSc Thesis, Air Transport and Operations (ATO)

ARTICLE

Aircraft Tail-Specific Performance Modeling for Fuel Efficient Flight Operations in the Cruise Phase

Frans Vossen[*,1,2]

[1]Faculty of Aerospace Engineering, Delft University of Technology, Delft, The Netherlands
[2]KLM Royal Dutch Airlines, Schiphol, The Netherlands

[*]Corresponding author: fransvossen1@gmail.com

Daily Supervision by Dr. Junzi Sun[1] and Ir. Jasper de Wilde[2]
Supporting Supervision by Dr.ir. Bruno F. Lopes dos Santos[1] and Ir. Christiaan Evertse[2]

Abstract

Fuel-efficient flight operations and improved Air Traffic Management (ATM) operations are identified as one of the main pillars in achieving net-zero CO_2 emissions by 2050. While considerable research has focused on airspace management and ATM operations, flight operations as managed by airlines have received little attention. Accurate aircraft/tail-specific performance modeling is crucial for identifying savings while existing models such as Euro-Control's BADA and manufacturers' book models remain too generic. Additionally, trajectories including optimal routes, altitudes, and airspeeds, must be determined to minimize fuel consumption. Emerging solutions leverage in-flight data connectivity and Machine Learning (ML) methods to provide pilots with real-time decision support. However, quantifying and validating saving potentials present challenges due to unpredictable variables and performance modeling complexities. This thesis aims to address these challenges by developing a tail-specific performance modeling framework using high-fidelity flight data and ML methods. The framework identifies and corrects tail- and flight-specific biases from the flight data, allowing fuel savings to be identified on a per-flight basis in post-flight analysis. The tail-specific performance model shows different Maximum Range Cruise (MRC) speeds than generic values determined by the aircraft. The benefits emerging from these optimal speeds are determined by high-accuracy simulations of different cost index strategies on flight-specific and network-wide levels. Three cost index strategies are evaluated and compared to generic MRC operations. Savings in both fuel and time are observed of 75 kg and 93 s, 96 kg and 111 s, and 127 kg and 107 s, on an average per-flight basis. In conclusion, this research demonstrates the existence and magnitude of fuel and time savings by flying tail-specific cruise speeds compared to generic values determined by the aircraft.

Keywords: aircraft performance modeling; cost index; economy cruise flight; uncertainty estimation; machine learning; simulations; fuel efficiency; airline operations

Abbreviations: **APM**: Aircraft Performance Monitoring, **APU**: Auxiliary Power Unit, **ATM**: Air Traffic Management, **BADA**: Base of Aircraft Data, **CG**: Center of Gravity, **CI**: Cost Index, **DOC**: Direct Operating Costs, **DOW**: Dry Operating Weight, **ECON**: Economy, **EWM**: Exponential Weighted Moving Average, **FF**: Fuel Flow, **FFF**: Fuel Flow Factor, **FMS**: Flight Management System, **ISA**: International Standard Atmosphere, **IQR**: Inner Quantile Range, **LS**: Load Sheet, **MAC**: Mean Aerodynamic Chord, **ML**: Machine Learning, **MRC**: Maximum Range Cruise, **MSL**: Mean Sea Level, **OFP**: Operational Flight Plan, **QAR**: Quick Access Recorder, **RMSE**: Root Mean Squared Error, **TOC**: Top Of Climb, **TOD**: Top Of Descent, **TSFC**: Thrust Specific Fuel Consumption, **ZFW**: Zero Fuel Weight,

1. Introduction

Aviation has seen a general movement toward improving operational efficiency. This has resulted in annual improvements of around 2.0% between 2000 and 2019, while passenger demand increased at an annual rate of 5% [1]. With the goal of net zero CO_2 emissions by 2050 established by Europe's aviation sector (Destination 2050) [2], rigorous actions are required and more research is needed to accelerate our way towards this goal.

Destination 2050 provides an outline of the required improvements to reach net zero CO_2 emissions. These improvements are characterized by: 1. Aircraft and engine technology, 2. ATM and flight operations, 3. Sustainable aviation fuels, and 4. Smart economic measures. To reach the final goal, 6% of reduction in CO_2 emission is required by ATM and flight operations [2]. Research into the area of airspace management and ATM is well-

Thesis paper written by Frans Vossen to obtain the Master of Science at the Delft University of Technology. To be defended publicly on the 24th of October 2023. An electronic version of this thesis is available at https://repository.tudelft.nl/.

known, however, the area of flight operations as managed by the airlines is still relatively unexplored. Therefore, this thesis aims to explore methods to identify and quantify saving potentials from tail-specific performance[1].

1.1 Analyzing Fuel Efficient Flight Operations

Airlines and pilots use fuel-efficient flight operations to reduce fuel consumption. This involves various practices throughout the flight, including efficient flight planning, trajectory optimization, fuel-efficient procedures, disruption management, and maintenance activities. Accurate tail-specific performance models are crucial to identify saving potentials emerging from different performances between tails. Euro-Control's Base of Aircraft Data (BADA) [3, 4] is commonly used in scientific research for performance modeling. Although its generic format works well for strategic decision-making, it cannot capture tail-specific performance deviations. Other performance models, like OpenAP [5] and Piano [6], have similar limitations. In industry, aircraft manufacturers provide performance data and tooling to operators, such as Boeing's Performance Engineers Tool (PET). These performance models describe the average type-specific performance of a new aircraft/engine combination determined from flight tests, the so-called book performance. Book performance achieves improved accuracy and is certified for fuel planning and in-flight usage. However, tail-specific performance deviations remain undetected.

Besides modeling aircraft performance, variables used to control the trajectories have to be determined to minimize fuel consumption. This includes finding optimal routes, altitudes, and airspeeds while considering payload, environmental conditions, airspace restrictions, and on-time performance. The Flight Management System (FMS) aids pilots in achieving efficient operations. The FMS was introduced in the late 1970s and has undergone several improvements since. Although its capabilities in flight planning, communication, surveillance, and navigation, have drastically improved, the methodology for performance predictions has remained unchanged [7, 8].

Given the rise of in-flight data connectivity and Electronic Flight Bags (EFB), new optimization solutions appear focusing on utilizing the latest information in weather, traffic, and aircraft performance data, together with ML techniques, to provide pilots with in-flight decision support tooling that cannot be provided by the FMS [9]. These software products offer optimized profiles in climb, vertical and speed optimization in cruise, and optimal profiles in descent. Although these improvements are generally small in isolation, consistent results on a per-flight basis can lead to significant savings on a network-wide scale [9].

A problem that arises with these new solutions is determining and verifying potential savings. Due to the many variables that affect aircraft performance, evaluations can become biased toward one's own interpretation. Without a clear evaluation standard and access to high-accuracy performance models, it is unclear what benefits can be expected on a network-wide or per-flight basis.

To answer these questions, flight operations can be analyzed through experimental flight tests. By conducting two sets of flights, one with the new strategy and one without, a comparison can be made to determine the benefits. However, since differences in flight conditions are inevitable, numerous flights are required to arrive at statistically significant results. Instead of expensive experiments, simulations can be used to assess benefits. These simulations must accurately model real-life operations and tail-specific performance, to arrive at similar results to those obtained in real life. Nonetheless, it's important to note that practical flight experiments still play a critical role in validating these simulations and fine-tuning new strategies.

Figure 1 provides an overview of the elements to be considered in a benefit analysis. The aircraft tail performance model is seen to lie at its center. Flight operations and environmental conditions affect the control variables from which the trajectory follows. Furthermore, an FMS model is required to simulate certain types of operations, e.g., economy flight, where the FMS determines flying speeds from a so-called cost index provided by the pilot. The elements provided in this figure are further discussed in the coming sections.

1.2 Contribution and Outline

The objective of this thesis is to investigate how fuel-efficient flight operations can be analyzed such that:

1. benefits from improvements in aircraft tail-specific performance can be quantified;
2. savings can be validated and explained on a per-flight basis;
3. strategies can be evaluated on a network-wide scale without performing costly experiments.

[1] Tail-specific performance means modeling the performance of a single aircraft rather than the average of its family (type-specific performance). Tail relates to the tail number, which is a unique identification of every aircraft.

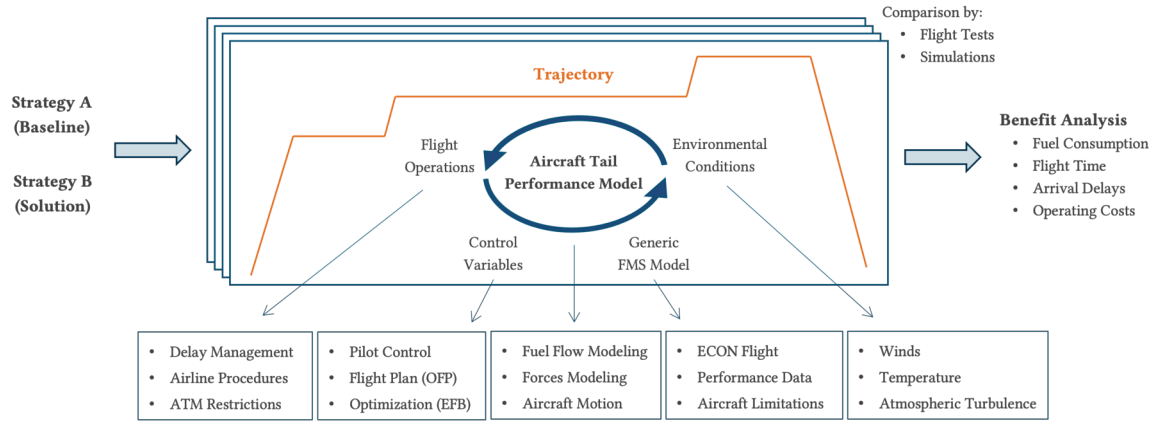

Figure 1. Overview of elements affecting aircraft performance and benefit analysis.

More specifically, this entails the development of a tail-specific performance model based on high-fidelity flight data and ML techniques; identifying and removing flight- and tail-specific biases from important parameters in the flight data; and designing and conducting high-accuracy simulations to assess benefits from different strategies.

This research is focused on a specific type of flight operation: the economy cruise. This operation is characterized by a cost index from which the FMS determines optimal cruise speeds by balancing fuel and time costs. Given that the focus of this thesis is on fuel-efficient flight, the research mainly covers the relation between cost index, cruise speed, and fuel consumption, while time and cost considerations are reserved for a future study. Although the main case study presented is focused on economy cruise flight, the proposed performance modeling framework and simulation methodology can also be extended to cover other flight phases or operations.

The remainder of this paper is structured as follows. In Section 2, the fundamentals of economy cruise flight are presented and the fuel mileage is introduced to relate cost index, flight conditions, and cruise speed. Section 3 provides the basics of generic physics-based fuel flow modeling as used in academia and industry. Section 4 presents the novel framework for tail-specific data-driven fuel flow modeling that identifies and corrects tail- and flight-specific biases from the flight data. Section 5 follows by analyzing the performance modeling improvements and shows deviations in true tail-specific MRC speeds from generic book values. Eventually, all elements are combined in Section 6 where a benefit assessment is presented by simulating different cost index strategies on flight-specific and network-wide levels. Finally, Section 7 presents the conclusion and outlook.

2. Economy Cruise Flight

This thesis is focused on evaluating fuel-efficient flight operations in the cruise phase. Airlines generally employ a certain strategy known as economy cruise, which lets the aircraft compute optimized speeds based on a cost index provided by the pilots. The fundamentals of the cost index, including its definition, how it follows from airline operations, and its relation between cruise speed and generic aircraft performance modeling are presented.

2.1 Cost Index

The cost index, with unit kg/h, can be defined by:

$$CI = \frac{C_T}{C_F}, \tag{1}$$

where C_T and C_F are average values for time-dependent costs expressed per unit flight time (\$/h) and fuel costs expressed per unit mass (\$/kg). The time costs include crew salaries, maintenance costs, and depreciation or leasing costs, and the fuel cost is the fuel price at the origin airport [10]. Manufacturers generally convert this cost index to a scaled dimensionless coefficient that ranges either from 0-100, 0-1000, or 0-9999 [11].

Considering a small cruise distance s in nautical miles and ISA conditions, the total costs (C_{tot}) can be expressed by a fixed cost (C_{fix}) and a variable cost. The variable cost is often referred to as Direct Operating Cost (DOC):

$$C_{tot} = C_{fix} + DOC, \quad \text{with } DOC = C_T\ t + C_F\ m_{fused}, \tag{2}$$

where t and m_{fused} are the time in hours and fuel burned in kg, respectively, to fly distance s. To minimize total costs in cruise, DOC has to be minimized. These costs can be related to the trajectory parameters by rewriting Equation 2 in the form of Equation 3, defining an economy cruise cost function as τ by assuming s and C_F to be fixed, and combining both equations to arrive at Equation 5:

$$DOC = s\, C_F \left(CI \frac{t}{s} + \frac{m_{fused}}{s} \right), \quad (3) \qquad \tau = \frac{DOC}{s\, C_F}, \quad (4) \qquad \tau = CI \frac{t}{s} + \frac{m_{fused}}{s}. \quad (5)$$

By considering that $\frac{s}{t}$ is the airspeed (V) and defining $\frac{m_{fused}}{s}$ to be the Fuel Mileage (FM), the final form follows:

$$\tau = \frac{CI}{V} + FM. \quad (6)$$

From this equation, it follows that lower cost index values encourage a flight path that lowers fuel consumption, whereas higher cost index values promote a flight path with higher cruise speed. When costs of time are high, a larger cost index reduces flight time and lower total operating costs. Conversely, when fuel prices are high, a lower cost index reduces fuel consumption and lower total operating costs.

2.2 Cost Index Practices by Airlines

For an accurate trade-off to be made between fuel and time costs, knowledge of the cost structure of an airline is essential. Based on [10], airlines struggle to integrate such practices as time costs are difficult to quantify and the importance and the concept of the cost index are largely unknown to the decision-makers. Another limitation is that costs related to arrival delays are excluded from the time costs. Being a discontinuous function that depends on the time of arrival, delay costs can not effectively be transformed into an average cost value required for the cost index framework. This is especially problematic for hub-and-spoke airlines, where on-time performance is essential. Still, most airlines heavily rely on the cost index to manage their operations. Five cost index strategies are identified in airline operations [10, 12]:

1. **Intended cost index** The optimal cost index is determined from an airline-specific cost analysis that quantifies crew, maintenance, and leasing costs either on a route, network, or flight-specific level. Furthermore, fuel costs are determined from the actual fuel price at the departure airport. A cost index is then obtained for each flight, where the effects of arrival delays are not considered.
2. **Standard cost index values** Aircraft manufacturers provide adequate values for cost index that can be adopted. Although a simple solution, this practice does not capture the airline-specific cost structure.
3. **Neglecting time costs** Cost index values are determined only by considering fuel prices. Although dynamic fuel prices are included in this strategy, it does not consider time-related costs.
4. **Adopting cost index as a performance setting** The standard cost components are no longer considered to determine the cost index. Rather, the cost index is used as a performance setting to directly control fuel consumption, trip time, and/or arrival delays. Subsequently, a different cost formulation may be used to combine these considerations into a new objective function. This approach also allows stable flight schedules to be developed based on standard cost index values. On the day of operation, this cost index is modified such that arrival delays are minimized considering the actual route and winds.
5. **Not using the cost index** Airlines are sometimes seen to fly at constant Mach instead of using a cost index. Especially on short-haul flights, this is seen to occur frequently. This also occurs on long-haul flights, where constant Mach operations are enforced during ocean crossings.

The fourth strategy is most often observed in practice. This thesis therefore considers this strategy for the remainder of the research when referring to cost index practices. The cost index is used as a performance-setting by the pilot to directly control fuel consumption, flight time, and arrival delays. The cost index is first determined in the flight planning phase to fit the schedule. In case of disruptions, a higher cost index can be opted to reduce arrival delays, given enough fuel was loaded for this higher speed.

With the selection of a cost index, the aircraft computes the corresponding cruise speed by minimizing Equation 6. Instead of iteratively solving this equation for the Mach number, a predetermined mapping is established by the FMS that directly relates observed flight conditions to the Economy (ECON) Mach number by:

$$Econ\ Mach = \mathrm{f}(m, h, CI, T, wind), \quad (7)$$

where m, h, and T are the instantaneous gross weight, altitude, and temperature obtained from the aircraft sensors, and *wind* is the combination of wind speed and direction relative to the track angle. This mapping requires a

performance model to determine fuel consumption at different speeds and flight conditions. The aircraft makes use of the book performance data that are loaded into the FMS. This results in the FMS delivering cruise speeds that are optimized for the average type-specific performance of a new aircraft/engine combination, rather than for the performance of the specific tail.

2.3 Fuel Mileage

The relation from Equation 7 is further described by the fuel mileage. Fuel mileage[2] is an instantaneous measure of aircraft performance efficiency. It relates the fuel consumption (m_{fused}) to traveled distance (s), or equivalently, instantaneous fuel flow (FF) to true-airspeed (V) or ground speed (V_g) by:

$$FM = \frac{m_{fused}}{s} = \frac{FF}{V_g}. \tag{8}$$

Equation 8 can be expressed relative to air or ground distance, where the effects of wind are excluded when considering fuel mileage relative to air. In economy flight, fuel mileage is considered relative to ground.

Considering a cost index of zero (CI0) is seen to reduce Equation 6 to a fuel mileage minimization problem. This condition is commonly known as Maximum Range Cruise (MRC) and is characterized by being the most fuel-efficient flight. The airspeed that resembles MRC and ECON flight given the flight conditions, is determined using performance graphs, as shown in Figure 2. This figure shows the contour lines of book performance at a constant weight, ISA conditions, and no winds, and includes ECON speeds indicated by the cost index lines. Following the definition of MRC, this condition follows the locus of minimum fuel mileage while increasing cost index values increase fuel mileage and airspeed. From this graph, it becomes clear that determining economic speeds is a non-linear problem with five degrees of freedom.

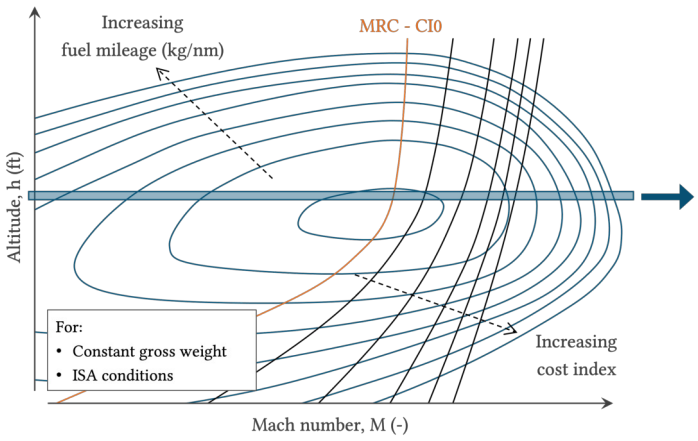

Figure 2. Contours of constant fuel mileage as a function of altitude and Mach (modified from [11]).

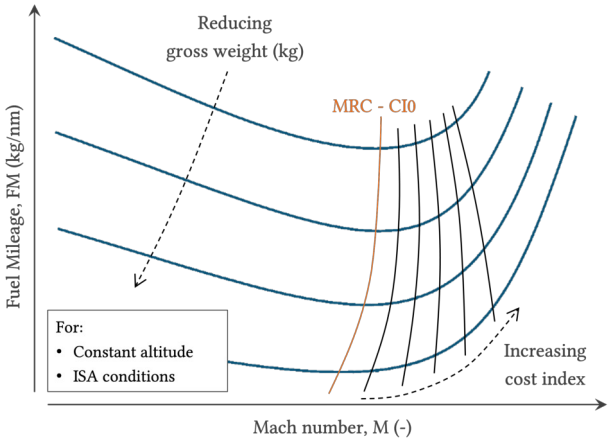

Figure 3. Influence of gross weight on the performance curves (modified from [11]).

2.3.1 Influence of Gross Weight

To see the influence of gross weight on economic speeds, Figure 2 is reduced by considering an altitude restriction describing a constant flight level. The performance graphs representing this new situation are shown in Figure 3, for a fixed altitude, temperature, and no winds. Lower gross weight improves fuel mileage, while economic speeds are seen to change non-linearly. Similarly, the MRC condition follows the minimum fuel mileage, and increasing cost index values increase fuel mileage and airspeed.

[2]Fuel mileage is often referred to as specific range. The general unit of fuel mileage is nm/kg which translates to traveled distance per fuel quantity. However, in this thesis, the inverse fuel mileage is used as the standard (consumed fuel quantity per traveled distance in kg/nm). The main difference now is that better fuel efficiency is obtained by reducing fuel mileage instead of increasing it.

2.3.2 Influence of Wind

Wind can be described by the wind speed (V_w), wind direction relative to the track angle (ϵ)[3], and a wind correction angle (δ)[4] which models a slight offset in heading to resolve drift angles caused by crosswinds. Fuel mileage relative to ground distance is determined by considering the ground speed in Equation 8, which is calculated by:

$$V_g = V \cos \delta + V_w \cos \epsilon. \tag{9}$$

Figure 4 shows the effect of head and tailwinds on fuel mileage and economic speeds. It follows that MRC and economic speeds are achieved at higher airspeed with headwind and lower airspeed with tailwind. In-flight these effects are directly managed by the FMS by changing speed when observing different winds.

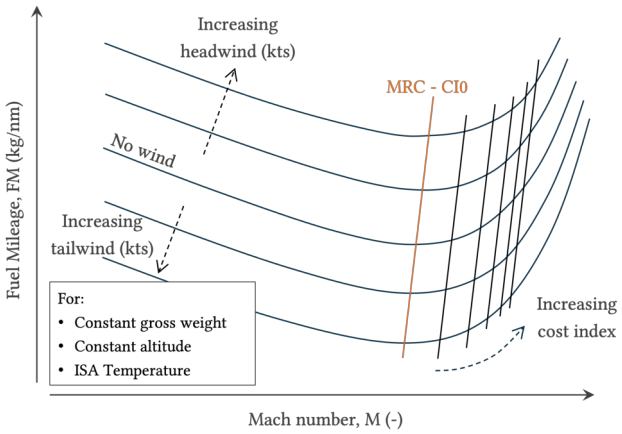

Figure 4. Influence of wind speeds on the performance curves (modified from [11]).

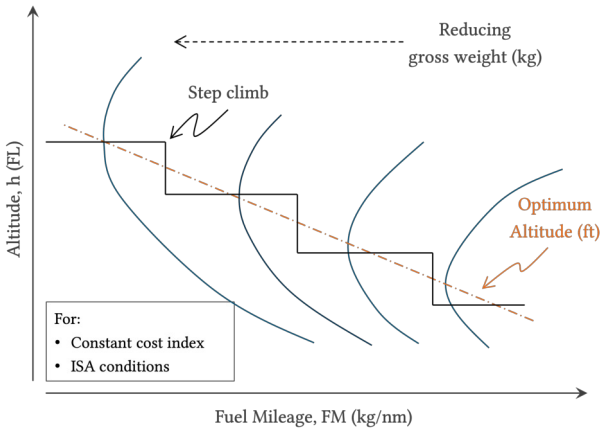

Figure 5. Visualization of how optimal altitudes follow from the performance curves (modified from [11]).

2.4 Cruise Altitude

Altitude selection in cruise is subject to various performance limitations that are merged into a so-called ceiling. This ceiling is the maximum altitude at which the aircraft can be safely operated. These restrictions are caused by thrust limitations, required levels of maneuverability, buffet margin, and resilience from atmospheric turbulence, and are mainly affected by atmospheric temperature and aircraft weight [11].

Considering a cruise segment with a certain gross weight, temperature, and cost index, an optimal altitude can be determined where fuel mileage is minimized. This optimum altitude is shown in Figure 5 for decreasing aircraft weight and ISA conditions. Although steady continuous climb results in the most fuel-efficient flight, operation limitations restrict cruise altitudes to constant flight levels [11]. Consequently, step climbs are performed between these flight levels while the closest proximity to the optimum altitude is ensured. The FMS provides pilots with recommendations on when to perform a step climb [11].

Different flight levels can experience significant differences in wind. This may result in trip fuel savings by opting for an altitude different than the standard ISA optimum. However, since winds are difficult to observe and forecast with high accuracy, the additional fuel consumption induced by the steps may eventually outweigh the savings [9]. In current operations, altitude is therefore generally determined by ISA conditions and is subsequently altered through optimization or to comply with operating restrictions while abiding by the altitude ceiling [11].

3. Generic Physics-Based Performance Modeling

Optimal speeds in economy cruise flight are determined by the FMS through generic performance models. These models are used to relate and adjust cost index and cruise speed at different flight conditions. To investigate saving potentials emerging from tail-specific performance, differences in book performance have to be identified. Before

[3] An ϵ of 0°represents tailwind, while an ϵ of 180°represents headwind.

[4] δ is the angle between the airspeed vector and track angle and can be calculated from trigonometric relations using the track angle, wind angle, wind speed, and airspeed.

a modeling framework is introduced that captures tail-specific performance, generic physics-based performance modeling is discussed. This covers the basics of fuel flow modeling and identifies the influential factors.

Performance modeling deals with describing the behavior, capabilities, and characteristics of an aircraft in different flight conditions. There are several ways to approach this modeling. The most detailed approach makes use of non-linear six-degree-of-freedom models that are used in research focused on aircraft control theory [13]. In research focused on trajectory optimization and ATM practices, the aircraft performance is simplified to a point-mass approach that assumes steady motions [14]. This latter approach is presented in this section. Furthermore, this thesis only deals with a sub-part of aircraft performance modeling: the modeling of fuel flow in cruise flight. Cruise flight is considered as the segment between the Top Of Climb (TOC) and the Top Of Descent (TOD), where step climbs or descents are removed from this analysis. The parameters that are generally considered to describe aircraft performance are shown in Table 1:

Table 1. Common flight conditions used as input to describe aircraft performance.

Parameter	Notation	Remark	Symbol	Unit
Gross Weight	gw	Mass	m	kg
Altitude	alt	Pressure Altitude	h	ft
Airspeed	M	Mach	M	–
	tas	True Airspeed	V	kts
	ias	Indicated Airspeed	V_{ias}	kts
Temperature	oat	Outside Air Temperature	T	K
	ΔISA	ISA Temperature Deviation	ΔT_{ISA}	°C
Acceleration	acc	Flight Path Acceleration	a	m/s^2
Vertical Speed	vs	Rate of Climb	roc	ft/min

Generic fuel flow modeling describes the physics required to go from these conditions to fuel flow. Before we dive into the theory describing this mapping, it should be noted that different levels of complexities are considered in academia and industry. In academia, simplifying assumptions are often used by neglecting the effects of the Center of Gravity (CG) on fuel flow and using simplified relations to describe the drag polar and engine characteristics. In industry, manufacturers have access to much more details which enables them to establish more accurate relations. An overview of a generic performance modeling methodology is shown in Figure 6. The elements are further discussed in this section.

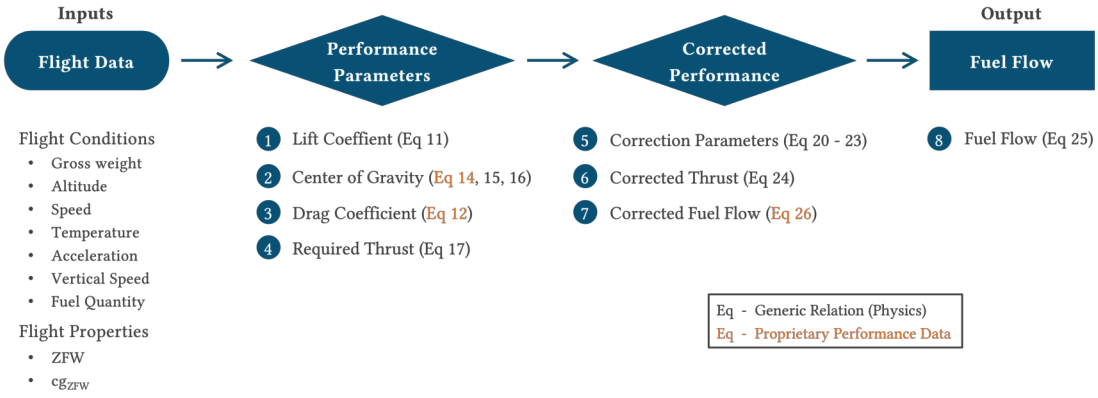

Figure 6. Overview of generic physics-based performance modeling framework in scientific research and industry. Elements that require proprietary performance data are indicated in orange.

3.1 Lift and Drag

The first step in determining fuel flow is the modeling of lift and drag. Given the steady-state consideration for cruise phase, vertical equilibrium of forces can be assumed [15]. This allows the lift coefficient (C_L) to be found:

$$C_L = \frac{W}{q\,S}\cos\gamma, \quad \text{with } \gamma = \tanh\frac{roc}{V}. \tag{10}$$

with W, q, S, and γ being the weight, dynamic pressure, wing surface area, and flight path angle, respectively.

Knowing the lift coefficient allows for determining drag. The drag of aircraft flying at subsonic speeds consists of parasitic drag, lift-induced drag, compressibility drag, and trim drag [15]. In performance modeling studies, drag is often simplified to the drag polar. This function specifies the relation between the lift coefficient and drag coefficient and comes in various forms of complexities [4, 5, 15]:

$$\begin{aligned} & \text{Standard (in-compressible)} && \rightarrow && C_D = \mathrm{f}(C_L), \\ + \quad & \text{Compressibility Effects} && \rightarrow && C_D = \mathrm{f}(C_L, M), \\ + \quad & \text{Viscosity (Re) Effects} && \rightarrow && C_D = \mathrm{f}(C_L, M, h, T), \\ + \quad & \text{Trim Drag (CG) Effects} && \rightarrow && C_D = \mathrm{f}(C_L, M, h, T, cg). \end{aligned} \tag{11}$$

Compressibility For commercial aircraft flying at subsonic speeds, compressibility effects have to be considered. These effects significantly increase aircraft drag when flying above certain Mach numbers. This requires the modeling of the drag polar as a function of the lift coefficient and Mach. Standard relations have been approximated in literature, but their accuracy remains limited [16]. Better approximations are obtained in BADA 4, which uses performance data generated by software from manufacturers to develop type-specific relations [17]. In industry, manufacturers provide their own closed-source method to approximate these Mach effects [11].

Viscosity The zero-lift drag coefficient is affected by different flight conditions through the Reynolds number [15]. These effects originate from different aerodynamic behaviors of surface roughness in viscous flows. The theory behind this goes beyond the scope of this thesis but can be found in [15]. In essence, the drag polar is affected by the Reynolds number (Re), which is calculated as:

$$Re = \frac{\text{inertia forces}}{\text{friction forces}} = \frac{\rho_\infty \, V_\infty \, c}{\eta_\infty}, \tag{12}$$

with ρ_∞, V_∞ and η_∞, being the free-stream air density, velocity, and dynamic viscosity, respectively, and c being a characteristic length. Different values in altitude, temperature, and Mach affect the Reynolds number, and thereby the flow properties. To include these effects in the drag polar, manufacturers normalize flight test data to a given reference flight condition for each Mach number. Correction factors are then determined in the form of ΔC_D, in the order of ± 0.0003 to 0.0005, to account for different flight conditions [15]. Performance models in ATM research generally ignore these effects.

Trim Aircraft trimming is required to ensure balanced horizontal flight. To ensure static stability, the CG is required to be positioned in front of the neutral point, which is the location where the combined aerodynamic forces of the aircraft body act [15]. To counterbalance the resulting pitch-down tendency, an opposite moment is provided by the trimming surface located on the elevator. The additional lift that is generated creates in effect additional lift-induced drag, known as trim drag. Similar to viscosity effects, CG effects are ignored in ATM performance modeling research. Their sole effects have been studied in [18], which shows an effect in drag in the order of -1% to 3%. Manufacturers provide data on trim drag as a function of CG to correct the drag polar [15].

3.2 Center of Gravity

The CG position of the aircraft is dependent on the location and masses of several components, including, passengers, luggage, cargo, and fuel in each tank. In practice, these components are combined into a Zero Fuel Weight (ZFW) and a Fuel Quantity (FQTY) component. The CG and mass of the ZFW are estimated by the load controller, which manages all items that are loaded onto the aircraft and ensures proper and optimal weight & balance. Given that passengers and luggage are not weighted, standard values are used for both mass and centroid. Cargo is generally weighted, but its centroid is assumed to be centered. Right before departure, the ZFW and CG are corrected for last-minute changes and are documented in the load sheet. Different from the ZFW estimations, fuel weight can be determined from quantity measurements in the fuel tanks and an estimated fuel density. The individual CG centroid of each Tank Body (TB) is subsequently found by considering the actual amount of fuel in the tank and using interpolation functions provided by manufacturers:

$$x_{cg,tb} = \mathrm{f}(FQTY_{tb}). \tag{13}$$

To calculate the CG position and its movement during flight, use is made of the following expression:

$$x_{cg} = \frac{\sum_{i=1}^{k} m_i x_i}{\sum_{i=1}^{k} m_i} = \frac{ZFW\ x_{cg,ZFW} + x_{cg,ctb}\ FQTY_c + 2\ x_{cg,wtb}\ (FQTY_{lbw} + FQTY_{rbw})}{ZFW + FQTY_{lbw} + FQTY_{rbw} + FQTY_{cbw}}, \tag{14}$$

where $x_{cg,ZFW}$, $x_{cg,ctb}$, and $x_{cg,wtb}$ are the centroids of the ZFW, center tank body, and wing tank body, respectively, as measured from the nose of the aircraft; and $FQTY_c$, $FQTY_{lbw}$, and $FQTY_{rbw}$, are the fuel quantities from the center tank, left bound wing tank, and right bound wing tank, respectively. It is common practice to express CG as a percentage in Mean Aerodynamic Chord (MAC), which can be done through:

$$cg = \frac{x_{cg} - LEMAC}{MAC} \times 100\%, \tag{15}$$

where $LEMAC$ is the distance from the aircraft nose to the leading edge of the MAC. Modeling of the CG position is generally not considered in scientific research given the required knowledge of sensitive parameters related to the weight & balance of the aircraft.

3.3 Thrust and Fuel Flow

Fuel flow is closely related to the provided engine thrust. Given that engine thrust cannot be physically measured in flight, a workaround is required to find estimates of this thrust. From the steady-state assumption of cruise flight, equilibrium of forces can be assumed. The provided engine thrust can therefore be considered as the required engine thrust (F_N) found through the total energy equation:

$$F_N = D + m\ a + m\ g\ \frac{roc}{V}, \tag{16}$$

where the drag D is estimated using the drag model previously discussed. When considering steady cruise flight, acceleration and vertical speed are set to zero, reducing this function to $F_N = D$. Since aircraft flying in cruise generally operate away from conditions limiting engine thrust [11], no separate thrust model is required to model limitations where thrust cannot be equal to drag.

Once the required thrust is known, the fuel flow can be calculated by considering engine characteristics graphs. Two different calculation methods can be used for this: using the Thrust Specific Fuel Consumption (TSFC) or using corrected performance properties.

Thrust Specific Fuel Consumption TSFC directly relates net thrust to fuel flow (FF) by:

$$FF = F_N\ TSFC(\cdot), \tag{17}$$

where $TSFC(\cdot)$ represents the characterization graphs as provided by engine manufacturers. TSFC is seen to vary with net thrust, pressure altitude, Mach, outside air temperature, and bleed air [11], and thereby, can be computed from the trajectory and aircraft system parameters:

$$TSFC = \mathrm{f}(F_N, h, M, T, \text{bleed-air}). \tag{18}$$

This approach requires a multi-dimensional relationship to be developed, which is often reduced by simplifying assumptions.

Corrected Performance Corrected performance properties are defined based on dimensional analysis. This allows reducing the order of a functional relationship into generalized graphs that are valid at multiple flight conditions [11]. Corrected performance properties are obtained by considering pressure and temperature ratios relative to Mean Sea Level (MSL) ISA conditions. These ratios include the ambient pressure (δ) and temperature (θ) ratio:

$$\delta = \frac{p}{p_{0,ISA}}, \tag{19}$$

$$\theta = \frac{T}{T_{0,ISA}}, \tag{20}$$

as well as the total pressure (δ_t) and temperature (θ_t) ratio, which corrects the ambient ratios for compressibility:

$$\delta_t = \delta\ \left(1 + 0.2\ M^2\right)^{3.5}, \tag{21}$$

$$\theta_t = \theta\ \left(1 + 0.2\ M^2\right). \tag{22}$$

These correction parameters can subsequently be used to express thrust as corrected (or generalized) thrust (F_{N_c}) and fuel flow as corrected fuel flow (FF_c) using:

$$F_{N_c} = \frac{F_N}{\delta}, \tag{23}$$

$$FF_c = \frac{FF}{\delta_t\, \theta_t^x}, \tag{24}$$

where the power x is used to tailor the corrected engine performance for engine-specific characteristics. This value is determined by the engine manufacturer and ranges from 0.50 to 0.67 [11]. Subsequently, corrected thrust can be related to corrected fuel flow only by considering the Mach number:

$$FF_c = \mathrm{f}\left(M, F_{N_c}\right). \tag{25}$$

This results in a two-dimensional relationship to model fuel flow. To convert back to actual fuel flow, Equation 24 is used together with the ambient conditions. Although this method works particularly well for initial studies and engine facility tests, it remains an approximation of reality that comes with a reduction in accuracy [11].

4. Tail-Specific Data-Driven Performance Modeling

Generic physics-based performance modeling is based on modeling assumptions, makes use of reduced-order functional relationships, and describes type-specific performance. To address these limitations, a methodology is proposed based on empirical relations such that inconsistencies between theoretical modeling and verifiable results are resolved. Although ML methods are well suited for this type of modeling, a new problem arises where biases and uncertainties in the flight data can highly affect model results, and consequently, benefit assessments. Therefore, several methods are presented to identify and quantify tail- and flight-specific biases from uncertainties to arrive at true aircraft tail-specific performance.

4.1 Flight Data Biases and Uncertainties

Before diving into the details of the proposed modeling framework, the uncertainties and biases that affect performance parameters are determined. Two main causes of uncertainties are identified: 1. measurement errors from aircraft sensors, and 2. uncertainties in estimated flight parameters. Both sources of uncertainty can be described by several tail- and flight-specific biases. Flight-specific biases describe offsets between measured/estimated values and true/expected values as an average value for each flight. Tail-specific biases describe offsets between tails and are identified by offsets in the flight-specific biases. This is further illustrated in the next section. By carefully analyzing the flight data, several sources of uncertainties and their biases are identified:

ZFW Bias ZFW is estimated using standard weights for passengers and luggage determined by aviation authorities. These standard weights are constant values, while in reality, seasonality effects, weight characteristics on routes, and the number of children on board are all sources of uncertainty that may combine into significant offsets. Discrepancies in cargo weight and aircraft Dry Operating Weight (DOW) further add to these offsets. Given that the ZFW bias directly translates to gross weight, a constant offset in fuel flow prediction error can be observed over the entire flight. By reducing this offset, the ZFW bias can be determined.

Performance Degradation Another source that leads to steady offsets in fuel flow prediction error is performance degradation. Each aircraft experiences gradual deterioration in engine and aerodynamic characteristics, leading to increasing fuel consumption over time. The performance model that is generated represents the average tail-specific performance over the period covered by the data and does not capture changes within this period. By investigating such gradual offsets in fuel flow prediction error, tail-specific offsets can be found.

CG Bias CG position is computed based on an initial estimate of the ZFW CG. Similar to the ZFW, standard values for passenger weight and centroid are assumed. Discrepancies in payload weight and centroid may lead to further offsets in ZFW CG. Given that CG position directly affects control surface deflections and aircraft attitude, offsets can be found for each flight by comparing the documented value to the expected value determined from the flight data. Besides the flight-specific biases, tail-specific biases can be found by analyzing the relation between control surface deflection/aircraft attitude and CG position between tails. In essence, a correction value can be determined for each tail such that all aircraft have the same aerodynamics (surface deflection and attitude) when considering a single CG position.

FQTY Measurements FQTY measurements are sensitive to the sloshing of fuel during movement and have low measurement resolutions with steps of 100 kg. Given that FQTY measurements are used to determine gross weight and CG position, more accurate values improve performance modeling. Therefore, corrected FQTY measurements are determined from the fuel flow measurements, which is not affected by sloshing and low resolutions.

Flow Flow Measurements Fuel flow measurements show offsets in fuel consumption when comparing the integrated values to the net change in the FQTY measurements over the entire flight. To rectify this, a correction factor is determined that matches the integrated fuel flow to the FQTY. Instead of providing a flight-specific correction, a smoothened average is determined that approximates the time-dependent correction for each tail. The difference between this average value and the flight-specific value represents the remaining uncertainty.

4.2 Proposed Modeling Framework

To model tail-specific performance, a data-driven framework is proposed. This framework is based on high-fidelity flight data and ML techniques to capture the non-linear mapping between flight conditions and fuel flow. Within this framework, the uncertainties and biases are also quantified and correction factors are established to remove their influence on model predictions.

An overview of the presented framework is shown in Figure 7. The first step consists of data processing where cruise flight is identified and characterized from the flight data. In step two, a fuel flow bias is determined by restoring differences to the FQTY indicator. In step three, a CG model is developed that describes the standard type-specific relation between CG and control surface deflection/aircraft attitude. CG correction factors are then found and described by an offset in the ZFW CG. The corrected flight data is then used to train the fuel flow model in step four, where model form uncertainty is analyzed through ensemble models. Finally, fuel flow prediction errors are investigated on a per-flight basis to identify performance degradation and to find the ZFW bias.

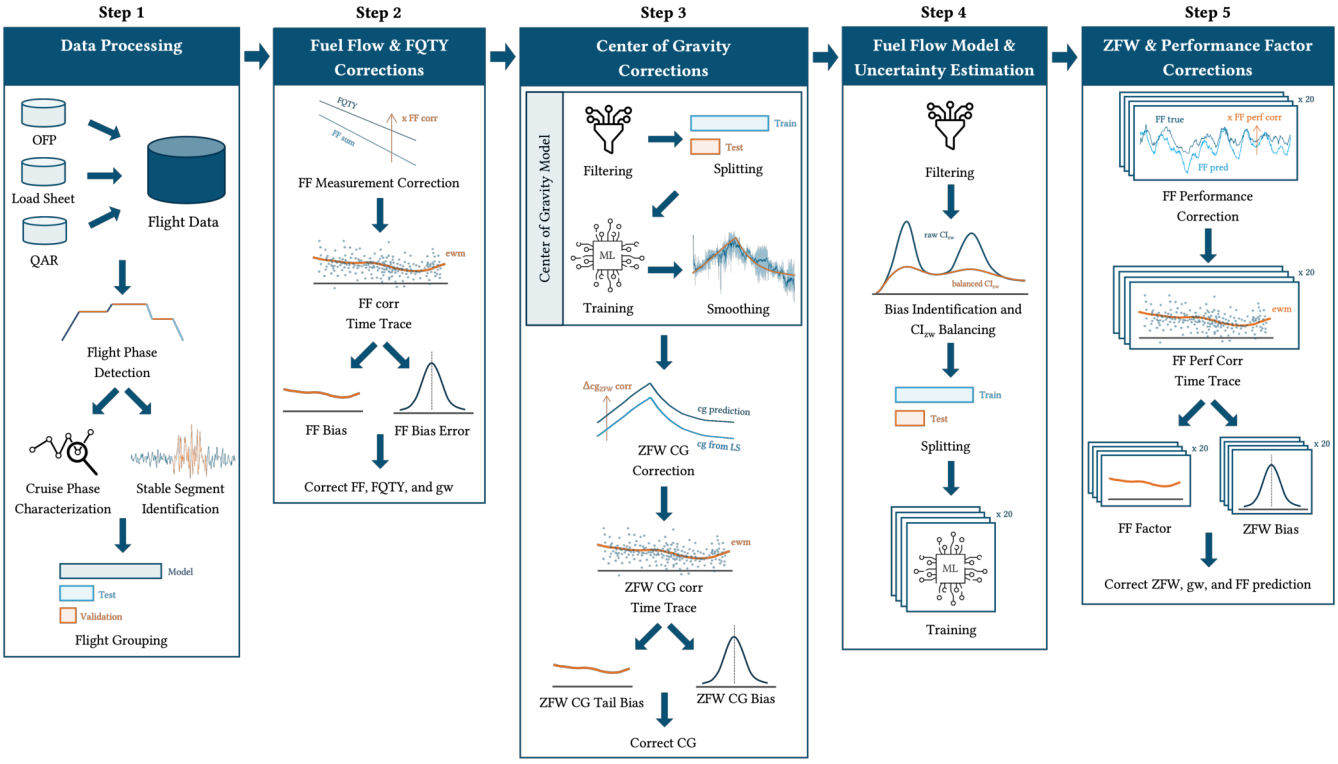

Figure 7. Overview of proposed tail-specific data-driven performance modeling methodology.

Step 1: Data Processing

The research has access to data from 2906 long-haul flights provided by a major airline carrier. These flights are flown by 8 tails of a specific sub-type. The data includes flight properties obtained from the Operational Flight Plan (OFP), Load Sheet (LS), and high-fidelity flight data from the Quick Access Recorder (QAR) which includes many flight parameters measured with a frequency of 1 Hz.

Flight Phase Detection The QAR data does not provide any information on the flight phase. The methodology proposed by [19] is therefore chosen to perform this classification task. [19] makes use of fuzzy logic identification by investigating the combination of instantaneous values in altitude, vertical speed, and airspeed. To improve classification performance, the membership function parameters are tailored to fit the flight data. Following this classification, every flight is segmented into the following phases: ground, initial climb, climb, cruise, descent, and final approach. The step climb and descent are furthermore identified in the cruise phase.

Cruise Phase Characterization The cruise segments are further characterized by certain types of cruise performances. As presented in Section 3, cruise performance is modeled for steady horizontal flight which requires the removal of all data points from steps or that experience a bank angle larger than a certain amount[5]. These conditions represent a so-called clean cruise type I and can be used to filter data for the aerodynamic CG model. Furthermore, engine performance, and therefore fuel flow, is affected by engine-bleed, anti-ice[6], and APU usage, which is required to be off. These additional considerations represent a so-called clean cruise type II and can be used to filter data for the fuel flow model:

Clean Cruise (type I): cruise phase, no step, no bank angle
Clean Cruise (type II): cruise phase, no step, no bank angle, no engine bleed, APU off, and anti-ice off

Stable Segment Identification To improve data quality in clean cruise, stable segments can be identified. This is done by monitoring flight parameters and requiring that the measured value stays within a certain threshold range from the average over a window of 100 seconds. Filtering on stable segments removes turbulent moments in flight reducing scatter. Two main forms of stability can be characterized: atmospheric and engine stability. Flight parameters should be chosen to distinguish between these forms. However, by over-selecting parameters describing similar forms of stability, multicollinearity effects can cause the results to be dominated by this form [20].

After investigating different combinations of flight parameters proposed by [21], the stability criteria shown in Table 2 were utilized, resulting in approximately 45 stable segments per flight. It is important to note that in standard Aircraft Performance Monitoring (APM) activities performed by operators, more strict stability criteria are used [21]. These criteria are also implemented resulting in approximately 4 stable segments per flight.

Table 2. Stability criteria used for stable segment identification

Parameter	Notation	Threshold	Unit
Altitude	alt	150	ft
Mach	M	0.008	–
Total Air Temperature	tat	1.1	°C
Ground Speed	gs	6	kts
Vertical Acceleration	vert acc	0.03	g
Roll Angle	roll	0.8	°
Fuel Flow	FF	5	%
Fan Speed	N1	2	%

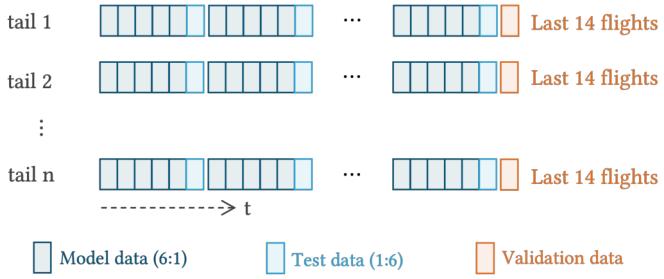

Figure 8. Method used for grouping of flights.

Flight Grouping Finally, all data is merged into a pool of model data, test data, and validation data. Here, it is important to make sure that temporal effects, such as aircraft degradation, are gradually spread over model and test data, and are secluded from the validation data. Tail-specific data should also be evenly distributed between these pools. To achieve this, the flights are sorted by date and time for each tail and then grouped into sets of six. The first five flights in each set are assigned to the model data, while the last flight is assigned to the test data. The final 21 flights of each tail are allocated to the validation data. A visual representation of this grouping is shown in Figure 8. In the remainder of this thesis, model data is randomly split into train/test sets for developing the CG and fuel flow models, and validation data is used to evaluate the final performance of the methodology. Flights from the test data are therefore no longer used.

[5] It was found that an absolute angle of 0.8°was effective for this.

[6] Airframe anti-ice does not have to be considered for the Boeing 787, since the required power for this is provided by the electrical systems onboard. However, other aircraft deduce the power required from the main engines which directly affects fuel flow.

Step 2: Fuel Flow and Fuel Quantity Corrections

Fuel Flow Corrections Fuel flow errors are quantified by comparing fuel consumption from the fuel flow to fuel consumption from the FQTY. Instead of focusing on the cruise phase only, more stable results were obtained by considering the entire flight, that is, from gate to gate. By doing so, the aircraft can be considered stationary when reading the FQTY measurements, reducing the errors induced by sloshing. Subsequently, a simple correction factor (FF_{corr}) is determined for every flight, such that Equation 26 is minimized:

$$\text{Minimize:} \quad \underbrace{\Delta\, FQTY_{meas}}_{\text{from FQTY}} - \underbrace{FF_{corr} \sum FF_{meas}\, \Delta t}_{\text{from Engines}} - \underbrace{\sum FF^{APU}_{meas}\, \Delta t}_{\text{from APU}}. \tag{26}$$

By considering all fuel flow corrections for a single tail, a scatter plot can be constructed describing its evolution over time, as shown in Figure 9 for Tail 1. This evolution can be decomposed into an average trend (the tail-specific bias), found by an Exponential Weighted Moving (EWM) average of three months, and the remaining flight-specific bias. These two components are the FF Bias and FF Bias Error, respectively, and are shown in Figure 9 and Figure 10 for five different tails. The fuel flow measurements are then corrected by multiplying the measured fuel flow from the QAR data with the tail-specific FF bias.

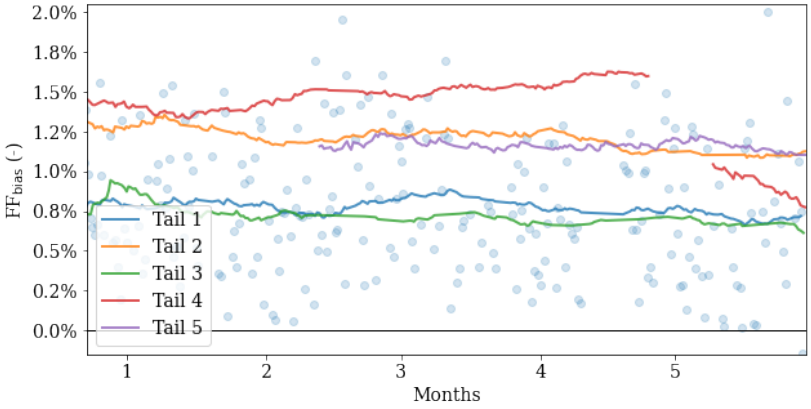

Figure 9. Tail-specific fuel flow Bias, including flight-specific corrections for Tail 1.

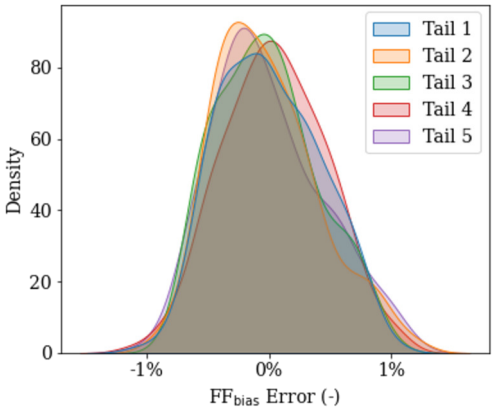

Figure 10. Flight-specific fuel flow bias.

Figure 9 shows a clear difference in FF bias between tails. A positive value indicates a higher actual fuel consumption than measured. Tail 5 covers only part of the graph which is caused by an inactive period of this aircraft. Interestingly, a sudden change in trend is observed for tail 4, which may be caused by the replacement of a faulty fuel flow indicator or an engine change. The resulting gap follows from the minimum time required to arrive at a new stable value in the EWM. When considering the flight-specific bias, uncertainties in fuel consumption remain in the order of ±1% as shown in Figure 10. This may be caused by the discretized measurements every second or by the poor resolution in the FQTY measurements.

FQTY Corrections FQTY measurements experience inaccuracies caused by sloshing and are characterized by poor resolution of 100 kg. With the measured fuel flow being corrected, a more accurate FQTY measurement can be computed from the FQTY at the beginning of the flight and the corrected fuel flow data. Subsequently, the recorded gross weight is enhanced by utilizing this new FQTY measurement.

Step 3: Center of Gravity Corrections

CG biases are quantified by comparing in-flight CG calculated from the load sheet to in-flight CG predictions from the flight data. The in-flight CG values are calculated using Equation 14 where the estimated ZFW CG and the corrected FQTY measurements are used. The predicted CG values are determined from a baseline type-specific ML model that provides independent values in the CG position.

Baseline CG Model Design

Several studies are presented in the literature targeted at estimating in-flight CG position. [22] proposes a methodology that computes CG position by combining a physics-based approach with multi-accelerometer measurements. A different approach is proposed by [23] which uses a kinematics approach and Kalman filters, and [24]

presents a novel approach to both CG and weight estimation from aircraft trim data. Although these methods show impressive performance in CG prediction, they are considered too complex for the problem at hand, require unknown aerodynamic characteristics, and are difficult to integrate with real-life flight data. Instead, this thesis proposes a more simplified approach where ML techniques are used to identify the mapping from aircraft trajectory, attitude, and control surface deflection to the CG position calculated from the load sheet.

Model Description The open-source ML library CatBoost [25] is used to perform the regression task. CatBoost is a gradient-boosted decision tree algorithm that has shown impressive performance in prediction accuracy and has great characteristics in handling large amounts of data and reduced training time [25].

Different model features were investigated to perform this mapping. Eventually, the features shown in Figure 11 were found to give adequate performance in predicting CG. It should be noted that the Mach FMS is used as input instead of the measured Mach. Mach FMS is the recorded speed by the FMS and is equivalent to the selected speed by the pilot. Different from the measured Mach, Mach FMS does not contain noise from atmospheric turbulence, improving model accuracy.

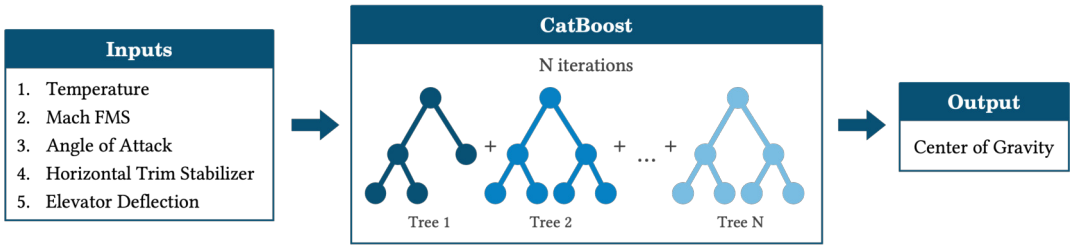

Figure 11. Overview of inputs and outputs for the baseline type-specific CG model.

Prediction Results Model training is performed using the data from the model data pool. This data is filtered on clean cruise type I and stable segments, after which the data is randomly split into a train and test set (2/3 and 1/3, respectively). The CatBoost was trained using the Root Mean Squared Error (RMSE) loss function and was found to give good performance using 300 iterations, a learning rate of 0.4, and a max depth of 10.

The prediction results are shown in Table 3. Based on the similarities between the two sets, it can be concluded that the model is well-generalized and there is no over-fitting. Prediction accuracies found by other studies are seen to be higher, with mean errors in the order of 0.1 - 0.5 [22, 24]. However, these studies are based on simulations where the exact CG position is known. The larger errors found in Table 3 are a result of uncertainties in the true CG position, random noise from the flight data measurements, and tail-specific characteristics not captured by this type-specific model.

Table 3. Prediction performance in type-specific CG.

Data Set	RMSE (% MAC)	MAE (% MAC)	MAPE (%)	R (–)
Train	1.212	0.925	3.476	0.922
Test	1.214	0.926	3.482	0.921

RMSE: Root Mean Squared Error, **MAE**: Mean Absolute Error, **MAPE**: Mean Absolute Percentage Error, **R**: Coefficient of Determination

Smoothing The flight data measurements are characterized by high-frequency noise. This noise is also translated to the model predictions. Considering that in-flight changes in CG are mainly caused by fuel consumption, a steady and slow transition is expected. A smoothing is therefore introduced consisting of two steps: 1. Computing the EWM for the model prediction, and 2. Fitting the physics-based CG to the weighted averaged prediction. A smoothing step could also be added to the input data, from which further smoothing can be expected. However, this was not deemed necessary.

The smoothing steps are visualized in Figure 12. The first step reduces the model prediction (light blue) to the EWM curve (dark blue) by utilizing a window of 120 seconds. Subsequently, Equation 14 is fitted to this EWM curve by iteratively finding a corrected ZFW CG ($cg_{ZFW_{corr}}$) such that Equation 27 is minimized:

$$\text{Minimize MAE:} \quad \underbrace{cg(cg_{ZFW_{corr}}, ZFW_{LS}, FQTY)}_{\text{from physics (eq.14)}} - \underbrace{cg(T, M_{FMS}, \alpha, \delta_t, \delta_e)_{EWM}}_{\text{from type-specific ML model}}, \tag{27}$$

where α, δ_t, and δ_e, are the the angle of attack, horizontal trim stabilizer deflection, and elevator deflection, respectively. This results in the corrected CG shown by the green line in Figure 12.

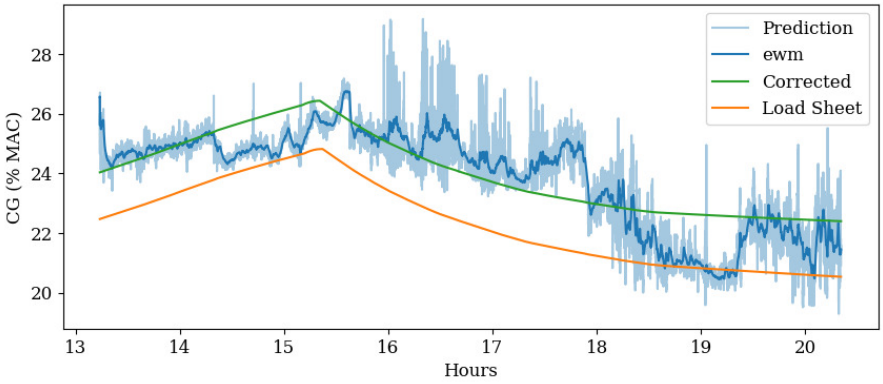

Figure 12. Smoothing steps to arrive at stable CG predictions.

Tail- and Flight-Specific CG Corrections

CG corrections are identified using a similar approach as used for the fuel flow corrections. CG biases are quantified by comparing the estimated ZFW CG from the load sheet to the corrected ZFW CG from the flight data. A simple correction factor ($\Delta cg_{ZFW_{corr}}$) is then determined for every flight. This offset in ZFW CG is translated to in-flight CG offsets shown Figure 12 by the vertical shift between the orange and green lines. By decomposing the evolution into the EWM of three months and the remaining error, the ZFW CG tail bias ($\Delta cg_{ZFW,tail}$) and ZFW CG flight bias (Δcg_{ZFW}) are found as shown in Figure 13 and 14, respectively:

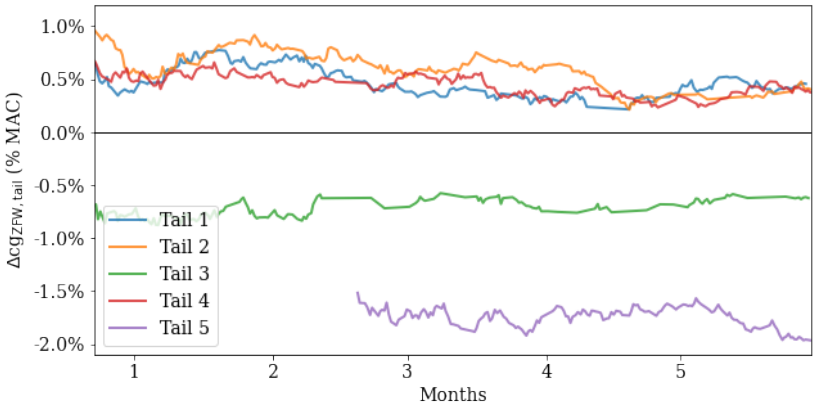

Figure 13. Tail-specific ZFW CG bias.

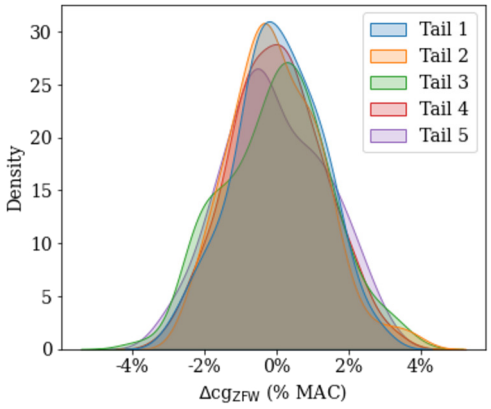

Figure 14. Flight-specific ZFW CG bias.

Figure 13 shows a clear tail-specific component in the CG parameter. Since the baseline CG model maps the attitude/deflections to the average type-specific CG, the identified offsets indicate that this mapping is tail-specific. A negative value for the ZFW CG tail bias indicates a more forward CG for the same attitude/deflections, or inversely, less attitude/deflection for the same CG. When comparing performance between tail 4 and 5 at constant CG, this would result in tail 5 appearing to have a relatively better performance caused by the lower drag. The CG flight data is therefore corrected by adding the ZFW CG tail bias to the ZFW CG obtained from the load sheet and then computing the in-flight CG from Equation 14. This guarantees that aerodynamic CG biases between tails are removed from the flight data. No clear cause is identified for these biases, but in theory, they may be attributed to small discrepancies in aircraft DOW and balance or airframe deterioration affecting aerodynamics. Furthermore, Figure 14 shows a remaining flight-specific bias in ZFW CG in the order of ± 4% MAC. This correction factor can be considered when evaluating or comparing performance between single flights.

Step 4: Fuel Flow Model Design & Uncertainty Estimation

After identifying and correcting tail-specific biases in the flight data, the performance model describing fuel flow can be developed. Different methodologies can be found in the literature that utilize QAR data and ML to perform

this task. These can be divided into methods employing neural networks [26, 27, 28, 29], random forest [29, 30, 31], and LSTM [32]. Although the methods are extensively investigated, the features used to predict fuel flow have received little attention. Except for [29], most research is seen to use an extensive number of features, ranging from air data, engine parameters, control surface inputs, and environmental data. By including features related to engine or control surface parameters the accuracy of fuel flow predictions is greatly increased in post-flight analysis. However, little can be said about these features beforehand. In order to develop a performance model that provides a practical structure to perform simulations and analyze flight operations, this research is restricted to a similar set of features as used by common performance models like BADA, OpenAP, and PET.

Besides modeling fuel flow, this research tries to estimate its uncertainties. Quantifying uncertainties has several benefits in terms of providing a measure of reliability, enabling the development of more robust strategies, and determining areas for improvement. Various types of uncertainties can be considered, including input uncertainty discussed in Subsection 4.1, and model form uncertainty [33]. Model form uncertainties originate from the selected type of model, for example, point-mass, high-fidelity, linear, or non-linear modeling; a lack of knowledge caused by data coverage; and the inherent randomness of a system [33]. As we will see later on, data coverage and system randomness are two main challenges that can be dealt with by estimating uncertainties.

Model Description The regression task is again performed using CatBoost. Two approaches were investigated to capture tail-specific performance, either by using the performance data from a single tail and creating multiple models or by using the tail number as a feature and creating a single model using all performance data. The latter approach was found to give the best results as this greatly increased data coverage in model training. To capture the effects of atmospheric turbulence on aircraft performance, acceleration and vertical speed are included as model features. When performing general cruise phase analysis, these features can either be reduced to zero, or analyzed using distributions describing atmospheric turbulence. This results in the final set of features shown in Figure 15:

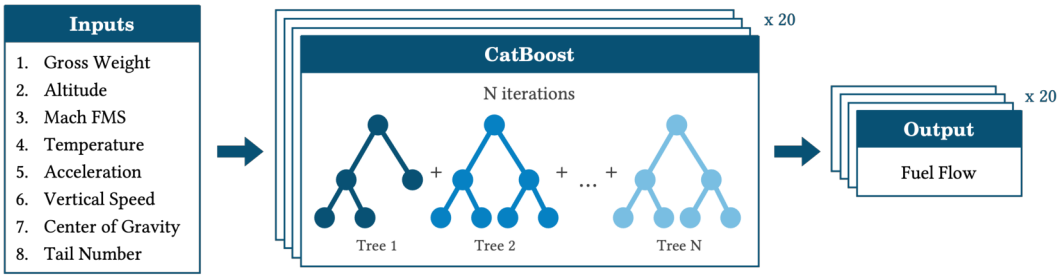

Figure 15. Model overview of inputs and outputs in tail-specific fuel flow prediction.

To quantify model form uncertainties, the same model is independently trained 20 times using a different random seed. This value is found to provide a good balance between training time and capturing sufficient levels of system randomness. Evaluating the differences in predictions between these models enables identifying levels of reliability in fuel flow predictions and establishing robust strategies, as will be seen later on.

Bias Identification and Data Balancing This research introduces a type of balancing that removes a performance bias induced by the economy cruise operation. As presented earlier, airlines typically operate using a cost index. The FMS uses this cost index to calculate the cruise speed from the flight conditions. Given that airlines operate using standard cost indices, certain performance conditions are seen to be dominated by the flight data. Performance conditions are characterized by the unique combination of parameters as shown in Equation 7 that directly relate flight conditions to economy cruise speed. To remove the effects of winds from this mapping, this research introduces a so-called Zero-Wind Cost Index (ZW CI). This is a normalized cost index that is inversely calculated from the FMS Mach, gross weight, altitude, and temperature while setting winds equal to zero. Different from the generic FMS cost index that is expressed relative to ground distance, the ZW CI is expressed relative to air distance. This results in a unique mapping between gross weight, altitude, temperature, and Mach.

By plotting the calculated ZW CI distribution of all flight data, the airline-specific cost index strategy becomes apparent. Since this information is considered confidential, the effects of a fictitious strategy with standard cost indices of 50 and 200 are shown in Figure 16 (blue). The peaks appearing at CI 50 and 200 are flattened, resulting from removing the effects of winds. Furthermore, performance conditions are seen to be flown covering all cost

indices. This is caused either by deviations from the standard cost indices pre- or in-flight or by constant Mach operations, resulting in variable equivalent cost indices. By directly fitting a model on this flight data, fuel flow predictions become biased towards the dominated performance conditions. In order to develop a model that is unbiased on cost index, the flight data has therefore to be balanced.

Simply balancing the data set on ZW CI has the issue of affecting the data coverage in the operating envelope. Therefore, an approach is developed that resolves this issue. This consists of two steps performed for each tail:

1. Establish the operating envelope by binning and grouping all data into unique sets of (gw_{bin}, alt_{bin}, T_{bin})[7], a so-called operating point;
2. For each operating point:
   (a) Construct the probability density function of the ZW CI;
   (b) Calculate the sample probability and convert it to inverse sample probability;
   (c) Sample 30% of unbalanced data with inverse ZW CI probability weights.

This approach is seen to remove the data unbalance, as shown in Figure 16.

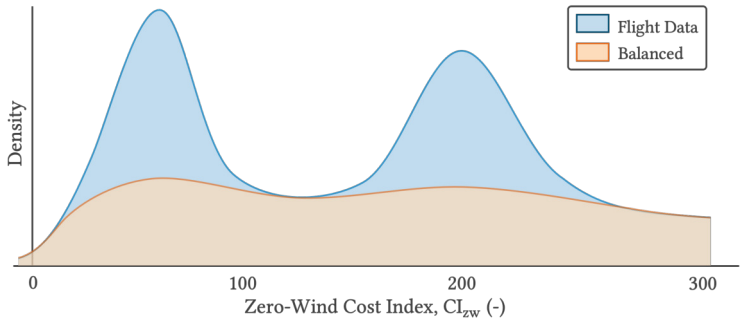

Figure 16. Data balancing to remove a performance bias in ZW CI.

Table 4. Prediction performance of tail-specific fuel flow.

Data Set	RMSE (kg/h)	MAE (kg/h)	MAPE (%)	R (–)
Train	154.17	109.47	1.906	0.930
Test	154.17	109.45	1.906	0.930

Prediction Results Model training is performed using the data from the model data pool. This data is filtered on clean cruise type II, balanced on zero-wind cost index, and randomly split into a train and test set (2/3 and 1/3, respectively). It should be noted that both stable and unstable segments are included in the data. The main reason for this is to enable the model to learn all effects related to atmospheric turbulence. The 20 CatBoost models are trained using the RMSE loss function and are found to give good performance using 300 iterations, a learning rate of 0.4, and a max depth of 10.

The prediction results are shown in Table 4. These results are the average performance of the 20 models. The spread in evaluation metrics between these models was found to be negligible. From this, it may seem that the ensemble model is ineffective at identifying uncertainties. However, uncertainties are still identified when looking at instantaneous moments in flight, as will be seen later on. Both the train and test set give very similar results, even after using a relatively large depth of 10. This is most likely caused by both considering the average performance of the ensemble model and the CatBoost methodology that only performs single symmetrical splits. By doing so, the methodology greatly improves training time and prevents over-fitting. However, greater accuracy could be achieved from other ML methods that enable a more extensive model to be designed to balance between generalization and over-fitting.

Step 5: ZFW Bias & Performance Factor Corrections

The final step consists of finding correction factors by analyzing differences between true and predicted fuel flow. This is done by finding a constant average offset for each flight. This offset becomes apparent from Figure 17, where the predicted fuel flow has a slight vertical offset compared to the true fuel flow. Directly comparing both fuel flow values and minimizing the error resulted in unstable results. Instead, a similar approach to traditional APM activities is used, where fuel flow deviations from book levels are determined by analyzing fuel mileage deviations averaged over stable segments [21]. Given that stable segments in APM analysis result in too few data points to find corrections on all flights, the stability criteria presented earlier are adopted and further reduced

[7] A bin width of 2,000 kg, 1,000 ft, and 2 °C was used for gw, alt, and T, respectively.

into sub-segments with a maximum duration of 60 seconds. An average fuel mileage deviation is then computed for each sub-segment using Equation 28, which results in the scatter plot shown in Figure 18:

$$FM_{error} = \underbrace{\left[\frac{FF(m, h, M_{FMS}, T, a, vs, cg, tail)}{V_g}\right]_{sub-segm,avg}}_{\text{predicted FM}} - \underbrace{\left[\frac{FF_{true}}{V_g}\right]_{sub-segm,avg}}_{\text{true FM}}. \tag{28}$$

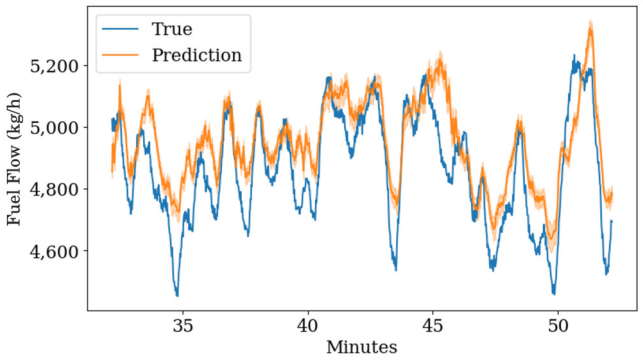

Figure 17. Fuel flow prediction error over a cruise segment.

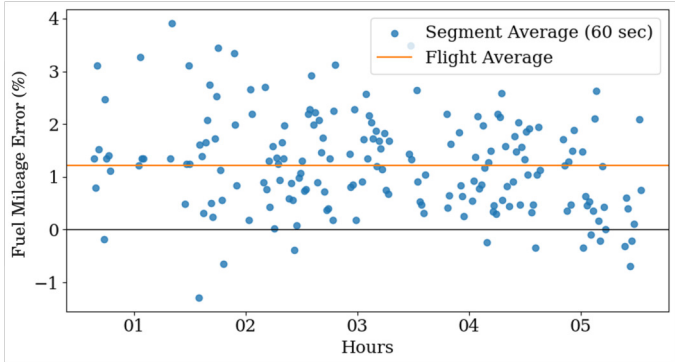

Figure 18. Fuel mileage deviations from stable segments.

A clear offset can be identified from the scatter plot indicated by the orange line. This offset is corrected by finding a multiplication factor ($FF_{perf,corr}$) to the predicted fuel flow in Equation 28 that minimizes the MAE. This correction is found for each model in the ensemble, from which uncertainties are determined.

Similar to the fuel flow and CG corrections, the evolution of the fuel flow performance correction can be decomposed into the EWM of three months and the remaining error. The first component describes the performance degradation of the tail, termed the Fuel Flow Factor (FFF). The remaining error is used to quantify an offset in gross weight, being the ZFW bias (ΔZFW). This ZFW bias is iteratively found by minimizing the MAPE between the true and predicted fuel flow while filtering on stable segments, considering the FFF previously found, and the CG corrected for the flight bias:

$$\text{Minimize MAPE:} \quad \frac{FFF \cdot FF(m + \Delta ZFW, h, M_{FMS}, T, a, vs, cg_{corr}, tail) - FF_{true}}{FF_{true}} \times 100\%. \tag{29}$$

Both the FFF and ZFW bias determined using this approach are shown in Figure 19 and 20, respectively:

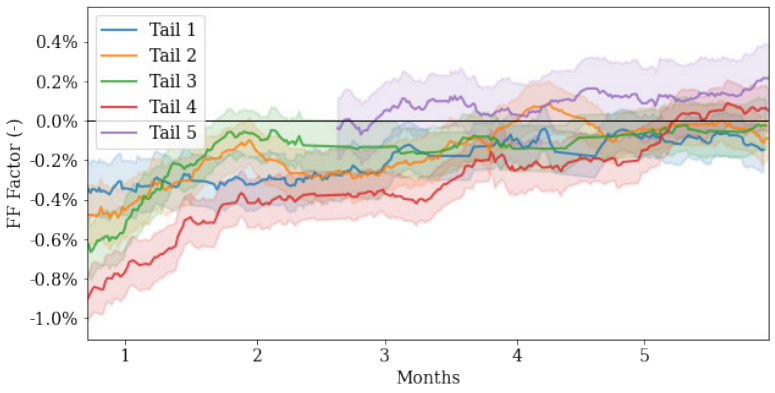

Figure 19. Tail-specific performance degradation, fuel flow factor.

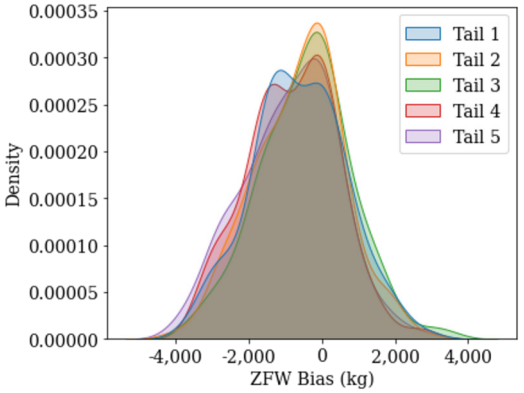

Figure 20. Flight-specific ZFW bias.

Figure 19 shows a clear presence of performance degradation with an average value of approximately 0.5% over 5 months. This figure also shows the minimum and maximum values determined from the ensemble models, indicating an uncertainty in the order of ± 0.1%. Figure 20 shows the ZFW bias, indicating a range in magnitude of -4,000 kg to 3,000 kg. This result is obtained from the average ZFW bias computed by the ensemble. By considering the spread, an average uncertainty range of approximately ± 450 kg is found for single-flight ZFW bias estimation. Interestingly, by further investigating the ZFW biases, a clear correlation is found to the region. Flights to Asia tend to have a more negative ZFW bias than those flown to, e.g., North America.

5. Performance Modeling Analysis and Deviations

In the previous section, a novel performance modeling framework is proposed that captures tail-specific performance characteristics and corrects biases and uncertainties from flight data. This section presents a further analysis of the corrections and their effect on fuel flow and trip fuel predictions. Furthermore, the tail-specific performance model is used to analyze the performance curves presented in Section 2, from which deviations in optimal speeds can be found from the generic MRC speeds determined by the FMS.

5.1 Flight Data Corrections and Model Evaluation

Various correction factors are introduced that describe average tail-specific biases (FF bias, CG tail bias, and FFF), and flight-specific biases (CG bias, and ZFW bias). The importance of flight-specific corrections becomes apparent when considering practical experiments on a per-flight basis. Ideally, after each flight, an evaluation should be delivered where benefits in fuel and time are identified and quantified with high accuracy, and where cumulative savings are explained over the flight. This can only be achieved by identifying and correcting flight-specific biases. To illustrate the influence of these corrections, fuel flow, and trip fuel errors are evaluated. This analysis makes use of the validation flights shown in Figure 8, which ensures that results are obtained independently from model training. This set includes 14 flights for each tail.

5.1.1 Fuel Flow Predictions

The tail-specific performance model is evaluated by considering the effects of the CG and ZFW bias:

$$\begin{aligned} \text{Uncorrected:} \quad & FF = FFF \cdot \mathrm{f}(gw, h, M_{FMS}, T, a, vs, cg, tail), \\ \text{Corrected:} \quad & FF = FFF \cdot \mathrm{f}(gw + \Delta ZFW, h, M_{FMS}, T, a, vs, cg_{corr}, tail). \end{aligned} \tag{30}$$

Figure 21 shows the difference in prediction error for one flight, filtering on stable segments. From the offset in the uncorrected error distribution, an under-prediction in the fuel flow, or equivalently, over-consumption of the aircraft, is observed. After applying the correction methods, an offset in ZFW CG is found of 1.2% MAC, which indicates an overestimation in aircraft drag and therefore fuel flow. This may seem counter-intuitive, as it suggests that the aircraft should perform better than predicted despite the observed over-consumption. The ZFW bias is then determined such that this offset is removed. This resulted in a ZFW bias of 2,960 kg with an uncertainty of ± 620 kg. This suggests that the observed over-consumption can be explained by the true aircraft weight being higher. The corrected prediction error is shown in Figure 21, where the offset is seen to be removed.

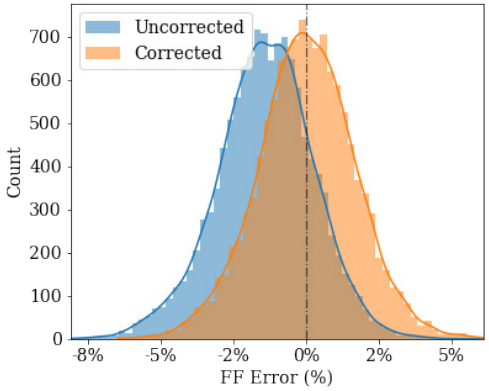

Figure 21. Improved prediction accuracy in fuel flow by removing the flight-specific bias.

Table 5. Prediction performance in fuel flow on the validation flights.

Filter	Correction	RMSE (kg/h)	MAE (kg/h)	MAPE (%)	R (–)
Clean cruise type II	Uncorrected	146.46	102.02	1.79	0.933
	Corrected	142.97	98.44	1.73	0.936
+ stable segments	Uncorrected	108.77	82.68	1.48	0.954
	Corrected	104.04	78.63	1.40	0.958
+ APM segments	Uncorrected	65.51	49.44	0.93	0.968
	Corrected	59.24	44.60	0.84	0.974

Besides the improved accuracy on single flights, the overall improvements are investigated. This is done by considering all flights from the validation set and evaluating their combined performance. Since academia and industry do not define standard baseline conditions for accuracy evaluation, the impact of different filtering schemes is presented in Table 5. The results indicate that flight-specific corrections slightly enhance accuracy by 6 to 9%. However, different filtering schemes are seen to have a more significant impact. For instance, filtering on APM segment improves accuracies by 50% compared to no stable segment filtering. One's own interpretation of appropriate cruise conditions therefore highly affects the values obtained in model performance.

5.1.2 Trip Fuel Predictions

Achieving small errors in trip fuel prediction is essential to arrive at statistically significant results in a single post-flight analysis. If the errors emerging from the performance model are larger than the anticipated savings, it becomes challenging to provide explainable flight-specific evaluations.

Figure 22 shows the cumulative trip fuel error for all flights in the validation set as a function of covered ground distance, filtered on clean cruise type II. Uncorrected performance shows trip fuel errors of up to ± 600 kg (1.50%). However, after applying the corrections, these errors are reduced to ± 100 kg (0.25%). The overall performance is also shown in Table 6 from which a 75% improvement is observed from the corrections.

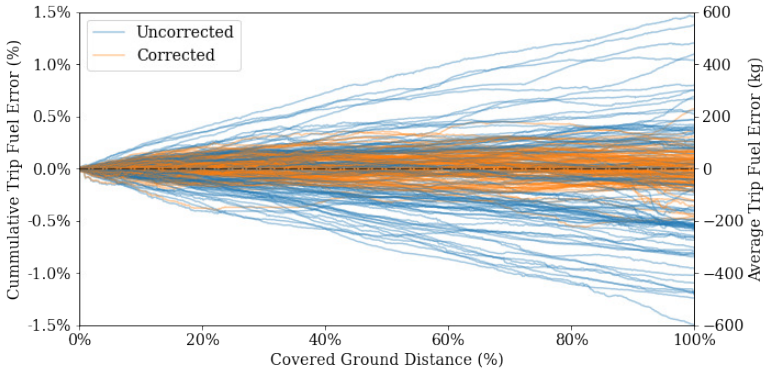

Figure 22. Cumulative trip fuel prediction error for all validation flights.

Table 6. Prediction performance in trip fuel for the validation flights.

Correction	RMSE (kg)	MAE (kg)	MAPE (%)
Uncorrected	237.7	187.4	0.47
Corrected	63.3	47.5	0.12
Corrected with IQR outlier removal	51.4	40.4	0.10

Trip fuel errors are significantly reduced by removing the average bias for each flight. However, discrepancies in cumulative prediction errors still exist when looking at individual flights. These discrepancies are described by flight-specific error profiles, which are unique to each flight and influenced by factors such as trajectory, flight conditions, and model form uncertainties. This is further discussed in Appendix 1. Less common trajectories and flight conditions can result in excessive trip fuel errors, which are identified and removed through a process that considers the error in final trip fuel and the Inner Quantile Range (IQR) outlier removal method. This process removes five flights from the validation set, resulting in the final accuracy shown in Table 6.

5.1.3 Discussion

Overall, the flight-specific corrections are effective in removing biases from the flight data. This results in a significant reduction in the 95% confidence interval in trip fuel predictions from ± 431 kg (1.04%) to ± 102 kg (0.26%) for the validation flights after outlier removal. However, the remaining errors are still too large to provide consistent evaluations of cumulative savings lower than these values. To solve this problem, a methodology is proposed where simulations are used to identify fuel savings irrespective of the error profile. This reduces the confidence interval to flight-specific values in the order of ± 20-50 kg (0.05-0.15%), shown in the next section.

Furthermore, the correction identification method used has some limitations. While it can identify flight-specific biases and provide explainable results, a more thorough approach is needed to fully identify performance deviations. Various factors, such as maintenance activities, engine washes/replacements, errors in sensor measurements, malfunctioning items, and uncertainties in CG and ZFW, can cause performance deviations. The proposed methodology allows the CG bias to be determined independently, but the remaining error is described by an offset in aircraft weight. Sudden improvements resulting from, for example, an engine wash, malfunctioning items, or other effects, are translated to the ZFW bias. This is reflected in the rather large uncertainty range of ± 450 kg.

To improve the accuracy and explainability for single flight performance deviations, the correction identification method can be extended by developing a method to determine both CG and ZFW bias independently from the fuel flow model. Subsequently, a correction factor that describes the remaining flight-specific performance deviation can be determined, from which abnormalities can be detected.

5.2 Fuel Mileage Deviations

So far, the focus has been on evaluating performance of individual or overall flights. As previously mentioned in Subsection 2.3, MRC speeds are identified from performance curves that illustrate fuel mileage at given flight conditions. These curves can now be created using the tail-specific performance model. As a result, any differences in MRC speeds from standard book levels can be determined and expressed through the cost index.

5.2.1 Standard Performance Curves and Uncertainties

To better understand the relationship between flight data and performance, a specific moment during flight can be considered. By narrowing down to a small range of values for gross weight, altitude, and temperature, all flight data can be plotted within that range based on measured fuel air mileage on the y-axis and Mach (or cost index imposing the zero wind condition) on the x-axis. This is shown in Figure 23, where significant scatter follows from varying values in CG, acceleration, and vertical speed that have not been filtered.

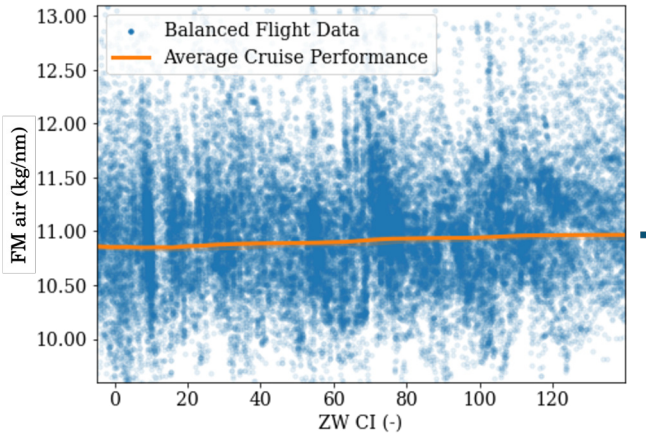

Figure 23. Performance curve showing the flight data filtered for constant weight, altitude, and temperature; and the standard performance obtained from the performance model.

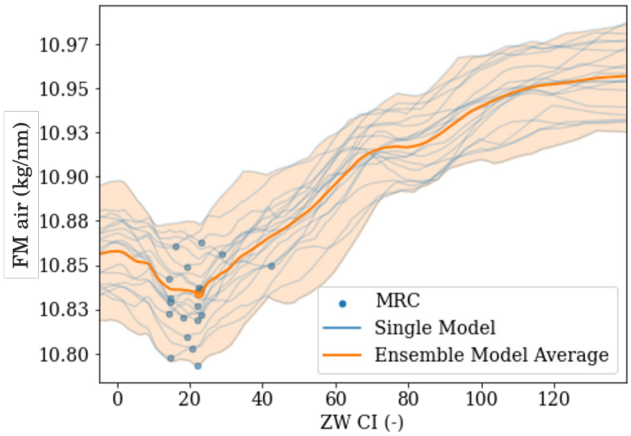

Figure 24. Isolated view of the orange line/area in the left figure, indicating the standard cruise performance.

To determine the standard performance of the aircraft, a standard CG of 30% MAC, zero acceleration, and zero vertical speed is used. These values are plugged into the performance model, which generates the orange line/area shown in Figure 23 and isolated in Figure 24. The blue lines in Figure 24 represent individual model predictions from the ensemble, while the orange line represents the average. The uncertainty range is determined by considering the minimum and maximum values. From this figure, a deviation in MRC speed can be seen from generic values determined by the FMS (CI0). It can be determined that by flying at a CI of 22 under these zero wind conditions, less fuel will be consumed than when flying at the supposedly optimal CI0 determined from the generic performance model. Despite the large amount of spread visible in Figure 23 and the small deviation in fuel mileage from MRC, tail-specific optimal speeds do result in fuel savings, shown in the next section.

Furthermore, Each tail shows a different performance curve, as shown in Figure 25 for the same five aircraft mentioned before. A vertical and horizontal shift in fuel mileage can be observed between the tails. The vertical shift represents the aircraft's overall efficiency, with lower values indicating better fuel efficiency. The horizontal shifts show differences in MRC deviations, indicating that each tail has its own optimal speed. Additionally, the first two and last three tails show similar shapes, suggesting that similarities exist between these tails. Although the reason for these similarities cannot be clearly explained, it is most likely due to inherent similarities in aerodynamic and engine performance characteristics.

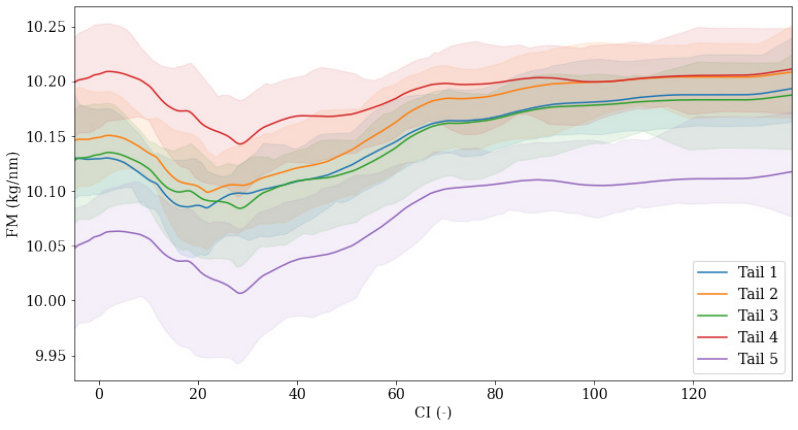

Figure 25. Tail-specific characteristics in performance at a given flight condition (gw, alt, T, cg, and wind).

5.2.2 Sensitivity Analysis

A sensitivity analysis is conducted for fuel flow predictions and all influential parameters. From this analysis, the influence of gross weight, altitude, temperature, winds, CG, and atmospheric turbulence is determined on the performance curves and MRC deviations from book levels across flight conditions. The analysis presented in Appendix 2 found that atmospheric turbulence does not affect the horizontal shift in performance curves. Therefore, the curves can be modeled by setting acceleration and vertical speed to zero in the performance model. The sensitivity of fuel mileage and MRC deviations from the flight conditions are shown in Figure 26. It is observed that MRC deviations are affected by all parameters. To maximize fuel savings, different cost indices should therefore be flown during flight to continuously operate the aircraft at the most optimal speed.

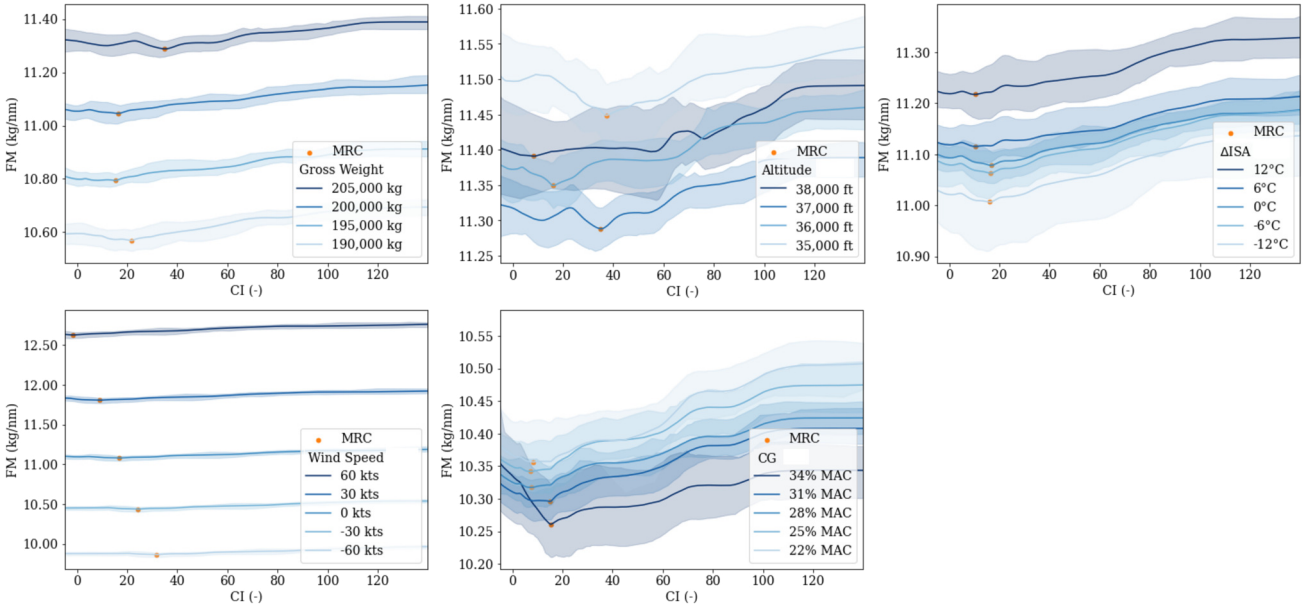

Figure 26. Sensitivity analysis of flight condition parameters on the performance curves.

Furthermore, the performance curves follow expected physics-based relations. Fuel mileage is improved with a decrease in gross weight, temperature, and headwinds. Fuel flow is also observed to increase with a more forward CG, worsening fuel mileage, conforming to the discussion on trim drag in Subsection 3.1. Interestingly, altitude follows the parabolic relation from Figure 5, with FL 370 resulting in the lowest fuel mileage and higher and lower altitudes resulting in less efficient values at the considered conditions.

5.2.3 Discussion

The tail-specific performance model is able to effectively distinguish differences between generic book performance and tail-specific characteristics. True MRC speeds are determined for different flight conditions, which differ from the values determined by the FMS. By providing pilots with optimal cost indices during flight, fuel savings can be achieved compared to generic MRC (CI0) flights. Yet, the optimal cost indices vary for all flight conditions, leading to operational difficulties that are addressed through simulations in the next section.

In addition, there are inherent uncertainties in true MRC predictions that pose some challenges. The different performance curves obtained from the ensemble often produce inconsistent and varying values in MRC deviation, as shown in Figure 24. The cause of these uncertainties is similar to the trip fuel prediction errors discussed in Appendix 1 and likely stems from model type uncertainties and the system's inherent randomness. Although the inconsistencies are effectively addressed by considering the average predictions from the ensemble, the MRC deviations should be viewed as an average estimate and not strictly interpreted.

Finally, it is discovered that flight conditions with sparse representation in the flight data produce varying performance curves. This follows from the knowledge uncertainty previously discussed for trip fuel and the limitations of ML models in under-represented or unseen conditions. Although using the tail number as model input instead of constructing multiple model on tail-specific data reduces drawbacks, performance predictions on individual flights can still be impacted. Although such cases are effectively identified as discussed in Appendix 1, more consistent results can be obtained from more flight data, especially in flight conditions that are under-represented.

6. Benefit Assessment Through Simulations

Fuel consumption is minimized by operating at MRC speeds. Tail-specific performance models describe different values than those determined by the generic model from the FMS. Given that these deviations change throughout the flight and that inherent uncertainties are present in both fuel mileage and optimal speed, the question remains what the achievable benefits are in practical flight operations?

To answer this question, simulations are performed for different cost index strategies. Benefits emerging from optimized cruise speed are quantified by comparing the simulated trip fuel and flight time to a baseline simulation described by a cost index of zero (FMS MRC). Two types of strategies are investigated. The first strategy determines the saving potential for flying at a constant cost index that minimizes average tail-specific fuel consumption over the entire network. The second strategy is more sophisticated, where saving potentials are determined for in-flight cost index optimization. Optimal cruise speeds are found at certain intervals by considering the actual flight conditions and finding the deviation in MRC speed at that moment in time. Two sets of intervals are considered. The first set performs an update at the beginning of a new altitude and after each hour, while the second set determines optimum speeds every minute. Although this latter strategy is considered impractical for real-life operations, it provides a measure of maximum potential savings for tail-specific cruise speed optimization.

6.1 Simulation Set-Up

The simulations are based on previously flown flights. The flight data provides information on the trajectory (route, altitude, distance, weight, and CG) and atmospheric conditions (temperature, winds, and turbulence). These baseline conditions are converted to linear interpolation functions using the ground distance (s).

Each simulation is characterized by its speed profile, controlled by the cost index. The flight data is first filtered for the cruise phase and then divided into constant altitude segments. A discretized time step of 30 seconds is used to progress in space and time. At each step, the simulation finds the flight conditions from the baseline interpolator and computes the ECON Mach from these values and the cost index. Subsequently, fuel flow is determined from the performance model. It should be noted that the net change in parameters over a step climb/descent is not simulated, but adopted from the flight data. Atmospheric effects are also included by obtaining acceleration and vertical speed from the baseline trajectory and the simulation does not consider the effects of engine bleed, bank angle, anti-ice, or the occasional switch between constant Mach and economy cruise. The pseudo-code for both types of simulations can be found in Appendix 4.

Finally, the simulations can be performed with an *average* or a *stochastic* setting. The *average* setting ensures that the ensemble model returns the average value, resulting in a single simulation output. The *stochastic* setting uses each model from the ensemble to perform individual simulations, resulting in 20 independent outputs describing flight-specific uncertainties.

6.2 Simulation Results

280 and 430 flights are simulated for the constant cost index and in-flight optimization, respectively, which are randomly assigned to one of the five tails presented before.

6.2.1 Constant Cost Index Strategy

The results from the first type of simulations are shown in Figure 27 and 28, showing the fuel and time savings, respectively. Each point represents one simulated flight at a constant cost index compared to the baseline CI0 simulation. By fitting a smoothing line to the results, average benefits in fuel are determined for each tail. Time savings follow from the generic FMS model, which therefore does not show tail-specific characteristics. Both figures show a range of benefits between flights operated at similar cost indices. This spread follows from the different trajectories and flight conditions, which results in different savings to be maximally achieved. To determine the range of saving potentials observed on single flights, a smoothened 0.1 - 0.9 quantile bound is provided. This removes the effects of excessive benefits resulting from less common trajectories and flight conditions.

Based on Figure 27 flying at speeds higher than CI0 results in average fuel savings. The lowest fuel consumption is achieved at an average constant cost index of around 26, leading to average fuel savings of 75 kg (0.17%) and time savings of 93 seconds, as shown in Table 7. Furthermore, each tail has a unique optimal cost index and saving potential. Although the reason for this cannot be clearly identified, it is most likely related to underlying aerodynamic and engine characteristics or the trajectory and flight conditions that are assigned to its flights.

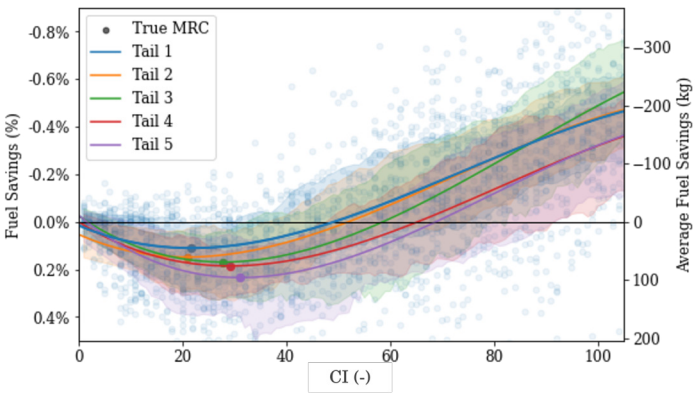

Figure 27. Fuel savings from constant cost index simulations.

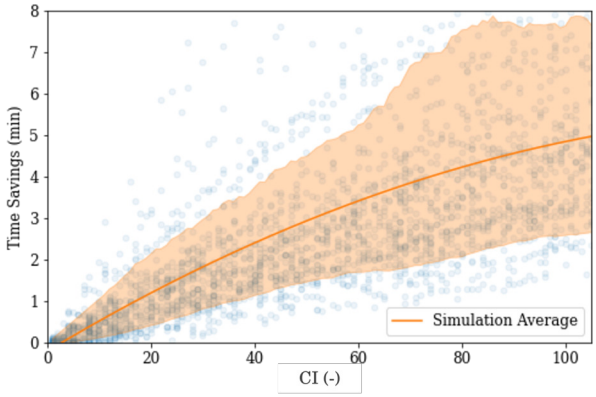

Figure 28. Trip savings from constant cost index simulations.

Table 7. Overall results from constant cost index simulations.

Aircraft Tail	MRC CI	Fuel Savings (kg)		Fuel Savings (%)		Time Savings (s)	
		Avg	Bound	Avg	Bound	Avg	Bound
Tail 1	22	48	[5, 126]	0.11	[0.01, 0.29]	60	[34, 86]
Tail 2	21	66	[13, 123]	0.15	[0.03, 0.28]	77	[42, 118]
Tail 3	28	80	[20, 148]	0.17	[0.04, 0.28]	108	[69, 169]
Tail 4	29	82	[51, 140]	0.19	[0.04, 0.33]	113	[73, 164]
Tail 5	31	100	[22, 169]	0.23	[0.12, 0.31]	106	[52, 181]
Average	**26**	**75 kg**		**0.17% trip fuel**		**93 s**	

6.2.2 In-Flight Cost Index Optimization Strategy

The second type of simulation considers two different in-flight cost index strategies characterized by the interval to find optimal speeds: after every 60 minutes and at new altitudes (60 min), and after every minute (1 min). The results from these two simulations are shown in Figure 29, 30, and 31, showing the in-flight deviation to the optimal cost index, fuel savings, and time savings, respectively. The deviations to the optimal cost index are seen to be smallest for the 1 min interval, which is increased to ± 35 units for the 60 min interval. The distributions in fuel savings show positive values for both intervals, with the 1 min strategy showing larger savings. The savings in time can be considered equal for both strategies. Similar to the constant cost index simulations, a spread in values is observed between flights, following the flight-specific characteristics in trajectories and flight conditions.

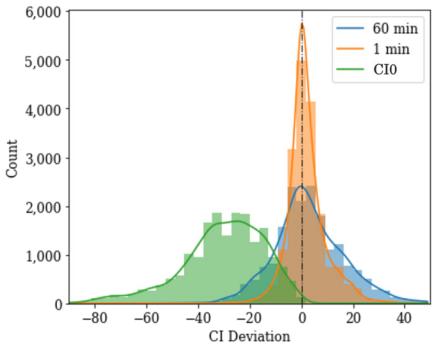

Figure 29. Cost index deviations from true optimal MRC condition.

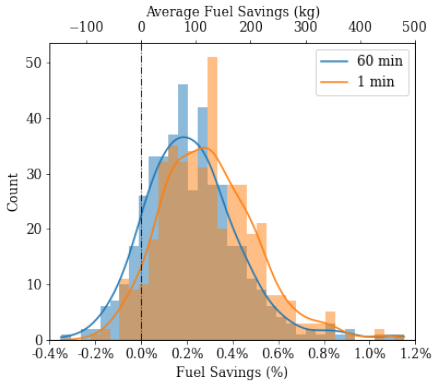

Figure 30. Fuel savings from in-flight cost index optimization simulation.

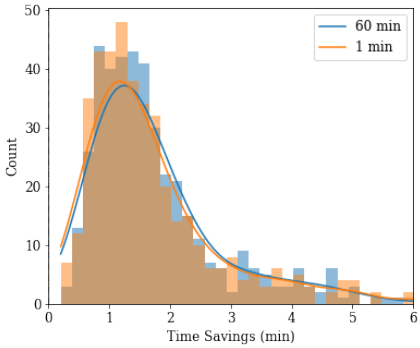

Figure 31. Time saving from in-flight cost index optimization simulation.

The overall results are shown in Table 8, from which average savings of 96 kg (0.23%) and 127 kg (0.30%) are determined for the 60 min and 1 min strategy, respectively, and time savings are found of around 110 seconds. Similar to the constant cost index simulations, each tail achieves distinct savings while flying at different average cost indices. By considering the 0.1 - 0.9 quantile from the distributions in Figure 30 and 31, a range is found for the savings observed on single flights. This is shown in Table 8 for the 60 min strategy.

Table 8. Overall results from in-flight cost index optimization simulations.

Aircraft Tail	Avg CI (1 min)	Fuel Savings (kg)		Fuel Savings (%)		Time Savings (s)	
		Avg (1 min)	Bound	Avg (1 min)	Bound	Avg (1 min)	Bound
Tail 1	28.1 (25.9)	93 (122)	[-15, 239]	0.22 (0.29)	[-0.03, 0.52]	98 (92)	[30, 193]
Tail 2	28.8 (27.5)	97 (130)	[-18, 195]	0.23 (0.30)	[0.05, 0.46]	99 (98)	[40, 197]
Tail 3	30.5 (28.9)	81 (104)	[-24, 208]	0.19 (0.24)	[-0.08, 0.45]	99 (91)	[44, 186]
Tail 4	36.4 (34.6)	113 (152)	[8, 235]	0.27 (0.36)	[0.02, 0.47]	127 (124)	[57, 262]
Tail 5	38.1 (36.8)	98 (127)	[2, 204]	0.23 (0.30)	[0.01, 0.45]	132 (128)	[58, 243]
Average	**32 (31)**	**96 (127) kg**		**0.23 (0.30)% trip fuel**		**111 (107) s**	

6.3 Post-Flight Benefit Evaluations

In Subsection 5.1, the importance of accurate and explainable benefits in post-flight evaluations was discussed. Given that the savings presented above are in the order of 75-127 kg (0.17-0.30%), the identified uncertainty range of ± 102 kg (0.26%) remains limited to identify fuel savings on a per-flight basis. Therefore, a different strategy is presented to achieve more consistent benefit evaluations post-flight.

Instead of quantifying benefits by comparing actual to simulated fuel consumption, benefits can be determined from relative differences between direct predictions and simulations. This is shown in Figure 32, where the blue line/area indicates the cumulative fuel error directly obtained from the model prediction and flight data, and the orange line/area indicates the simulated fuel burn for the same flight with a different cost index. As discussed previously, each flight contains a flight-specific error profile that can be determined post-flight. By investigating the difference between both lines, this error profile is seen to remain constant, indicating that the gradual shift describes the isolated effect of different cruise speeds on aircraft performance. This effect is shown at the bottom of Figure 32, indicating a clear and steady benefit in fuel consumption. The remaining uncertainties can now be determined directly from the ensemble model, which provides a measure for flight-specific uncertainty in the order of ± 20-50 kg (0.05-0.15%) across different flights. The uncertainty range for the simulation is larger than for the direct prediction, which follows from the step-wise progression in time. Each flight can be further examined by considering the fuel mileage deviations across the route, as discussed in Appendix 3.

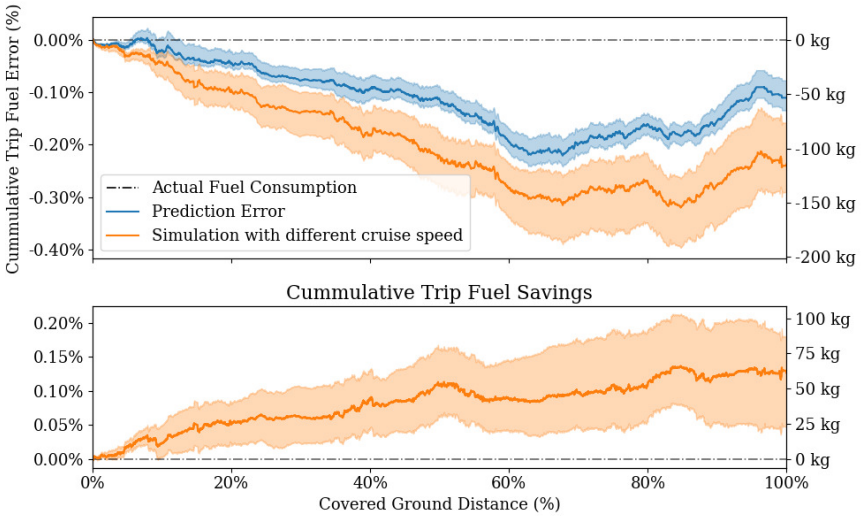

Figure 32. Approach used to determine flight-specific benefits in fuel consumption.

6.4 Discussion

The simulations show that using tail-specific speeds instead of generic MRC values can reduce fuel consumption. Given that tail-specific speeds lie above CI0, this automatically results in accompanying time savings of around 1.5 to 2 minutes. According to the 1 min simulations, the maximum attainable fuel savings are 127 kg (0.30%). In real-life situations, simpler strategies are required. Two strategies are examined, with constant cost index operations achieving 59% of the potential, and in-flight cost index optimization (60 min) increasing this value to

76%. To achieve further savings, advanced decision support tools are necessary, which allows cost index updates to be triggered automatically when entering sensitive areas, as presented in Appendix 3.

It should be noted that the potential savings identified are relatively small. Therefore, high-accuracy performance models and flight-specific corrections are crucial when moving to practical experiments. Although the corrections do not affect simulation results, they are essential to validate proposed strategies post-flight. Only after correcting for the ZFW bias, CG bias, and error profile, fuel savings can be identified and explained on a per-flight basis.

Finally, it is important to consider that by selecting higher cost indices, fuel planning may increase, leading to additional weight being carried along the route. This can result in increased fuel consumption, known as transport loss. The generic book performance model used for fuel planning was investigated and found to be rather flat in the considered cost index ranges. This results in insignificant increases in trip fuel and transport loss.

7. Conclusion and Outlook

Airlines generally manage fuel efficiency in the cruise phase by the cost index. Given its definition of a single constant that relates flight conditions to fuel consumption and flight time, it is a simple and powerful parameter used by pilots to manage cruise speed. However, given the complexities in performance modeling and the limited capabilities of the FMS, simplified performance models are used by the aircraft to determine optimal speeds.

This thesis proposes a methodology to identify potential savings in cruise speed cost index optimization by using tail-specific performance models. The methodology creates a data-driven modeling framework using high-fidelity flight data and ML techniques. It involves several steps, including developing a model for CG and fuel flow, identifying tail- and flight-specific biases, and accounting for model form uncertainties by considering an ensemble of similar fuel models trained with different random seeds. This methodology shows very good results in predicting fuel flow and obtains impressive results after correcting the flight bias in trip fuel predictions.

The remaining uncertainties are effectively identified by the ensemble model on a single-flight basis. The ensemble model shows great applicability in identifying both flight-specific error profiles and knowledge uncertainties. Given that the proposed framework provides limited accuracies in off-nominal flight conditions, the identification of knowledge uncertainty is of special importance to effectively manage these cases.

The tail-specific performance model is also used to construct standard performance curves at different flight conditions. These curves are compared to generic values determined by the aircraft, from which deviations in MRC speeds are found that differ between tails. Although model form uncertainties and system randomness complicate finding true optimal speeds, the average prediction from the ensemble model is able to provide consistent values. The sensitivity analysis showed different deviations across all flight conditions, which requires a more thorough examination to determine saving potentials emerging from tail-specific performance.

Therefore, simulations are established to assess the fuel and time savings for different cost index strategies. The first strategy evaluates the benefits emerging from constant cost indices, while the second strategy performs in-flight cost index optimization steps at certain intervals during the flight. Both strategies effectively capture fuel and time savings compared to generic MRC (CI0) flight. The first strategy achieves savings of 75 kg (0.17%) and 93 seconds on an average flight basis, while the second strategy increases this value to 96 kg (0.23%) and 110 seconds. By exploring more advanced decision support tooling, the fuel savings can be increased to a maximum of 127 kg (0.30%) with similar time savings on an average flight basis. By combining the simulations with the flight-specific corrections and error profile, single-flight fuel savings can be determined post-flight with certainty ranges in the order of ± 20-50 kg (0.05-0.15%) determined by the ensemble model.

Overall, the proposed methodology can be valuable to an airline, where true savings from aircraft tail performance can finally be detected and validated for its benefits. New solutions can be developed and implemented to maximize fuel efficiency. This research lays the groundwork for broader application, where the proposed work can be extended to other flight phases and operations. The next logical step would be to include a wind model, and extend the performance model to climb and descent flight, such that cruise altitude optimization, including penalties from step climb/descent, can be added to the presented analysis. Furthermore, time and cost considerations can be added and combined with optimization techniques like reinforcement learning or optimal control theory to extend the proposed methodology to in-flight multi-phase trajectory optimization.

Appendix 1. Model Form Uncertainties and Trip Fuel Analysis

Although flight-specific corrections significantly reduce trip fuel errors, discrepancies still exist for isolated flights. These stem from the model form uncertainties previously presented. This can be further investigated by considering the cumulative trip fuel prediction error from the individual models in the ensemble, from which two types of uncertainties can be characterized.

The first type is a slow and steady increase in uncertainty as the flight progresses, along with sudden changes in the error, as shown in Figure 33 up to 80% covered ground distance. These sudden changes in prediction error are unique and present on most flights, as shown in Figure 34 for six flights from the validation set. While no clear explanation can be provided for this behavior, it may originate from uncertainties not captured by the model or general randomness in the system. This behavior is also related to the trajectory of a flight, where less common trajectories and flight conditions result in larger discrepancies. A further investigation into these flight-specific errors may be worthwhile in the future to identify possible improvements to enhance the performance model.

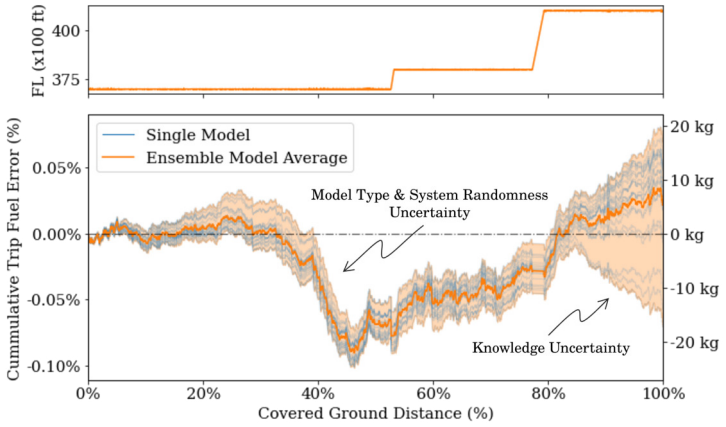

Figure 33. Identification of two types of uncertainties by the ensemble model on a single flight basis.

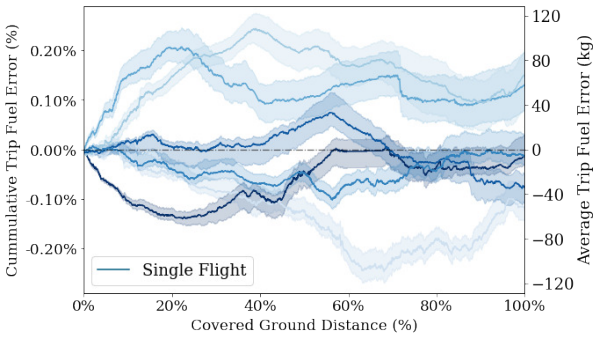

Figure 34. Examples of error profiles that are specific to each flight.

The second type is a sudden increase in uncertainty, as seen in Figure 33 from 80% covered ground distance onward. This is a clear example of knowledge uncertainty, where the combination of flight conditions is underrepresented in the training data. As a result, the ensemble predictions tend to diverge. This behavior directly follows from the modeling approach used, where ML models deliver limited performance in unseen or underrepresented conditions. By using the ensemble model, these cases are effectively identified.

Appendix 2. Influence of Atmospheric Turbulence on Fuel Mileage Deviations

The influence of atmospheric turbulence on the performance curves is investigated to see whether unsteady flight conditions contribute to MRC deviations. Unsteady conditions affect various components related to aircraft performance. First of all, oscillatory behaviors are observed in acceleration and vertical speed that translate to unsteady states in altitude, airspeed, angle of attack, and control surface deflections. Secondly, unsteady autothrottle behavior may be observed followed by the autopilot correcting for the oscillations.

Although identifying isolated effects of unsteady flight conditions on fuel consumption is rather challenging, an attempt is provided to investigate overall effects by relating measured disturbances in acceleration and vertical speed to fuel consumption. Given that the fuel flow model is trained from cruise data including unsteady segments, the performance model is able to provide meaningful insights into unsteady conditions.

Average distributions in acceleration and vertical speed are determined by considering unsteady segments from the data. Both parameters are seen to follow a clear normal distribution that can be approximated by $N(0, 0.0009)$ and $N(0, 1296)$ in m/s^2 and ft/min, respectively. Subsequently, random values can be drawn from both distributions to describe a single moment in time. These values can be plugged into the performance model, together with the other flight conditions, to compute a single (blue) line in the performance curve, as shown in Figure 35. To find the required number of samples to capture average performance in unsteady conditions, the average value in fuel mileage is investigated. This value was seen to approach a stable value after approximately 300 samples.

The average performance curves of the 300 lines are shown in Figure 36 indicated by the orange line. The orange area follows from the average performance curves considering each model from the ensemble individually. Subsequently, the standard performance curve is obtained for the same conditions, but by setting both acceleration and vertical speed to zero, indicated by the blue line. By observing that the shapes of both curves are very similar, it can be concluded that average performance in turbulent conditions is identical to the standard performance obtained by setting acceleration and vertical speed to zero.

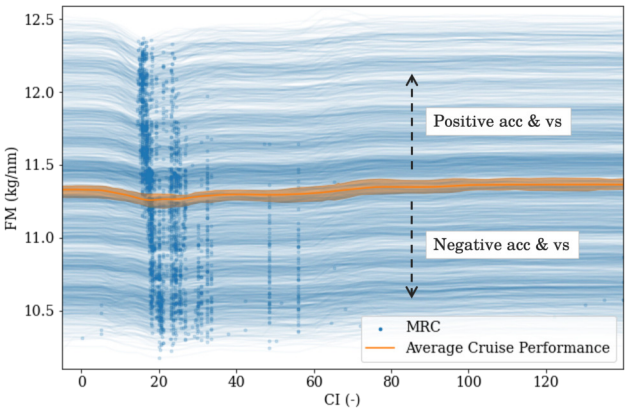

Figure 35. Simulated effect of atmospheric turbulence expressed by random sampling of acc and vs.

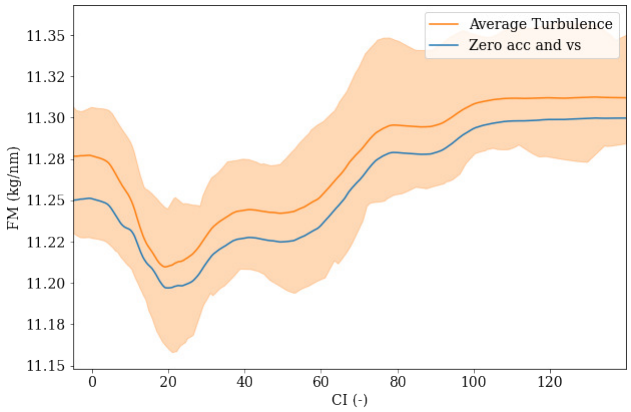

Figure 36. Comparison of average cruise performance on turbulent segments and general aircraft performance.

Appendix 3. Post-flight Performance Analysis

A method to identify the benefits in fuel consumption emerging from a cost index strategy is already presented in Subsection 6.3. To explain the cumulative savings identified from such an analysis, the relative efficiency in fuel mileage can be analyzed across a flight.

This is shown in Figure 37 for a simulated flight using the in-flight cost index optimization strategy (60 min). The orange line indicates the optimal cost index profile determined by the strategy, while the heat map indicates the relative fuel mileage increment from MRC along the route. At each cost index update, a new value is found that matches the speed with the best-estimated fuel mileage. Following the strategy, the new cost index remains constant for the next hour, given that no change in altitude is performed. This may be problematic when flying in sensitive areas, where flight conditions (e.g., winds, altitudes, or ECON Mach) change significantly before the next update. As a result, the orange line may enter blue regions as shown in Figure 37 to occur at the start and end of the flight. Based on this analysis, the strategies can be evaluated post-flight or monitored in-flight.

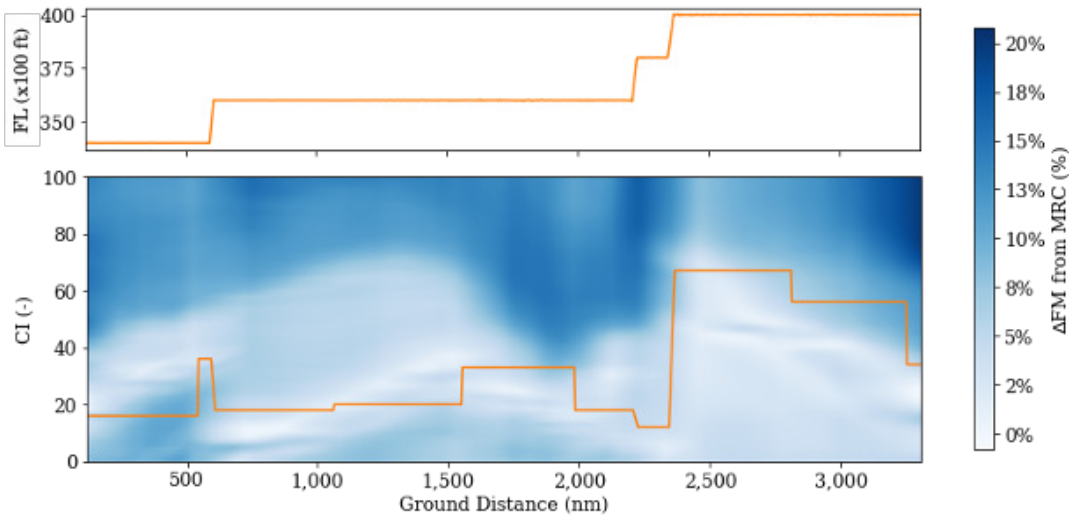

Figure 37. Relation between the cost index profile determined by the in-flight cost index optimization strategy and the relative efficiency in fuel mileage over the entire flight.

Appendix 4. Pseudo-Code of Economy Cruise Simulations

Simulation: Constant OFP Cost Index

```
initialize trajectory and performance model
assign aircraft tail
for trajectory ← max flights do
    filter on cruise phase
    sample 10 CIs from 1, 2, 3, 4, ..., 130
    for CI = CI0, and CI samples do
        initialize flight parameters at start cruise phase
        identify cruise segments at constant flight level
        for segment ← cruise segments do
            while s < max ground range segment do
                t ← t + Δt
                s ← s_{t-1} · gs_{t-1} · Δt
                m ← m_{t-1} − FF_{t-1} · Δt
                FQTY ← FQTY_{t-1} − FF_{t-1} · Δt
                get h, Δ_ISA, a, vs, track, V_w, and ϵ, from
                  base interp(s)
                compute cg from
                  cg(cg_ZFW, ZFW, TOW, FQTY)
                compute ECON Mach from
                  M(m, h, CI, Δ_ISA, track, V_w, ϵ)_FMS
                compute gs from gs(V, track, V_w, ϵ)
                compute FF from
                  FF(m, h, M, Δ_ISA, a, vs, cg, tail) · FFF
                store flight parameters
            end
            add step to flight parameters
        end
        save flight data
    end
end
```

Simulation: In-Flight Cost Index Optimization

```
initialize trajectory and performance model
assign aircraft tail
for trajectory ← max flights do
    filter on cruise phase
    for sim type ← CI0, 1 min, 60 min do
        initialize flight parameters at start cruise phase
        identify cruise segments at constant flight level
        for segment ← cruise segments do
            while s < max ground range segment do
                t ← t + Δt
                s ← s_{t-1} · gs_{t-1} · Δt
                m ← m_{t-1} − FF_{t-1} · Δt
                FQTY ← FQTY_{t-1} − FF_{t-1} · Δt
                get h, Δ_ISA, a, vs, track, V_w, and ϵ, from
                  base interp(s)
                compute cg from
                  cg(cg_ZFW, ZFW, TOW, FQTY)
                if t > update time then
                    compute new CI_opt from tail model
                compute ECON Mach from
                  M(m, h, CI_opt, Δ_ISA, track, V_w, ϵ)_FMS
                compute gs from gs(V, track, V_w, ϵ)
                compute FF from
                  FF(m, h, M, Δ_ISA, a, vs, cg, tail) · FFF
                store flight parameters
            end
            add step to flight parameters
        end
        save flight data
    end
end
```

Acknowledgement

I had the privilege to perform my Master's thesis in collaboration with KLM Royal Dutch Airlines. I would like to extend my gratitude to Jasper de Wilde, Christiaan Evertse, and Frans Huisman for their support during my internship and thesis. Additionally, I would like to thank Junzi Sun, Bruno Santos, and Marta Ribeiro from TU Delft for their assistance during my thesis.

References

[1] IEA. *Aviation*. https://www.iea.org/reports/aviation. Accessed on Aug 08, 2023.

[2] ES Van der Sman, B Peerlings, J Kos, R Lieshout, and T Boonekamp. *Destination 2050*. Netherlands Aerospace Centre NLR, 2020.

[3] Eduardo Gallo, Francisco A Navarro, Angela Nuic, and Mihai Iagaru. "Advanced aircraft performance modeling for ATM: BADA 4.0 results". In: *2006 ieee/aiaa 25TH Digital Avionics Systems Conference*. IEEE. 2006, pp. 1–12.

[4] Angela Nuic, Damir Poles, and Vincent Mouillet. "BADA: An advanced aircraft performance model for present and future ATM systems". In: *International journal of adaptive control and signal processing* 24.10 (2010), pp. 850–866.

[5] Junzi Sun, Jacco M Hoekstra, and Joost Ellerbroek. "OpenAP: An open-source aircraft performance model for air transportation studies and simulations". In: *Aerospace* 7.8 (2020), p. 104.

[6] D.Simos. *PIANO: PIANO user's guide version 4.0*. Lissys Limited. London, UK, 2002.

[7] Sam Liden. "The evolution of flight management systems". In: *AIAA/IEEE Digital Avionics Systems Conference. 13th DASC*. IEEE. 1994, pp. 157–169.

[8] Sam Miller. "Contribution of flight systems to performance-based navigation". In: *Aero magazine* 28 (2009).

[9] David Lax, Mark Darnell, Owen O'Keefe, Brandon Rhone, Nick Visser, Reza Ghaemi, and Eric R Westervelt. "Quantifying operating cost reduction from aircraft performance optimization". In: *2018 Integrated Communications, Navigation, Surveillance Conference (ICNS)*. IEEE. 2018, pp. 3C4–1.
[10] Airbus. "Getting to Grips with Cost Index". In: *Flight Operations Support & Line Assistance; SmartCockpit: Geneva, Switzerland* (1998).
[11] Trevor M Young. *Performance of the Jet Transport Airplane: Analysis Methods, Flight Operations, and Regulations*. John Wiley & Sons, 2017.
[12] Geoff Burrows, Christine A Brown, Trevor W Thom, John MC King, and John Frearson. "Real-time cost management of aircraft operations". In: *Management Accounting Research* 12.3 (2001), pp. 281–298.
[13] Brian L Stevens, Frank L Lewis, and Eric N Johnson. *The kinematics and dynamics of aircraft motion*. John Wiley & Sons, 2015.
[14] Junzi Sun. "Open Aircraft Performance Modeling: Based on an Analysis of Aircraft Surveillance Data". PhD thesis. Delft University of Technology, 2019.
[15] Ed Obert. *Aerodynamic design of transport aircraft*. IOS press, 2009.
[16] John David Anderson and Mary L Bowden. *Introduction to flight*. Vol. 582. McGraw-Hill Higher Education New York, 2005.
[17] María del Pozo Domínguez, Javier López Leonés, and Paul C Roling. "QAR Data-Driven Calibration of Physics-based Aircraft Performance Models using a Machine-Learning Approach". In: *AIAA AVIATION 2023 Forum*. 2023, p. 4498.
[18] Yitao Liu, Zhenbo Yang, Junxiang Deng, and Junjie Zhu. "Investigation of fuel savings for an aircraft due to optimization of the center of gravity". In: *IOP Conference Series: Materials Science and Engineering*. Vol. 322. 7. IOP Publishing. 2018, p. 072018.
[19] Junzi Sun, Joost Ellerbroek, and Jacco Hoekstra. "Flight extraction and phase identification for large automatic dependent surveillance–broadcast datasets". In: *Journal of Aerospace Information Systems* 14.10 (2017), pp. 566–572.
[20] Robert Sklorz, Adrian Zieliński, and Jarosław Brodny. "Analysis of Selected Factors' Influence on the Specific Range of Modern Jet Transport Aircraft as a Complex Mechatronic System". In: *Mechatronics 2017-Ideas for Industrial Applications 4*. Springer. 2019, pp. 360–376.
[21] L Airbus. "Getting to grips with Aircraft Performance Monitoring". In: (2002).
[22] Andy Komendat and Agamemnon Crassidis. "Center of gravity estimation of an aircraft solely using standard aircraft measurement sensors". In: *AIAA Atmospheric Flight Mechanics Conference*. 2012, p. 4411.
[23] AD Manshadi and F Saghafi. "In-Flight Estimation of Time-Varying Aircraft Center of Gravity Position Based on Kinematics Approach". In: *Journal of Aircraft* 55.5 (2018), pp. 2037–2049.
[24] Shaobo Zhai, Guangwen Li, Penghui Huang, Mingshan Hou, and Qiuling Jia. "A novel estimation method for weight and center-of-gravity via the aircraft trim data". In: *Measurement* 220 (2023), p. 113362.
[25] Anna Veronika Dorogush, Vasily Ershov, and Andrey Gulin. "CatBoost: gradient boosting with categorical features support". In: *arXiv preprint arXiv:1810.11363* (2018).
[26] S Baumann and U Klingauf. "Modeling of aircraft fuel consumption using machine learning algorithms". In: *CEAS Aeronautical Journal* 11.1 (2020), pp. 277–287.
[27] Mevlut Uzun, M Umut Demirezen, Emre Koyuncu, and Gokhan Inalhan. "Design of a hybrid digital-twin flight performance model through machine learning". In: *2019 IEEE Aerospace conference*. IEEE. 2019.
[28] Mevlut Uzun, Mustafa Umut Demirezen, and Gokhan Inalhan. "Physics guided deep learning for data-driven aircraft fuel consumption modeling". In: *Aerospace* 8.2 (2021), p. 44.
[29] Vehbi Emrah Atasoy. "Detailed Analysis of Aircraft Fuel Flow Using Data from Flight Data Recorder". In: *Transportation Research Record* (2023), p. 03611981221150401.
[30] S Baumann, T Neidhardt, and U Klingauf. "Evaluation of the aircraft fuel economy using advanced statistics and machine learning". In: *CEAS Aeronautical Journal* 12.3 (2021), pp. 669–681.
[31] Sebastian Baumann. "Using machine learning for data-based assessing of the aircraft fuel economy". In: *2019 IEEE Aerospace Conference*. IEEE. 2019, pp. 1–13.
[32] Weizhen Luo, Zixuan Wu, and Cong Chen. "An Aircraft Fuel Flow Model of Cruise Phase Based on LSTM and QAR Data". In: *2020 13th International Symposium on Computational Intelligence and Design (ISCID)*. IEEE. 2020, pp. 118–121.
[33] Casey L Denham, Mayuresh Patil, Christopher J Roy, and Natalia Alexandrov. "Framework for estimating performance and associated uncertainty for modified aircraft configurations". In: *Aerospace* 9.9 (2022).

II

Literature Study
previously graded under AE4020

1

Introduction

Aviation has seen a general movement towards improving operational flight efficiency in the last decade. Operational efficiency, fuel-saving incentives, and more efficient aircraft have led to annual improvements in fuel efficiency of 2.4% between 2000 and 2010, and 1.9% between 2010 and 2019. Meanwhile, passenger demand increased at an annual rate of 5% between 2000 and 2019 [38]. With the recent announcement of the International Civil Aviation Organization (ICAO) to adopt the aspirational goal of net-zero 2050 for international flight operations [37], further research into more sustainable practices is of utmost importance.

Over the years, new incentives are adopted in order to control environmental impact. ICAO initiated a Carbon Offsetting and Reduction Scheme for International Aviation (CORSIA). With this incentive, carbon emissions are economized with the goal to reduce climate impact [53]. At the same time, airlines have a strong financial incentive that cannot be ignored. Most importantly, their operations have to be profitable. With a more prominent focus on sustainable practices, fuel-efficient flight operations become of more interest to airlines.

The cost index was introduced to aid aircraft operators in developing more efficient flight operations. It provides a trade-off between time cost and fuel cost, which is based on an airline-specific cost analysis. This value is generally chosen by the airline and is used to construct the corresponding flight trajectory. By being a single constant, it is a powerful tool that enables an airline to easily manage its flight operation.

However, the correct adoption of cost index practices in the airline operation is proven to be challenging. The problem is three-folded: there is a lack of knowledge of the cost index concept, time costs are overly simplified and hard to quantify, and delay costs are not considered [1, 11]. This has resulted in airlines deviating from the intended cost-based cost index practice and to rather use the cost index as a performance setting to manage flight time, arrival time, and fuel consumption.

Another difficulty that lies with analyzing and developing cost index practices, is its direct relation to the flight trajectory. By opting for a different cost index, a new trajectory is obtained that has a new speed and altitude profile and a different climb and descent schedule. Often, simplifications are assumed to capture this trajectory optimization problem and standard performance models are used to relate flight trajectory to fuel flow. In practice, deviations are observed between the intended cost index and the true cost index which emerge from such simplifications. This thesis is after to address this problem and evaluate different cost index practices.

This report is structured as follows. chapter 2 starts by providing a basic description of the cost index and describes its characteristics in relation to aircraft performance. It also provides a discussion of difficulties that airlines have with cost index practices. chapter 3 brings the focus towards scientific research related to the cost index. It identifies two research areas: delay management, and flight trajectory optimization. Both areas are reviewed on literature and evaluated on methodologies. chapter 4 summarizes the available literature and identifies the three main research gaps that exist. Finally, chapter 5 presents the research proposal, which includes the problem definition, research question and objective, and a breakdown of the work into work packages.

2

Background Information on Cost Index

Operational flight efficiency has been an important focal point in aviation. Airlines are after optimizing their flight operation to reduce operating costs, limit disruptions, and adhere to schedules while ensuring flight safety. The cost index has been introduced to aid aircraft operators in developing and managing such practices by combining flight trajectory optimization, flight execution, and operating cost, into a simple index. The cost index is therefore a powerful tool that can be generalized and adopted in airline operational practices.

This chapter serves to provide the basics of the cost index and present its characteristics. section 2.1 first gives a general description of the cost index. section 2.2 presents a more detailed practical description of how the cost index is related to aircraft performance and influences a flight trajectory, and section 2.3 discusses difficulties that airlines have with properly developing and using cost index practices.

2.1. Cost Index Description

The Cost Index (CI) is used as a relative measure to balance the objective of the flight operation between minimizing fuel cost and time costs. The combination of fuel and time costs is often referred to as *Direct Operating Costs* (DOC). The aircraft uses this index to compute the speed that it should fly. Low-cost index values result in the aircraft flying at a speed that results in low fuel cost, while high-cost index values result in the aircraft increasing its speed to reduce time cost. This matter is captured by the cost index curve. This curve is generally used to understand the cost index and includes several operational points that characterize cost index practices.

The cost index curve is discussed in subsection 2.1.1, after which the time and fuel costs are presented in subsection 2.1.2 and subsection 2.1.3, respectively.

2.1.1. Cost Index Curve

In order to perform the cost trade-off, the aircraft considers a unit measure of fuel quantity. Considering, e.g., 1 kg of fuel, the aircraft evaluates for different values of airspeed the ground distances that can be covered with the corresponding flight time. The ground distance covered by the unit fuel quantity is referred to as the Specific Ground Range (SGR). The fuel burn and flight time can subsequently be expressed in costs by considering average values for fuel and time cost.

This results in the cost index curve as shown in Figure 2.1. The cost index values are seen to range between 0 and max and correspond to the *Maximum Range Cruise* (MRC) and *Maximum Operating Speed* (V_{MO}) condition, respectively. The MRC condition is characterized by the airspeed at which SGR is maximized, that is, the airspeed at which the largest ground distance can be covered with a unit amount of fuel quantity. The V_{MO} condition is obtained from the performance envelope in the flight manuals and is characterized by the airspeed that results in the lowest flight time.

Besides the CI=0 (MRC) and CI=max (V_{MO}) condition, cost index practices are characterized by two other conditions: *Long Range Cruise* (LRC) and *Economical Flight* (ECON). The LRC condition is defined as the airspeed that results in an increase in fuel consumption of 1%, relative to the MRC condition. Its characteristic is that for a slight reduction in fuel efficiency, a significant increase in airspeed can be obtained. The ECON condition is defined as the airspeed that results in the lowest total operating cost. This airspeed is obtained

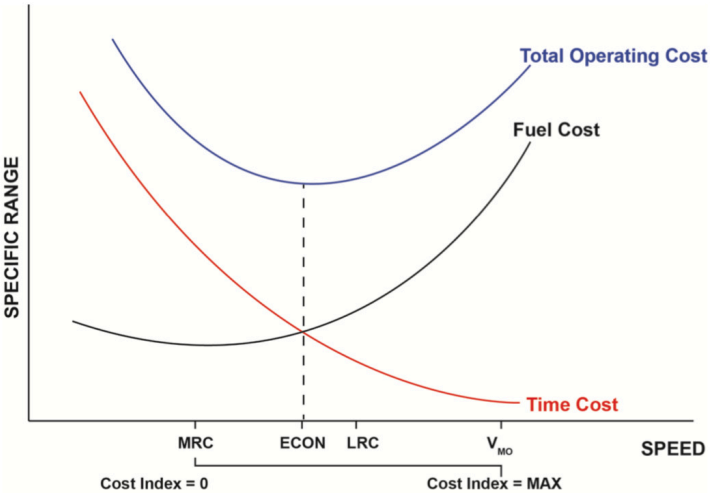

Figure 2.1: Cost index curve for a given flight condition, fuel price, and time cost. [39]

after evaluating both fuel and time costs and follows from the condition where its sum is minimized. Different to the other operating points, the ECON condition differs between flights. Since the average fuel and time cost are dynamic properties that may change over time and are influenced by local prices, the ECON cost index is calculated before a flight considering an airline-specific cost analysis. It should however be noted that this latter step is rarely performed by airlines, which will be further discussed in section 2.3.

2.1.2. Time Cost

When considering cost index practices, the time cost is defined by three components: *crew cost*, *maintenance cost*, and *depreciation or leasing cost* [2]. Each cost component is expressed as an average value per flight time. Because the cost index is a relative measure, it requires the cost value to be constant over the entire flight. Generally, the time cost is expressed per flight hour or minute.

Crew Cost Crew costs consist of cockpit and cabin crew salaries. While generally an average cost is assumed, the crew cost differs between flights dependent on the number of crew on board. Different wages should also be considered for captains, first officers, and other crew members. Besides the standard crew salaries, flights that experience delays, are above a threshold flight time, or encounter other types of disruptions may result in additional crew costs to be considered.

Maintenance Cost Maintenance cost is considered a measure to express the increase in maintenance activity that follows from operating an aircraft. While this matter is highly complex and may be affected by many different scenarios, the maintenance cost per trip is assumed to be simplified into an hourly cost component and a cyclic cost component [2]. An estimate of the average hourly cost component is used when considering the cost index.

Depreciation or Leasing Cost Depreciation or leasing cost describes the loss in value and the rental price of the aircraft per flight time, respectively. A depreciation cost value is difficult to compute and is generally obtained from statistics in literature. Lease cost is more easily computed for an airline, as it generally follows from the contractual agreements.

Finally, it should be noted that in the scientific literature often a single value is assumed for time cost. Furthermore, Airbus [2] states that the three time costs only cover part of the total operating costs for an airline, however, efforts to accurately capture such costs are not pursued.

2.1.3. Fuel Cost

Different to time cost, fuel cost does not require any calculation and is obtained simply from the local fuel price at the origin airport. Although this value is often taken as constant or as average over the entire airline network, obtaining the local flight-specific fuel cost for every flight is considered a better approach. Furthermore, different to time cost, fuel cost is considered to be very dynamic. With fast-changing oil prices, fuel

costs can drastically change over time. Revising the fuel price, or including it as a live parameter, is therefore important to consider.

2.2. Aircraft Performance and Cost Index

In order to evaluate different flight conditions on fuel and time cost, aircraft performance characteristics are used. These characteristics allow the computation of unit fuel consumption and unit travel time, based on aircraft speed, aircraft properties, and atmospheric conditions. To further illustrate this matter, the book of Ruijgrok [62] is used as the main reference for aircraft performance.

subsection 2.2.1 first describes the relation of SR to the performance curve in a graphical manner. subsection 2.2.2 discusses the relation of cost index to flight trajectory optimization, after which subsection 2.2.3 presents how the aircraft obtains the correct airspeed along the flight envelope.

2.2.1. Specific Range

As stated before, the relative fuel use is captured by the SR, which specifies how far the aircraft can travel with a unit amount of fuel. This is directly related to the airspeed (v) by:

$$SR = \frac{v}{ff} = \frac{v}{C_T\, T} \tag{2.1}$$

where ff, C_T, and T are the fuel flow, Thrust Specific Fuel Consumption (TSFC), and thrust, respectively. The thrust and TSFC are dependent on several aircraft properties and atmospheric conditions. These are: the altitude (h), aircraft mass (m), and local temperature (T_h). Different flight conditions, therefore, result in different mappings of the airspeed to the SR. The general relation between SR and airspeed is shown in Figure 2.2 and is referred to as the *performance curve*. The point on the performance curve that corresponds to the maximum SR is the MRC, previously discussed. Such performance curves are generally constructed using performance models or experimental flight tests.

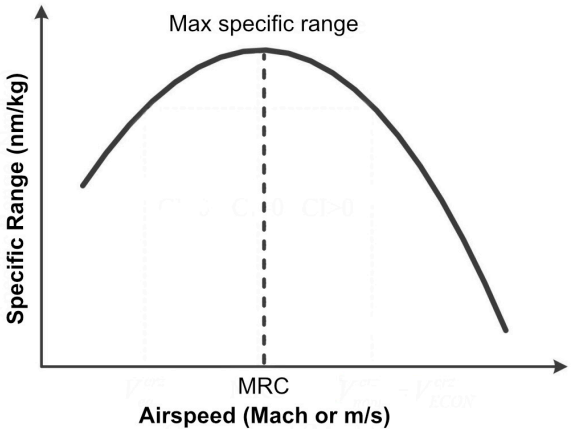

Figure 2.2: Performance curve for a given altitude, aircraft mass, temperature, and density.

It is important to note that such a performance curve is specific to the given flight condition. That is, for every combination of altitude, aircraft mass, and temperature, a different performance curve is obtained. This results that a single point on the performance curve, e.g. MRC, has a different airspeed for different flight conditions. A single point on the performance curve is referred to as a *performance setting*, which is equal to the cost index when considering the range of [MRC,V_{MO}]. The airspeed to the left of the MRC condition is generally not included in cost index practices. Flying at such speeds results in both an increase in fuel consumption and an increase in flight time, which is highly inefficient.

Influence of Wind When considering the influence of wind, the SR can be expressed as either SGR or Specific Air Range (SAR). While the performance curves are generally constructed using aircraft performance models that consider the airspeed around the aircraft as a reference (that is, SAR is considered as a distance metric), the cost index is based on the SGR. In order to construct the cost index curve for a given flight condition, the SAR has to be converted to SGR. This can be done through Equation 2.1 by considering the ground

speed (v_g) instead of the airspeed (v). This results in:

$$SGR = \frac{v - w}{C_T\ T} = SAR\ \left[1 - \frac{w}{v}\right], \tag{2.2}$$

where $v_g = v - w$, with headwind being defined positive. When a no-wind condition is considered, SGR is equal to SAR.

The effect of headwind and tailwind is shown in Figure 2.3. This figure is a graphical representation of Equation 2.2, where the SGR is equal to the inverse of the slope between the origin shifted by the wind speed and the fuel flow curve ($C_T\ T$). Tailwind is seen to lower the MRC airspeed and increase the SGR, while headwind is seen to increase the MRC airspeed and lower the SGR. The shift in performance curve and performance settings are shown in Figure 2.4.

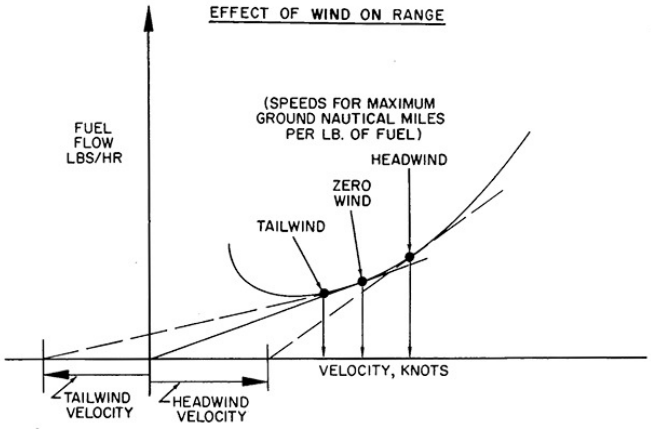

Figure 2.3: Maximum specific ground range for different wind scenarios. [62]

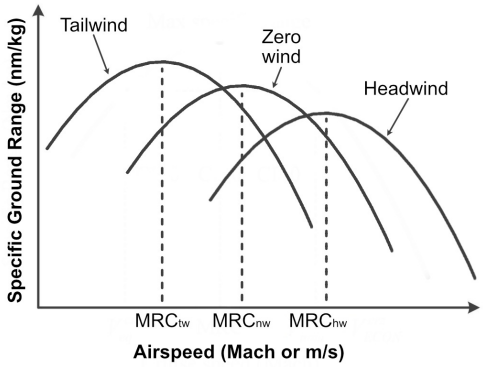

Figure 2.4: Performance curves for different wind scenarios.

Influence of Altitude The performance curve from Figure 2.2 describes the SR to airspeed at constant altitude. Flying at different altitudes results in a shift in the performance curve. The general relation of SAR, airspeed, and altitude is shown in Figure 2.5. This graph also contains a vertical plane, which represents an altitude restriction. By considering the intersection of the 3D performance curve with the vertical plane, the general performance curve from Figure 2.2 follows.

From this figure, it follows that the SAR varies in a similar manner with altitude as with airspeed. Considering a constant performance index on the 3D performance curve, e.g., MRC, a single altitude can be obtained that results in the absolute maximum SAR. By considering a 3D representation of the wind, Figure 2.5 can be converted to a 3D performance curve that maps the airspeed and altitude to the SGR. Such a graph is able to capture favorable altitude-dependent winds, which may result in local jumps of the 3D SGR performance curve.

Besides the value of the SR, when considering a constant performance setting, the airspeed is also seen to vary with altitude. An example of this is shown in Figure 2.6, which contains performance curves for constant cost index values. By considering a single performance index, e.g., the MRC condition, it can be seen that the airspeed is generally increased with altitude.

Influence of Aircraft Weight Similar deviations are observed when investigating the influence of aircraft weight on the performance curve, as shown in Figure 2.7. When considering a constant performance setting, altitude, temperature, and wind, it follows that, especially for low-cost index values, the airspeed reduces with a reduction in aircraft mass.

Influence of Temperature The performance curves are generally constructed considering International Standard Atmospheric (ISA) conditions. Changes in actual atmospheric conditions are expressed through temperature deviations. [2] states that an increase in temperature generally results in a higher airspeed, and a decrease in temperature results in a lower airspeed compared to ISA.

2.2.2. Flight Trajectory Optimization

It has become clear that cost index operations are influenced by altitude, aircraft weight, and atmospheric properties. In order to construct an optimal flight trajectory, a combination of speed and altitude profile has

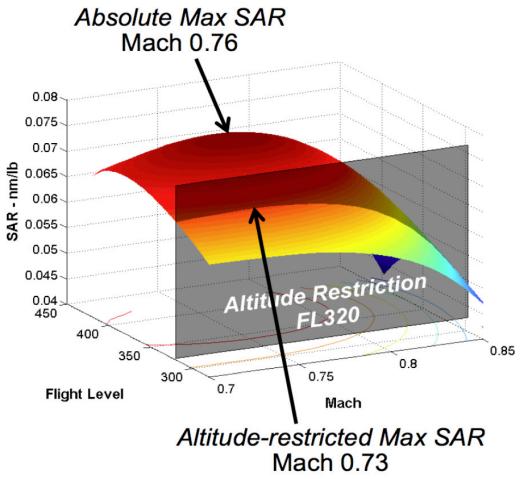

Figure 2.5: Three-dimensional performance curve for a given aircraft mass, and temperature. [40]

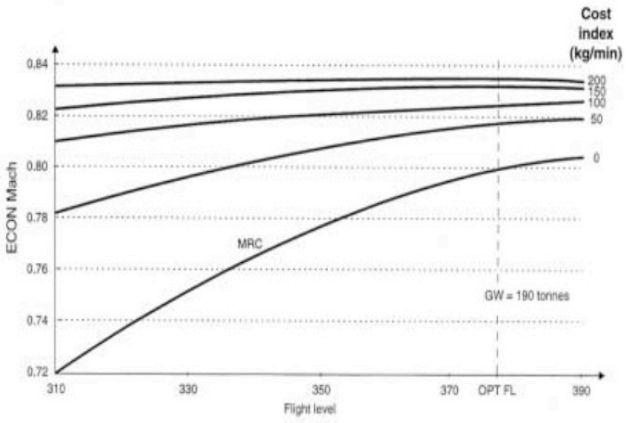

Figure 2.6: Cruise Mach number as a function of CI and altitude, for a given aircraft weight, temperature, and wind. [2]

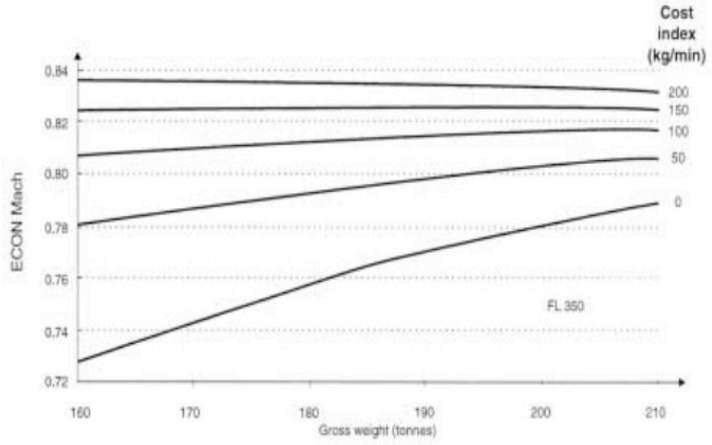

Figure 2.7: Cruise Mach number as a function of CI and aircraft weight, for a given altitude, temperature, and wind. [2]

to be determined that corresponds to the desired cost index and that includes the dependency of aircraft weight and atmospheric properties along the flight trajectory. A detailed description of such a trajectory optimization problem is presented in section 3.3.

Generally, a cost index is chosen before the flight, which is then used as a metric to construct the scheduled flight trajectory. This consists of path optimization and the creation of climb, cruise, and descent profiles. When considering the trajectory optimization problem for different cost index values in a general sense, each phase is seen to have some characteristics

Cruise Phase The cruise phase trajectory is mainly dictated by the cruise altitude and airspeed. With different cost index values, the total fuel consumption and total travel time of the cruise phase are being altered. While different values in cruise speed directly impact this matter, different cruise altitudes also affect the total fuel consumption or travel time. This relation is shown in Figure 2.8, where an increase in cost index generally results in a lower cruise altitude.

Climb and Descent Profile The climb and descent profile are optimized by considering the aircraft to move from point A to point B, as shown in Figure 2.9 and Figure 2.10, respectively. Low-cost index values are after minimizing total fuel consumption along this trajectory, while high-cost index values are after minimizing total flight time. For the climb phase, such a trade-off is obtained by altering the climb gradient. The minimum fuel consumption is obtained by reaching the cruise altitude as fast as possible, while minimum time is obtained by converting more energy into moving forward. In a similar sense to the descent profile, the lowest

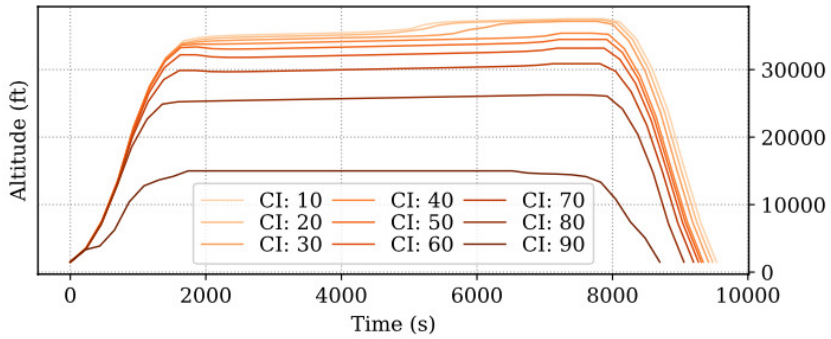

Figure 2.8: Deviation in cruise altitude profiles for different cost index values. [65]

fuel consumption is obtained by approximating a gliding flight, while the minimum time is obtained by starting the descent as late as possible and having a steep descent. Finally, it should be noted that the location of the Top of Climb (ToC) and Top of Descent (ToD) is changed by the cost index.

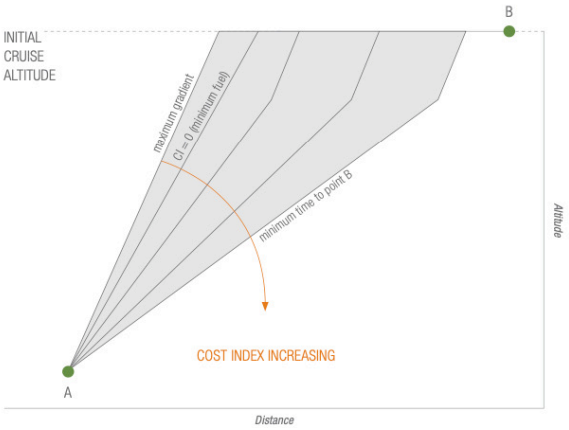

Figure 2.9: Deviation in climb profiles for different cost index values. [9]

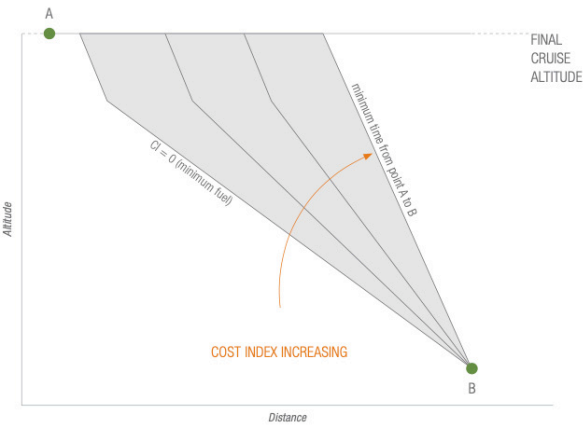

Figure 2.10: Deviation in descent profiles for different cost index values. [9]

2.2.3. Flight Management Computer

The cost index behavior of the aircraft is managed by the Flight Management Computer (FMC). Given the cost index input from the pilot in the Control Display Unit (CDU), the FMC finds the corresponding airspeed considering the aircraft weight, temperature, altitude, and wind. This computation is performed using the model and engine performance database that is stored inside the FMC [34]. This database contains multiple look-up tables that describe the performance of the aircraft. The performance tables are generated during the aircraft development and are constructed using manufacturer performance reports, flight simulators, and/or recorded flight data [31]. The tables consist of discretized instances of aircraft weight, temperature, altitude, etc., and contain performance values related to thrust, Mach, fuel flow, SR, and more. The FMC uses specific performance tables and interpolation to find the correct aircraft states.

An example of such a table is shown in Figure 2.11 in a graphical format. The aircraft performance is plotted for the Boeing 777-300ER aircraft with the GE90 engine. It shows the Mach number that corresponds to different cost index values and aircraft weight, given the altitude, temperature deviation, and wind, being equal to 31 000 feet, ISA temperature conditions, and no wind. Similar graphs are constructed for different altitudes, ISA temperature deviations, and wind speeds, which are converted to look-up tables that can be interpolated.

The approach of storing specific performance tables allows the FMC to quickly output performance parameters. These tables are, however, only generated once and are not updated. Since aircraft performance gradually changes with aircraft age, the actual performance deviates over time. Another problem with this

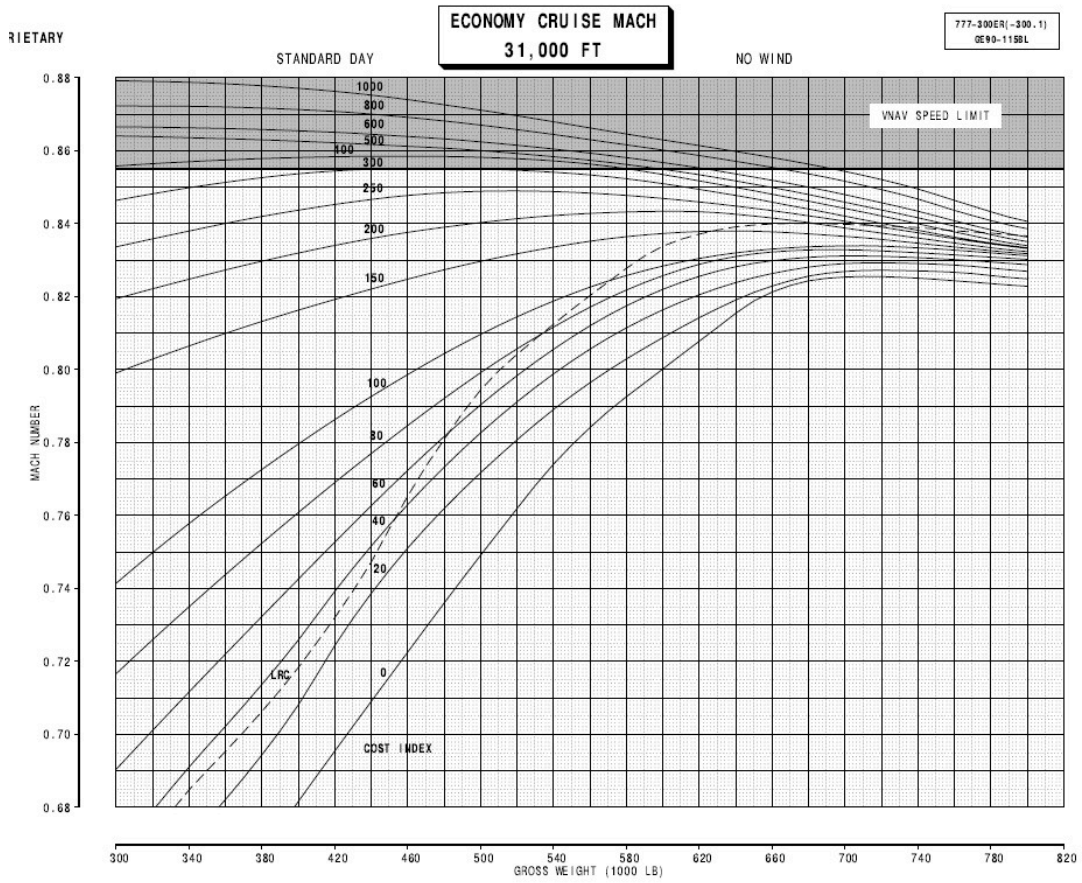

Figure 2.11: ECON cruise Mach number table for the Boeing 777-300ER with the GE90 engine. [8]

information is that aircraft manufacturers consider this data to be strictly confidential, resulting in limited data being available, or only being granted access under strict license agreements [31].

Finally, it should be noted that the FMC also contains a flight trajectory optimization module that computes the properties to fly an appropriate climb, cruise, and descent profile for a given cost index. However, these properties can also be defined separately by the pilot or Air Traffic Control (ATC), which results in the FMC simply computing the airspeed profile corresponding to the cost index input.

2.3. Airline Practices

For an accurate trade-off to be made between fuel costs and time costs, knowledge of the cost structure of an airline is essential. This requires an elaborate cost analysis to be performed by the financial department of the airline. Based on Airbus [2], airlines struggle to integrate such practices as the importance and the concept of the cost index are largely unknown to the decision-makers. This is also acknowledged in Boeing [9], which states that *"operators do not take full advantage of this powerful tool"*.

Furthermore, a major limitation of the cost index is that arrival delay costs are generally not included in the time costs. Being a discontinuous function that depends on the time of arrival, delay costs cannot effectively be transformed into an average cost value expressed in unit time, which is a requirement for the cost index. When considering hub operations, arrival and departure punctuality are of great importance to the airline. Following the intended cost index practice by calculating the ECON cost index through an airline-specific cost analysis neglects this aspect entirely.

The challenge in the cost index is therefore three-folded: there is a lack of knowledge in the cost index concept; time costs are hard to quantify [1]; and punctuality costs are generally not considered. Still, many airlines make use of the cost index to manage their flights in some sort of way. Different practices are presented

below, which is mainly based on Airbus [2], Burrows et al. [11].

1. Not using the cost index Airlines opt to not use the cost index. Instead, a constant airspeed or Mach number is used for the entire or part of the flight. This may lead from the fact that for short flight routes an increase in CI has a limited effect on flight time [1, 14]. Operational restrictions can also require a flight to operate at a fixed airspeed, which limits cost index practices.

While flying at a fixed airspeed results in more efficient management of air traffic flows [14], it results in lower flight efficiency compared to cost index practices. When flying at a constant airspeed, the performance setting changes throughout the flight. Instead of continuously flying at a fixed point on the performance curve, the performance setting is seen to gradually shift.

2. Making use of predefined performance settings to fit a schedule Another practice is to not consider any cost quantification but rather opt for either the LRC, MRC performance setting, or anywhere in between. Instead of calculating the economical cost index from the flight costs, a final cost index is chosen that complies with the flight schedule. This results that a cost index is being flown that might result in a large total DOC, but that limits the occurrence of arrival delays.

When making use of this approach, flight schedules are often generated considering a standard cost index. On the day of operation, this standard cost index is modified based on the calculated time of arrival following a trajectory optimization.

3. Discarding time cost Since the difficulty lies with quantifying time costs, airlines opt to only consider fuel prices in the cost index variation. This is a quick solution where local fuel prices are investigated to find routes that are more economical to fly with either a high or low-cost index value. A major limitation is that no time costs are considered, which limits operators from taking full advantage of the cost index. This approach might also result in difficulties with pre-determined flight schedules.

4. Adopting/adapting cost index values The third practice is to adopt cost index values from other aircraft models or manufacturers. Aircraft manufacturers often provide adequate values, which are then simply adopted. The main issue with this approach is that operating costs change with time. Since the published cost index values originate from the aircraft development phase, the current situation no longer reflects these values. This results that the aircraft is flying at a cost index that was optimal some years ago, but that no longer is.

5. Correct usage of cost index The correct/intended use of cost index practices is based on an airline-specific cost analysis. This consists of monitoring the fuel price (EUR/kg) and computing the average flight-specific time cost (EUR/min). The ECON cost index can then be calculated for every single flight as shown in Figure 2.1, which is used to construct the flight trajectory.

The major limitation of this approach is that no schedule considerations are included and by following this approach, arrival delays may come as a result. Furthermore, airline flight operations are very complex and can generally not be captured well by the very simplistic cost values. Therefore, this fifth practice is not used in airline operations [2].

3

Literature Review

From the earliest cost index research originating from 1984, until the latest state-of-the-art research, different topics and practices have gotten attention. More recent cost index research is seen to focus on two topics: delay management and flight trajectory optimization. Delay management investigates the opportunities behind dynamic cost index practices and capturing delay costs. Flight trajectory optimization is after researching different methods to increase accuracy and to allow balancing fuel cost and time cost using the cost index. Throughout the different research topics, emissions and climate impacts are increasingly adopted.

This chapter serves to provide an overview of the present and past scientific research on the cost index. Furthermore, it provides the mathematical theory required to construct a type of cost index flight trajectory optimization model. section 3.1 first gives a review of early cost index research. section 3.2 continuous by reviewing relevant research on delay management practices and providing a description of delay costs. Finally, section 3.3 reviews the literature on flight trajectory optimization, and provides a description of optimal control theory and aircraft performance modeling.

3.1. Early Cost Index Research

The first published cost index research originates from the year 1984 with the publications of Chakravarty [13], DeJonge and Syblon [18], Liden [47]. These papers were the first to introduce the concept of the cost index in academic literature. Their main focus was on establishing the associated cost components and researching the application of the cost index in relation to airline operations. They propose methods that allow the ECON cost index to be calculated from flight costs.

While the three papers include the DOC as introduced in chapter 2, they acknowledge the drawback of not including costs related to arrival delays. Therefore, both Chakravarty [13], Liden [47] propose a different method than the conventional cost index that includes an arrival error cost function in addition to the DOC. This is done through mathematical approximations of the crew overtime cost, losses due to missed connections, losses due to customer dissatisfaction, and imposing several assumptions. Although this approach results to be successful, it further complicates the understanding and adoption of airline-specific cost analysis, which still is seen to be a major limitation today [1].

Liden [48] investigates a different cost index practice: flight management through the cost index. Instead of considering flight costs to compute the ECON cost index, the sensitivity of the cost index on flight properties, including, altitudes, step climbs, airspeed, flight time, and fuel burn, is investigated. This enables 4D flight planning through the cost index and Required Time of Arrival (RTA). A major limitation identified is the required computational power.

From 1992 until 2008, little cost index research is conducted. In order to investigate the behavior of the cost index on flight properties, performance models are required. With aircraft manufacturers having direct access to such performance models, or airlines through performing costly flight experiments, operational cost index research was limited. Furthermore, fuel prices are seen to be stable, possibly reducing the need for fuel-saving research.

Burrows et al. [11] focused on cost management practices possible from the FMC. They identified cost

drivers and described cost behavior from an airline perspective by managing the cost index. Several issues are identified. It is concluded that the cost index is generally misused by airlines through the forms stated in section 2.3. Airlines are seen to fail to quantify cost components and do not operate at economical speeds. This is also acknowledged by two documents released by Airbus [2] and Boeing [9].

With fuel costs increasing drastically around 2008, a new interest in cost index research is observed. This is also seen to go together with the emergence of research and availability in performance models [3, 12, 22, 29, 55].

3.2. Delay Management

From 2008 until now, two streams of cost index research is observed. The first stream is related to quantifying delay costs and investigating flight management practices through the cost index. The focus of delay management is on in-flight cost index management practices termed Dynamic Cost Indexing (DCI). By describing arrival delay cost and relating this to cost index performance settings, delays can be managed by the cost index.

A review of relevant literature is first presented in subsection 3.2.1, after which subsection 3.2.2 describes how delay costs are generally considered.

3.2.1. Research Focus

The stream of research on delay management builds on Chakravarty [13], Liden [47]. However, instead of computing the ECON cost index before the flight including delay cost, the focus is shifted to in-flight delay management through different performance settings. Furthermore, time costs are generally no longer considered as these cost components are included in the delay costs.

Cook et al. [14] was the first to introduce the concept of DCI and present considerations and a general framework to enable this without developing a DCI model. The principle is to evaluate different cost index values on changes in fuel use and delay cost to prevent unnecessary losses incurred by delay recovery. The fuel use should be modeled using performance models and trajectory optimizers that compute fuel and time changes for different cost index values. The delay costs are captured through publicly available cost data, and the cost index is used to represent a performance setting rather than a cost trade-off.

In the following years, the delay management research is extended. Aktürk et al. [4] extends the problem by including aircraft swapping. Delgado et al. [20] performs analyses on DCI practices and proposes the strategy of Waiting For Passengers (WFP). Achenbach and Spinler [1] includes arrival time predictions to optimize the cost index pre-flight, and Mori [49] proposes a decision-support algorithm to aid pilots in dynamic cost index selection, without considering delay management.

The research of Rosenow et al. [58] provides an evaluation of different strategies to reduce flight delay costs. The considered strategies are fast turnaround, increasing aircraft cruise speed, re-booking of passengers, waiting for passengers, and flight cancellation. To evaluate each strategy, delay costs are calculated through statistically established relations that allow flight-specific delay costs to be computed that consider the number of transfer passengers per flight. By considering single flights and investigating the applicability of the strategy and the effectiveness in total cost reduction, the success rate is found. The fast turnaround and increasing cruise speed are found to be the most effective strategies to manage passenger-specific delay costs. While fast turnaround is not directly related to the cost index, increasing cruise speed is. Cost index management practices can therefore be considered to be a valuable strategy to limit flight and passenger-specific delay costs.

Research that includes both detailed delay cost and aircraft trajectory optimization is limited. While Aktürk et al. [4] allows non-linear and step function delay costs to be modeled, it significantly simplifies the aircraft trajectory problem. Only cruise speed adjustments are considered and fuel burn is modeled through a statistical relation with speed generated from the Base of Aircraft Data (BADA) project of EUROCONTROL. Furthermore, no trajectory modifications in terms of weight, altitude, or descent profiles are included. Similar limitations are observed in Delgado et al. [20], where the aircraft performance and trajectory optimization are simplified.

More recent research captures the Trajectory Optimization Problem (TOP) more accurately. Achenbach and Spinler [1] make use of aircraft performance and optimization models provided by Airbus to compute the change in trip time and trip fuel for different cost index values. The newly computed trip time is used in

a Machine Learning (ML) model to predict the arrival time for a single flight. By using the fuel price and an assumed average time cost, they provide a method to find the optimal cost index. By including the delay cost as an average value in the time costs, it does, however, not consider the effect of delays on total network costs or flight-specific passenger flows.

It should be noted that the research of Cook et al. [14] addresses the impact of carbon emissions on airline operations. Besides considering the fuel price and delay cost in its objective function, carbon pricing is set on fuel emission. Following this cost definition, Achenbach and Spinler [1], Aktürk et al. [4], Rosenow et al. [58] also include a carbon pricing in addition to fuel price. Edwards et al. [24] investigates the effect of carbon pricing and cost index in general on carbon emissions and concludes that carbon pricing itself has a limited impact to reduce this. The study acknowledges the limits in the crew, maintenance, and delay costs, and that airlines generally struggle with the complexities in cost index operations.

Finally, the effectiveness of speed management and cost index operations differs between flight operations. Based on Cook et al. [14], experts of Scandinavian Airlines state that speed management on short-haul flights under 60 minutes is limited, and should be operated at low-cost index values regardless. On the other hand, other airlines state that little time differences already result in large benefits on operational efficiency. No information is provided on fuel benefits. It is concluded that the greatest delay recovery opportunity lies with long-haul flights.

3.2.2. Delay Costs

Flight delays are manifested across the flight operation. Delays can be expressed as departure delays, ground delays, ATC delays, in-flight delays, arrival delays, and more. When considering cost index practices, both departure delay and arrival delays are of importance. Departure delays are defined as the difference between the Scheduled Off-Block Time (SOBT) and the Actual Off-Block Time (AOBT), and arrival delays are defined as the difference between the Scheduled Time of Arrival (STA) and Actual Time of Arrival (ATA) at the gate.

The arrival delay at the destination airport is termed a *primary delay*. If this delay cannot be recovered during the turnaround, the primary delay is carried over into the following flight events, which is then referred to as *reactionary delay* [58]. In order to quantify delay costs, the impacts of both types of delays have to be considered. Primary delays are mainly limited to personnel cost and passenger compensation claims and are therefore rather straightforward to evaluate. Reactionary delays consist of missed passenger or baggage connections, cargo- or postal-related delivery, and the propagation of flight operational disruptions, which are more complex to evaluate [58].

Cook and Tanner [15] published a comprehensive study of reference values for airline delay cost in Europe. In this study, three cost scenarios are assumed: low, base, and high. For every scenario averaged statistical relationships are constructed for 15 different aircraft types that describe the cost of delay as a function of discretized minutes of delay. This study is mainly targeted at providing a means to construct a high-level cost-benefit analysis and is not intended for considering flights on an individual basis. In order to perform trade-offs on specific flights, additional components have to be considered.

In order to develop the generic type-specific delay cost relationships as a function of delay minutes, Cook and Tanner [15] consider the following cost components:

Cost of Fuel: Average fuel cost per flight minute;

Maintenance: Average maintenance cost per flight minute;

Fleet: Average depreciation or leasing cost per flight minute;

Crew: Average crew cost per flight minute;

Passenger Hard Costs: Costs associated with passenger re-booking, compensation claims, and care, on a per-flight basis;

Passenger Soft Costs: Costs associated with passenger dissatisfaction and future value loss, on a per-flight basis.

It should be noted that the crew, fleet, and maintenance costs are the same components considered for the time costs in the cost index presented in section 2.1. The same holds for the cost of fuel. The difference between both cases is that for the cost index, the costs are expressed over the entire flight, while Cook and Tanner [15] only considers the additional costs incurred from delays. When considering delay costs in a cost index problem, care should therefore be taken to not include these costs twice.

Referring to the research of Rosenow et al. [58], they highlighted the importance of flight- and passenger-specific delay cost when considering single-flight airline operations. This is also acknowledged by Cook and Tanner [15], which states that their more generic approach is not suitable for daily flight operations. Evler et al. [25] and Evler et al. [27] therefore focus on developing flight-specific delay cost functions. This method is targeted to enable flight operators to distinguish delay costs between flights by considering flight-specific properties. These properties are shown in Figure 3.1, captured by either linearly assumed cost variables (blue), or step-wise cost increments (purple). As reference, the average type-specific delay cost function from Cook and Tanner [15] is displayed as-well (green).

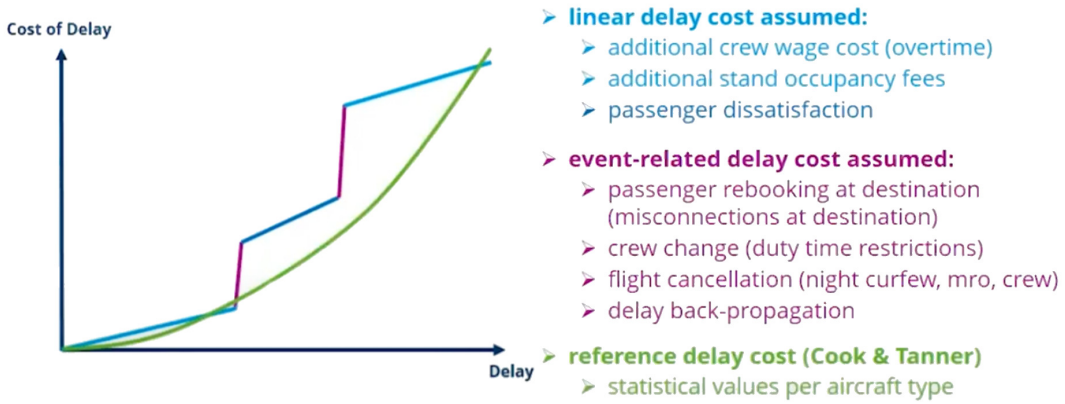

Figure 3.1: Flight- and passenger-specific delay cost function. [26]

3.3. Flight Trajectory Optimization

The second stream of cost index research is related to flight trajectory optimization. Over the years, Single-Objective Optimization (SOO) is evolved into Multi-Objective Optimization (MOO). Instead of optimizing a route for minimum fuel or time, factors related to weather, aircraft performance, terrain, airspace restrictions, operational businesses, noise, emissions, climate impacts, and contrails, are included to optimize for more complete and complex flight trajectories [30]. Such optimization problems are after optimizing single flight phases like climb, cruise, or descent, or attempting to optimize the entire flight, referred to as Single-Phase Optimization (SPO) and Multi-Phase Optimization (MPO), respectively. A distinction is also made between trajectory and profile optimization. The first refers to a 4-dimensional problem, where the lateral (route) and vertical (altitude and speed) profiles are optimized, either simultaneously or sequentially. The latter refers to a 3-dimensional problem, where the vertical (altitude and speed) profile is optimized for a fixed route.

This section serves to present the general scope of flight trajectory optimization. This includes a review of different optimization methodologies used in literature; a description of the optimal control approach and numerical methods to solve this; an overview of the objective function, and a description of performance modeling. This is presented in subsection 3.3.1, subsection 3.3.2, subsection 3.3.3, subsection 3.3.4 and subsection 3.3.5, respectively.

3.3.1. Optimization Methodologies

The topic of trajectory optimization has been extensively researched in the past. In recent years, several reviews were published on this matter. Delahaye et al. [19] presents a review of different mathematical models and describes their most suitable use-case; Gardi et al. [30] presents a review of MOO in the context of ATM and avionics, and provides an elaborate description of the different models and aspects related to flight trajectory optimization; Simorgh et al. [63] presents a review of flight trajectory optimization in relation to climate impact.

Based on [63], trajectory optimization models can be classified into two categories: optimal control (OC) approach, and non-optimal control (NOC) approach. Optimal control is characterized by having several control parameters that are used to control the aircraft states. The aircraft dynamics are modeled as a point-mass representation of 4D or 3D aircraft motions and are captured in a continuous time span. In order to

link physical aircraft performance to the control system, use is made of path constraints. These constraints prevent infeasible paths to follow from the optimization, as the control system is restricted to only applying controls that comply with aircraft physics [19]. Boundary constraints are used to enforce initial conditions such as start and end location, initial masses, airspeed, and more. This approach enables the control system to optimize trajectories by considering an objective function and non-linear aircraft dynamics. Compared to the NOC approach, OC provides more accurate results but is more difficult and requires more effort to set up.

Non-optimal control approaches are characterized by making simplifications to a dynamical optimization problem. Instead of capturing actual aircraft performance related to the modeled dynamics, they are disregarded or simplified through e.g. linearizations [63]. The advantage is that they are easy to set up and generally provide a fast and robust solution, although not the most optimal. Trajectories are often required to be discretized to allow for efficient performance. Popular methods to solve this optimization problem are geometric methods, path-planning (e.g. A^* and Dijkstra algorithm), combinatorial optimization, and meta-heuristics [63].

Both approaches can also be combined, resulting in a hybrid control approach. Such approaches generally consider a NOC approach for the lateral route optimization and perform an OC optimization to obtain the corresponding vertical profile. By decomposing both components the final trajectory is a combination of two separate optimization problems, which does not necessarily result in the optimal trajectory. Such hybrid methods address the limitations observed by the NOC approaches by including accurate flight performance characteristics in the trajectory optimization.

Table 3.1 presents an overview of the published research on flight trajectory optimization. This table characterizes the work into the three optimization approaches and states important characteristics related to the method, optimization problem, performance model, and objective function. The characteristics of the different optimization approaches are further discussed below.

Non-Optimal Control Approach The NOC approach is seen to be mostly limited to single-profile optimization. [50] and [28] consider Dijkstra's and A^* algorithms, respectively, to optimize the lateral route. The advantage of this discretized approach is that both methods effectively capture existing ATM constraints, including, airways, waypoints, and restricted airspaces. Both methods also incorporate wind into their optimization, which is evaluated at the discretized locations. The main limitation is the lack of aircraft performance in the optimization problem. Murrieta-Mendoza and Botez [50] makes use of an average fuel flow value during the cruise and [28] makes use of iterations to adapt the geographical graph cost factors on fuel burn after performing a vertical profile optimization.

Murrieta-Mendoza and Botez [51] and Dancila and Botez [17] consider a NOC approach for the vertical profile optimization. Both methods make use of a form of search algorithm to evaluate different altitude and speed profiles over a fixed route. Compared to lateral optimization, a more detailed representation of aircraft performance is considered. Murrieta-Mendoza and Botez [51] make use of a Performance Database (PDB), similar to the look-up tables of the FMC discussed in chapter 2. These tables are constructed from experimental flights and are generated for all flight phases. Dancila and Botez [17] makes use of a similar approach, but directly uses the performance tables from the FMC.

More advanced NOC approaches are seen to capture the lateral and vertical optimization problem at once. [70] make use of Genetic Algorithms to directly optimize the route and altitudes by modifying 6 design points in a 3D space. Aircraft performance is included using BADA3.9 and the DLR fuel flow method, which estimates the fuel burn and emissions between the design points. Trajectories are constructed considering the cruise phase only and operating constraints are not included. The application of this model is focused on researching routing options on climate impacts and is not suitable for practical use.

Hybrid Control Approach Compared to the NOC approaches, hybrid methods are seen to optimize the entire trajectory. Förster et al. [28] constructs the TOol-chain for Multi-criteria Aircraft Trajectory Optimization (TOMATO) and the Compromised Aircraft performance model with Limited Accuracy (COALA). These modules consist of the A^* path algorithm described above, and a PID controller to optimize the corresponding vertical profile. By linking both modules, the entire trajectory is optimized. TOMATO is targeted for single-flight multi-criteria trajectory optimization, where ATC cost charges, airspace structures, airline operating costs, emissions, and contrails, can be included. The performance model COALA includes type-specific aircraft characteristics obtained from BADA4 and performs a 3D vertical path optimization. TOMATO is able to model all flight phases, from take-off to landing, and assess trajectories on fuel, time, delay, and ecological costs. The main advantage of this model is the adherence to the existing navaid infrastructure, ATS route

network, and airline operations. In Rosenow et al. [59], the author acknowledges the increase in computational effort resulting from the NOC path-finding approach and recognizes the more suitable OC approach for such types of optimization problems. However, in order to accurately capture the current route infrastructure, the author argues that computational efforts and controller sensitivity are limiting OC methods for such applications.

The authors have published much work related to flight trajectory optimization using TOMATO and COALA. To name a few, Rosenow et al. [57] focuses on climate mitigating trajectory optimization, Rosenow and Schultz [56] studies trajectory effects on delay costs, Rosenow et al. [59] investigates the suitability on daily flight operations, Rosenow et al. [60] focuses on in-flight trajectory optimization, and [61] extends the research on arrival management practices.

Optimal Control Approach The OC approach is seen to focus mostly on 4D trajectory optimization. Instead of decomposing the lateral and vertical profile, OC approaches are able to directly optimize the entire trajectory. [64] performs a 4D Multi-Phase Trajectory Optimization (MPTO) focused on Trajectory Based Operations (TBO). The trajectory is modeled using a 3D dynamic point-mass model that assumes symmetric flight and includes the effect of wind. The aircraft is controlled using the bank angle, engine thrust, and lift coefficient, through which the state parameters (true airspeed, heading angle, flight path angle, longitude, latitude, altitude, and aircraft mass) are controlled. Furthermore, multiple constraints exist to manage the optimized trajectories. Besides the performance constraints set on the aircraft states, and control inputs, [64] consider path constraints to restrict the aircraft from flying a certain Standard Instrument Departure (SID) Procedure consisting of lateral, vertical, and speed constraints. In a similar manner Dalmau et al. [16] presents path constraints for standard arrival procedures. For the cruise phase, Soler et al. [64] assumes no airspace restrictions and a Continuous Descent Approach (CDA) from the ToD to the runway. The author also discusses the possibility of adding constraints to ensure discrete altitudes and manage the frequency of step climbs. For the atmospheric conditions, the ISA is assumed. The author states that the presented framework is also valid for a more detailed atmospheric model.

Vilardaga and Prats [68] published similar research with a focus on flight trajectory management and optimization practices in the context of TBO. Different from Soler et al. [64], more extensive use of RTA at fixes along the route is considered. Since future ATM structures from SESAR and NextGen tend to limit deviations from initially filled routes, the work considers a fixed lateral path that is added as a constraint to the control model. The atmospheric properties are obtained from weather forecasts.

Vitali et al. [69] presents a similar 4D MPTO optimization. Instead of including path constraints for TBO operations, this work considers free-route airspace for the entire flight. Its focus is on climate-mitigating flight trajectories, where DOC and climate cost based on GWP are included in the objective function. The climate impact is computed considering CO_2 emissions, non CO_2 emissions and aircraft-induced clouds. Use is made of an atmospheric model to capture spatial atmospheric conditions.

Finally, Sun [65] presents another study on 4D MPTO. Different from all other research, this work is focused on being an open-source flight trajectory optimizer that can be used for air transport and sustainability research. To this purpose, the work presents multiple optimization problems ranging from 4D Single Phase Trajectory Optimization (SPTO) to 4D MPTO. A description is presented of how the OC problem is set up for the different flight phases and how each flight phase combines to model the complete flight. Free-route airspace is considered for the routing problem and ISA conditions are assumed. Operational constraints related to flight planning and execution are therefore not considered. Furthermore, this study proposes multiple objective functions. Trajectories can be generated for minimum fuel, time, DOC, GWP, and GTP. Similar climate impact metrics are considered as in Vitali et al. [69], except for the aircraft-induced clouds.

The research from [32] goes in a different direction. Instead of considering the trajectory as being fully deterministic, the focus is on modeling wind uncertainty and how this can be included in an OC model. The general OC method is extended with probabilistic functions from which trajectory ensembles are constructed. A case study is presented for a flight from New York to Lisbon where trajectories are generated by balancing the cost index and increased predictability. The trajectories are constructed considering free-route airspace, and ISA atmospheric conditions, and model only the cruise phase at fixed altitude.

Similar research is observed in Kamo et al. [41] where probabilistic functions are included in the OC control. This research is focused on CDA operations including RTA that minimizes the expectation of overall operational costs. No path restrictions are mentioned in the work.

Table 3.1: Overview of published research on flight trajectory optimization.

Work	Method	Optimization Problem	Performance Model	Objective Function
		Optimal Control Approach		
Soler et al. [64]	Hermite-Simpson (direct-local-collocation)	4D MPTO in TBO	BADA 3.9	Fuel and time costs using the cost index
Vilardaga and Prats [68]	Direct-local-collocation	3D MPTO in TBO with RTA (fixed route)	Airbus PEP software suite	Fuel and time costs using the cost index
González-Arribas et al. [32]	Direct-global-collocation	3D robust (probabilistic) SPTO (cruise) in free-route airspace	BADA 3	Cost index and increased predictability
Kamo et al. [41]	LGPM (direct-global-collocation)	4D robust SPTO (CDA) in fixed-route airspace	BADA 4	Fuel and time costs using the cost index
Kang and Ryu [42]	Hermite-Simpson (direct-local-collocation)	SPTO (climb) to determine cruise altitude	Generic-type supersonic aircraft model	Fuel and time costs using the cost index
Vitali et al. [69]	Chebyshev Pseudospectral (direct-global-collocation)	4D MPTO in free-route airspace	FSAA (aero), BADA 3 (thrust), and BM2 (emissions)	DOC and Environmental Costs (environmental CI)
Sun [65]	Direct-local-collocation	4D MPTO in free-route airspace	OpenAP	Cost index, global warming and temperature potential
		Non-Optimal Control Approach		
Murrieta-Mendoza and Botez [50]	Dijkstra's algorithm	Lateral (at given altitude and Mach)	PDB describing fuel flow during cruise	Fuel burn, flight time, and cost index
Murrieta-Mendoza and Botez [51]	Search Space Reduction, and B&C optimization algorithm	Vertical (climb, cruise, and descent speeds, and altitudes)	PDB for each flight phase from experimental flights	Fuel burn, flight time, and cost index
Dancila and Botez [17]	Binary Search Algorithm	Vertical cruise segment for RTA (altitude and speed)	FMC PDB	DOC and RTA adherence
Yamashita et al. [70]	GA (AirTraf)	MPTO (lat, lon, and altitude)	BADA and DLR fuel flow method	Fuel, DOC, emissions, contrails
		Hybrid Control Approach		
Förster et al. [28]	Lateral and vertical profile are iteratively optimized; A* lateral (TOMATO); PID controller vertical (COALA)	4D MPTO (lateral with iterated flight characteristics; vertical with restricted path)	lateral with iterated fuel burn, vertical with COALA (Based on BADA 4)	DOC, delay costs, and ecological costs
Rosenow et al. [57]	TOMATO and COALA	4D MPTO (lateral and vertical profile separated)	COALA	DOC, delay costs, and GWP
Rosenow and Schultz [56]	TOMATO and COALA, with extended delay, contrail, and environm. costs	4D MPTO (lateral and vertical profile separated)	COALA	DOC, delay costs, and ecological costs
Rosenow et al. [60]	TOMATO and COALA	Hourly In-flight cruise phase re-optimization	COALA	DOC, delay costs, and ecological costs

B&C: Branch and Cut; BM2: Boeing Fuel Flow Method 2; COALA: Compromised Aircraft performance model with Limited Accuracy; FSAA: NASA Flight Simulator For Advanced Aircraft; GA: Genetic Algorithm; LGPM: Legendre-Gauss Pseudospectral Method; MPTO: Multi-Phase Trajectory Optimization; PDB: Performance Database; PEP: Performance Engineers Program; RTA: Required Time of Arrival; SPTO: Single-Phase Trajectory Optimization; TBO: Trajectory Based Operations; TOMATO: Tool-chain for Multi-criteria Aircraft Trajectory Optimization

3.3.2. Optimal Control Approach

As stated in Simorgh et al. [63], the OC control approach is known as being one of the most reliable dynamic optimization techniques. Working in continuous time, considering the system's dynamical behavior, and adopting numerical methods, are characteristics that make it a perfect fit for the flight TOP. The generic mathematical formulation of such a non-linear optimal control problem is presented below. This theory is obtained from [30] and [63], which is based on the book of [45].

Non-Linear Optimal Control Formulation The dynamics of the system are modeled as Differential Algebraic Equations (DAE) as shown in Equation 3.1. This equation functions as constraint on the *state parameters* ($\boldsymbol{x}(t)$), *control parameters* ($\boldsymbol{u}(t)$), and *system parameters* ($\boldsymbol{p}$), which ensure the correct (non-linear) dynamics of the system.

$$\dot{\boldsymbol{x}}(t) = \mathrm{f}\left(\boldsymbol{x}(t), \boldsymbol{u}(t), \boldsymbol{p}, t\right) \tag{3.1}$$

Besides the dynamical constraints, other non-differential constraints can be set. In order to limit the system between the initial and final condition use is made of path constraints. Two types of path constraints exist: *equality constraints* (h) and *inequality constraints* (g).

$$\begin{aligned} \mathrm{h}\left(\boldsymbol{x}(t), \boldsymbol{u}(t), \boldsymbol{p}, t\right) &= \boldsymbol{0} \\ \mathrm{g}\left(\boldsymbol{x}(t), \boldsymbol{u}(t), \boldsymbol{p}, t\right) &\leq \boldsymbol{0} \end{aligned} \tag{3.2}$$

In order to set the initial and final values of the system, use is made of *boundary constraints* (Ψ):

$$\Psi\left(t_0, t_f, \boldsymbol{x}(t_0), \boldsymbol{x}(t_f)\right) = \boldsymbol{0} \tag{3.3}$$

For the control system to arrive at a trajectory with optimal performance, use is made of a cost/objective function that is to be minimized. In optimal control theory, such a function is called the *performance index* (J). In order to model a specific performance, user-defined metrics should be included in the performance index. The general form is shown below:

$$J(t_0, t_f, \boldsymbol{x}, \boldsymbol{u}) = \mathcal{M}\left(t_0, t_f, \boldsymbol{x}(t_0), \boldsymbol{x}(t_f)\right) + \int_{t_0}^{t_f} \mathcal{L}\left(t, \boldsymbol{p}, \boldsymbol{x}(t), \boldsymbol{u}(t)\right) \mathrm{d}t \tag{3.4}$$

where $\mathcal{M}(\cdot)$ and $\mathcal{L}(\cdot)$ are called the terminal cost (or Mayer term) and running cost (or Lagrange term), respectively.

This results in the final general form of the deterministic OC problem, shown below:

$$\begin{aligned} \min J(t_0, t_f, \boldsymbol{x}, \boldsymbol{u}) = \; & \mathcal{M}\left(t_0, t_f, \boldsymbol{x}(t_0), \boldsymbol{x}(t_f)\right) + \int_{t_0}^{t_f} \mathcal{L}\left(t, \boldsymbol{p}, \boldsymbol{x}(t), \boldsymbol{u}(t)\right) \mathrm{d}t \\ \text{with respect to:} \quad & \dot{\boldsymbol{x}}(t) = \mathrm{f}(t, \boldsymbol{x}(t), \boldsymbol{u}(t)) \\ & \mathrm{h}\left(\boldsymbol{x}(t), \boldsymbol{u}(t), \boldsymbol{p}, t\right) = \boldsymbol{0} \\ & \mathrm{g}\left(\boldsymbol{x}(t), \boldsymbol{u}(t), \boldsymbol{p}, t\right) \leq \boldsymbol{0} \\ & \Psi\left(t_0, t_f, \boldsymbol{x}(t_0), \boldsymbol{x}(t_f)\right) = \boldsymbol{0} \end{aligned} \tag{3.5}$$

Dynamic Aircraft System Equations The aircraft's non-linear dynamics can be expressed in multiple ways. An example is presented from [65].

[65] defines four state parameters and three control parameters:

$$\begin{aligned} \boldsymbol{x}_t &= \begin{bmatrix} x & y & h & m \end{bmatrix} \\ \boldsymbol{u}_t &= \begin{bmatrix} M & vs & \psi \end{bmatrix} \end{aligned} \tag{3.6}$$

with (x, y), h, and m, being the 2D position, altitude, and aircraft mass, and M, vs and ψ, being the Mach number, vertical sate, and aircraft heading, respectively. By directly including the heading ψ as control, the aircraft turn dynamics are ignored. In order to include turn dynamics, the heading angle ψ should be defined as a state, and the bank angle (μ) should be added as control. Similarly, by directly including the vertical speed as control, aircraft vertical dynamics are simplified, which otherwise should be controlled using the

climb angle (ϕ), or lift coefficient (C_L). [63] state that these simplifications have little to no effect on the solution accuracy for TOPs.

Following the simplifications, both the true airspeed (v) and flight path angle (γ) are classified as intermediate variables and can be calculated with the state and control variables using:

$$\begin{aligned} \gamma &= \tan^{-1}\left(\frac{v_s}{v}\right) \\ v &= M\, a_0 \sqrt{\gamma_a\, R\, T_h} \end{aligned} \tag{3.7}$$

with a_0, γ_a, R, and T_h being the speed of sound at sea level, the ratio of specific heat for air, gas constant for air, and air temperature at altitude h, respectively.

The aircraft dynamics are then modeled using the following DAE:

$$\frac{\mathrm{d}}{\mathrm{d}t}\begin{bmatrix} x \\ y \\ h \\ m \end{bmatrix} = \begin{bmatrix} v\,\sin(\psi)\cos(\gamma) + w_x \\ v\,\cos(\psi)\cos(\gamma) + w_y \\ v_s \\ -\mathrm{ff}(m, v, h) \end{bmatrix} \tag{3.8}$$

where w_x, w_y, and ff, are the wind speed components and fuel flow for the given states. It should be noted that the fuel flow follows from the performance model and that by using this formulation of aircraft system dynamics, aerodynamic aircraft characteristics are included in the path constraints.

Path and Boundary Constraints In order to arrive at feasible solutions path and boundary constraints are required to be set up. These constraints are specific to every formulation of aircraft system dynamics. For the control formulation of Sun [65], three types of path constraints are defined related to: aircraft dynamics, aircraft performance, and smooth control variable changes.

The path constraints related to the aircraft dynamics are shown in Equation 3.9 and Equation 3.10. These enforce the dynamical system equations from Equation 3.8 and place bounds on the state and control parameter values to ensure the aircraft to stay within its flight envelope, respectively. It should be noted that the parameter k represents discretized points along the path and that 10 km is added to the lateral boundaries for the case when the origin and destination have the same latitude or longitude.

Path constraints for aircraft dynamics

$$\dot{\boldsymbol{x}}(t) = \mathrm{f}(t, \boldsymbol{x}(t), \boldsymbol{u}(t)) \tag{3.9}$$

$$\begin{aligned} \min(x_0, x_f) - 10 <\ & x_k < \max(x_0, x_f) + 10 \quad \text{(km)} \\ \min(y_0, y_f) - 10 <\ & y_k < \max(y_0, y_f) + 10 \quad \text{(km)} \\ h_{\min} <\ & h_k < h_{\text{ceiling}} \\ m_{\text{oew}} <\ & m_k < m_{\text{to}} \\ 0.1 <\ & M_k < M_{\max} \\ -2500 <\ & v_{s_k} < 2500 \quad \text{(ft/min)} \\ -\pi <\ & \psi_k < 3\pi \end{aligned} \tag{3.10}$$

Path constraints for aircraft performance

$$\begin{aligned} T_{\max,k} - D_k &> 0 \\ D_k &= \left(C_{D_0} + C_{D_i}\frac{2\, m_k\, g}{\rho_k\, v_k^2\, S}\right)\frac{1}{2}\rho_k\, v_k^2\, S \end{aligned} \tag{3.11}$$

$$\begin{aligned} L_{\max,k} - m_k\, g &> 0 \\ L_{\max,k} &= \frac{1}{2}\,\rho_k\, v_k^2\, S\, C_{L,\max} \end{aligned} \tag{3.12}$$

$$\frac{T_{\max} - D_k}{m_k} - \frac{g}{v_k}\frac{\mathrm{d}h_k}{\mathrm{d}t} - \frac{\mathrm{d}v_k}{\mathrm{d}t} > 0 \tag{3.13}$$

The path constraints related to aircraft performance are shown in Equation 3.11, Equation 3.12, and Equation 3.13. The first set of constraints ensures that the available thrust is always larger than the aircraft drag. The second set ensures that the available lift is always larger than the aircraft weight, and the third constraint is related to total energy changes to ensure that the available power is always more than the energy required for the change in kinetic and potential energy. It should be noted that all model coefficients related to aircraft thrust, drag, and aircraft properties are provided by the underlying performance model. Furthermore, [64, 68] opt for a more extensive dynamic system set-up, where the airspeed and flight path are included as state parameters, and subsequently modeled by DAE. In this case, the performance constraints are directly enforced by the aircraft dynamics and no separate aircraft performance path constraints are required.

The path constraints related to smooth control variable changes are used to limit sudden large variations in the control parameters. These are shown in Equation 3.14, where it should be noted that the last constraint

is only enforced on the discretized points k that are in the cruise phase. $\mathcal{K}_{\text{cruise}}$ is obtained from the kinematic model inside the performance model.

Finally, boundary constraints are enforced on the initial and final state parameter values, as shown in Equation 3.15.

Path constraints for smooth control variable changes

$$\begin{aligned} -0.2 < M_{k+1} - M_k < 0.2 \\ -2500 < vs_{k+1} - vs_k < 2500 \quad \text{(ft/min)} \\ -15 < \psi_{k+1} - \psi_k < 15 \quad \text{(deg)} \\ -500 < vs_{k+1} - vs_k < 500 \quad \text{(ft/min)}; \quad \forall k \in \mathcal{K}_{\text{cruise}} \end{aligned} \tag{3.14}$$

Boundary constraints

$$\begin{aligned} (x_0, y_0, h_0, m_0) &= (x_{\text{orig}}, y_{\text{orig}}, h_{\min}, m_{\text{to}}) \\ (x_f, y_f, h_0) &= (x_{\text{dest}}, y_{\text{dest}}, h_{\min}) \\ m_{\text{oew}} < \; & m_f < m_{\text{mlw}} \end{aligned} \tag{3.15}$$

As mentioned before, [65] does not consider operational constraints related to flight planning and execution. In order to add such limitations to the trajectory optimization, additional path constraints have to be enforced. [68] presents several operational constraints considered in their work. First of all, they state that the operating speeds used to control the trajectory are always expressed in Calibrated Airspeed (v_{cas}, CAS). As this parameter is not included in the system equations, it is added as an intermediate variable through:

$$v_{\text{cas}} = \sqrt{\frac{2\,\gamma_a}{\gamma_a - 1}\frac{p_0}{\rho_0}\left[\left(\frac{p}{p_0}\left(\left(\frac{\gamma_a - 1}{2\,\gamma_a}\frac{v^2}{R\,T} + 1\right)^{\frac{\gamma_a}{\gamma_a - 1}} - 1\right) + 1\right)^{\frac{\gamma_a - 1}{\gamma_a}} - 1\right]} \tag{3.16}$$

where p and T are the local air pressure and air temperature, respectively, and p_0, and ρ_0 are the air pressure and air density at sea level, respectively. Subsequently, additional path constraints can be included to enforce, e.g. a constant CAS during the climb, or CAS limits below certain altitudes.

Furthermore, [68] consider a fixed lateral route as a path constraint. They use it to model a SID procedure, however, a similar approach can be used to fix the route to pre-defined waypoints. In order to implement this, an additional parameter is included in the control problem: along path distance (s). This parameter is not included as a state parameter, but its dynamics are modeled as:

$$\frac{\mathrm{d}s}{\mathrm{d}t} = \sqrt{\left(\frac{\mathrm{d}x}{\mathrm{d}t}\right)^2 + \left(\frac{\mathrm{d}y}{\mathrm{d}t}\right)^2} \tag{3.17}$$

Subsequently, equality path constraints can be set on the aircraft position in the form of:

$$\begin{aligned} x(t) &= \Gamma_x(s(t)) \\ y(t) &= \Gamma_y(s(t)) \end{aligned} \tag{3.18}$$

where Γ_x and Γ_y are polynomials fitted to model the pre-defined lateral path that follows the way-points. In order to fit the optimization problem, the polynomials have to be a continuous and twice-differentiable function. Vilardaga and Prats [68] argues that cubic B-splines perform well under such optimization problems.

3.3.3. Numerical Approximations

The optimal control problem formulation in Equation 3.5 is generally solved using a numerical approach. The most common numerical approaches used for this are classified as either direct or indirect methods. Somewhat similar to finding the maximum of a simple function by setting its derivative to zero and checking that the curvature is positive, indirect methods are after numerically solving such an indirect optimization problem on the exact system equations. The final control and state trajectories are subsequently obtained by discretizing and considering the established optimality conditions [43]. Differently, direct methods are after directly optimizing the control and state trajectories. This is done by first converting (transcribing) the infinite-dimensional problem to a finite-dimensional approximation of the system equations (i.e. Non-Linear Program (NLP)). The optimization of the problem is subsequently performed on the approximated non-linear system to arrive at the final control and state trajectories [63].

The benefit of indirect methods is that they are generally more accurate than direct methods. However, they struggle with finding convergence and require analytical conditions to be constructed, which are quite

complex [43]. This results in the direct approach being more robust and generally provides better performance in the TOP.

Considering the direct methods, trajectories are directly modeled using some type of discretization. In order to model the trajectory, two different approaches can be used: *time-marching* and *simultaneous* [54]. An overview of the numerical approximation methods for optimal control is shown in Figure 3.2. Both methods are further discussed in this sub-section.

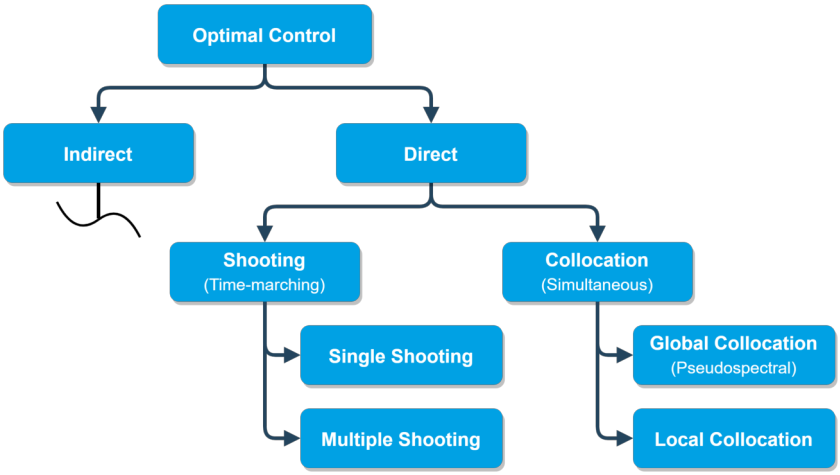

Figure 3.2: Overview of the different methods used to solve the optimal control problem numerically.

Direct Shooting (Time-Marching) Time-marching methods are classified as shooting methods. It is characterized by only parameterizing the control parameters, and obtaining the state trajectories through time-marching [44]. The evolution of the state parameters is obtained sequentially by:

$$\boldsymbol{x}_{i+1} = \boldsymbol{x}_i + \int_{t_i}^{t_{i+1}} \dot{\boldsymbol{x}}(t)\mathrm{d}t = \boldsymbol{x}_i + \int_{t_i}^{t_{i+1}} f(\boldsymbol{x}(t), \boldsymbol{u}(t), t)\mathrm{d}t \tag{3.19}$$

where $f(\cdot)$ are the system dynamics. The continuous time-span $[t_0,\ t_f]$ can be discretized into $\mathcal{K}$ time intervals resulting in time steps t_k, with $k = 0, 1, ..., f$. By considering multi-step numerical methods like Euler (single-step), Adams-Bashforth (two-step), or general Runge-Kutta (RK) (K-step), Equation 3.19 can be expressed as an implicit or explicit form using the discretized states x_k. When the entire time span is directly captured by this discretization method, the problem is called *single shooting*.

In order to find the optimal control and state trajectories with single shooting, different control inputs are generated over the piecewise segments $[t_k,\ t_{k+1}]$. These control inputs are generally modeled by a continuous function in the form of a constant, piecewise linear, or piecewise polynomial [44]. The control functions are changed iteratively, until the optimal trajectories are obtained that maximize some performance index, comply with the constraints, and have the correct final states.

An example of single shooting is shown in Figure 3.3, where the continuous time span is discretized into four equidistant time segments and the control input is parameterized by a piecewise linear function.

The time interval can also be divided into smaller sub-intervals. Each sub-interval can then be considered a single shooting problem and by imposing final state constraints at the end of each sub-interval, the optimization problem can be solved. This approach is called *multiple shooting* and is shown in Figure 3.4.

Single shooting performs well on simple problems where the control can be parameterized by a simple linear function and a small number of optimization parameters are present. Increasing the problem size and complexity results in numerical difficulties, of which some are overcome by multiple shooting [54]. Path constraints are also difficult to implement with shooting methods, and convergence issues result in the shooting methods being less robust than collocation methods [43]. Collocation methods are therefore generally chosen for the TOP [42, 65].

Direct Collocation (Simultaneous) Different from shooting methods, collocation methods directly parameterize both control and state parameters. Instead of performing time-marching operations to obtain the

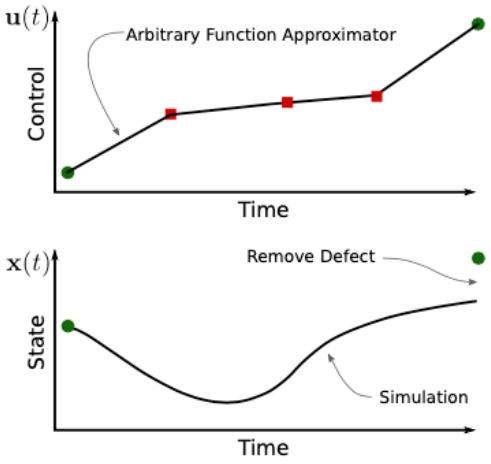

Figure 3.3: Control and state trajectory discretization for single shooting. [44]

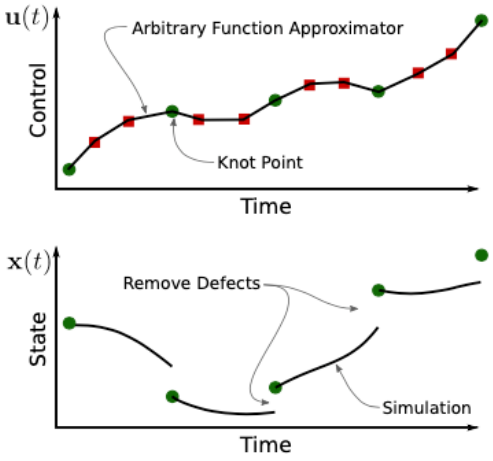

Figure 3.4: Control and state trajectory discretization for Multiple shooting. [44]

control trajectories sequentially, control and state trajectories are simultaneously obtained through solving a system of equations (NLP). An NLP is obtained by describing the infinite-dimensional problem from Equation 3.5 by a set of real values at discretized nodes, and by transforming integral and differential equations into simple algebraic equations.

The control and state trajectories can be approximated over the entire time span by a single Lagrange interpolating polynomial ($\mathrm{f}_p(t)$) of degree P, where use is made of $P+1$ discretization nodes [35]:

$$\begin{aligned} &\boldsymbol{x}(t) \approx \sum_{p=0}^{P} \mathcal{L}_p(t)\, \boldsymbol{x_p} \quad ; \quad \boldsymbol{u}(t) \approx \sum_{p=0}^{P} \mathcal{L}_p(t)\, \boldsymbol{u_p} \\ &\text{with } \mathcal{L}_p(t) = \prod_{j=0, j\neq p}^{P} \frac{t - t_p}{t_j - t_p} \qquad (p = 0, ..., P) \end{aligned} \tag{3.20}$$

In order to describe the integral present in the objective function as an approximated algebraic function, use is made of the (general) quadrature [35]:

$$\int_a^b f(t)\mathrm{d}t \approx \sum_{k=1}^{\mathcal{K}} w_k\, f(t_k) \tag{3.21}$$

where $t_1, ..., t_{\mathcal{K}}$ are the quadrature points, and w_k are the quadrature weights following a specific quadrature formulation.

To describe the differential equation $\dot{\boldsymbol{x}}(t) = \mathrm{f}(t, \boldsymbol{x}(t), \boldsymbol{u}(t))$ as an algebraic function, two numerical approaches can be used: differentiation of the state trajectory by finite-difference (left-hand side), or integration of the system dynamics by quadrature (right-hand side). The first approach is generally considered for direct collocation methods. The differentiation of the state trajectory is performed on the Lagrange polynomial from Equation 3.20, resulting in [35]:

$$\dot{\boldsymbol{x}}(t) \approx \sum_{p=0}^{P} \dot{\mathcal{L}}_p(t)\, \boldsymbol{x_p} = \sum_{p=0}^{P} D_p(t)\, \boldsymbol{x_p} \tag{3.22}$$

with $D_p(t)$ being the differentiation matrix. This equation is used to enforce the system dynamics at the discretized nodes, which are called the collocation nodes.

From these expressions, the transcribed NLP is formulated as:

$$\begin{aligned}
\min_{x_k,u_k} J = \; & \Phi\left(t_0, t_f, \boldsymbol{x_0}, \boldsymbol{x_f}\right) + \sum_{k=1}^{\mathcal{K}} w_k \, \mathrm{g}\left(t_k, \boldsymbol{p}, \boldsymbol{x_k}, \boldsymbol{u_k}\right) \\
\text{with respect to:} \quad & \sum_{p=0}^{P} D_{pk} \, \boldsymbol{x_p} - \mathrm{f}\left(t_p, \boldsymbol{x_p}, \boldsymbol{u_p}\right) = 0 \qquad (k = 0, ..., \mathcal{K}) \\
& \mathrm{h}_k\left(\boldsymbol{x_k}, \boldsymbol{u_k}, \boldsymbol{p}, t_k\right) = \boldsymbol{0} \qquad (k = 0, ..., \mathcal{K}) \\
& \mathrm{g}_k\left(\boldsymbol{x_k}, \boldsymbol{u_k}, \boldsymbol{p}, t_k\right) \leq \boldsymbol{0} \qquad (k = 0, ..., \mathcal{K}) \\
& \Psi\left(t_0, t_f, \boldsymbol{x_0}, \boldsymbol{x_f}\right) = \boldsymbol{0} \qquad (k = 0, ..., \mathcal{K})
\end{aligned} \tag{3.23}$$

where k are the discretization nodes, $\boldsymbol{x}_k \equiv \boldsymbol{x}(t_k), \boldsymbol{u}_k \equiv \boldsymbol{u}(t_k)$, and $\boldsymbol{x}(t)$ and $\boldsymbol{u}(t)$ are approximated by a P-order Lagrange polynomial. This NLP formulation can be solved by a numerical solver, from which the discretized states and controls follow. The trajectories within the nodes are subsequently obtained using the Lagrange interpolating polynomials (Equation 3.20). A further illustration of the characteristics and difficulties with the discretization nodes k is presented next.

The problem parameterization is done by representing the continuous states $\boldsymbol{x}(t)$ and controls $\boldsymbol{u}(t)$ at $\mathcal{K}$ specific points in time, referred to as a node, mesh, or grid-points (k):

$$\begin{aligned}
t &\rightarrow t_0, ..., t_k, ..., t_f \\
\boldsymbol{x}(t) &\rightarrow \boldsymbol{x_0}, ..., \boldsymbol{x_k}, ..., \boldsymbol{x_f} \\
\boldsymbol{u}(t) &\rightarrow \boldsymbol{u_0}, ..., \boldsymbol{u_k}, ..., \boldsymbol{u_f}
\end{aligned} \tag{3.24}$$

It should be noted that the numerical methods used to transcribe the problem make use of a similar discretization scheme, which is not necessarily equal to the grid points. Generally, the numerical methods make use of orthogonal roots obtained from a P-order Legendre polynomial. By using the orthogonal roots as discretization points, the accuracy and numerical efficiency of these numerical methods are increased [44]. These roots are subsequently used for the interpolating nodes, quadrature nodes, and collocation points.

There are three different types of Legendre polynomials that can be used to obtain the root locations: *Legendre-Gauss* (LG), *Legendre-Gauss-Radau* (LGR), and *Legendre-Gauss-Lobatto* (LGL). These sets of Legendre points are shown in Figure 3.5. The main difference between the three methods is the location of the start and end nodes. The Lobatto methods are defined such that the two endpoints are included as orthogonal roots. Radau methods include only the starting or end point as root, and Gauss methods do not include any boundary points.

Each method has its own characteristics. By forcing the roots to be located on the boundaries, a more expensive numerical approach is required. In general, the LG and LGR show the best convergence behavior for TOP problems, where the LGR is preferred for problems with fixed initial or final time [33]. Lobatto representations are most practical to relate the numerical discretization to the problem parameterization, however, high-order Lobatto collocation schemes should be avoided in the TOP [44].

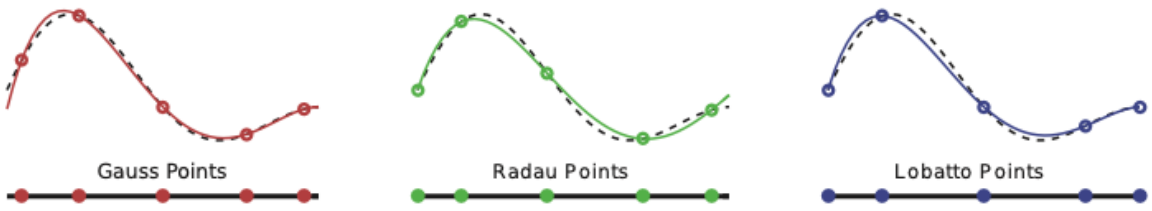

Figure 3.5: Orthogonal roots for different numerical discretization methods. [44]

Similar to single and multiple shooting, the collocation method can be divided into *global collocation* and *local collocation*. In global collocation (often referred to as *pseudospectral collocation*), the entire trajectory is modeled using a single polynomial. In local collocation, the trajectory is first divided into multiple segments, after which each segment is evaluated by a single polynomial, similarly to global collocation. With local collocation, care is taken to ensure continuity in the solution between segments.

Considering global collocation, the problem parameterization is generally adopted from the orthogonal roots. That is, the discretization nodes in Equation 3.24 are set equal to the chosen set of Legendre points. Dependent on the chosen discretization method, additional nodes may be defined at the endpoints to ensure

boundary constraints. This has to be considered separately in the NLP. The number of nodes k follows from the order $P+1$ of the Lagrange polynomial. In order to create a finer mesh, a higher-order polynomial has to be chosen.

Considering local collocation, the discretization process is performed differently. Generally, the problem is first parameterized into $\mathcal{K}$ segments, similarly as in Equation 3.24, after which each segment is again discretized by orthogonal roots. This results in a problem discretization that is more easily managed. In order to create a finer mesh, either more segments can be added, and/or a higher polynomial can be chosen. Both collocation methods are shown in Figure 3.6, and Figure 3.7, respectively.

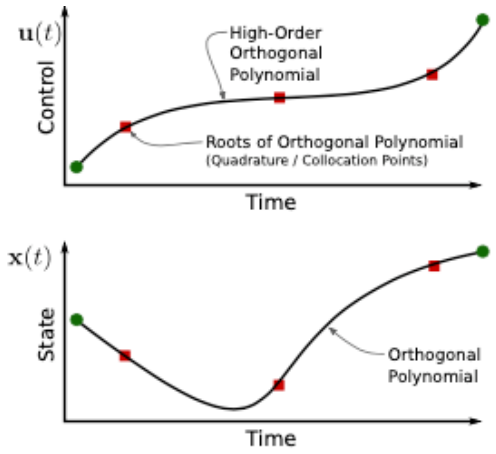

Figure 3.6: Control and state trajectory discretization for global collocation. [44]

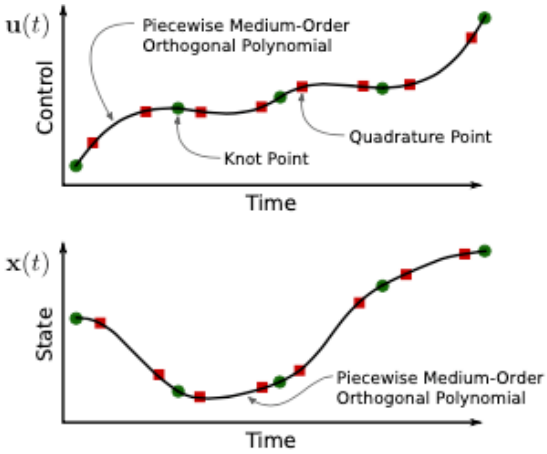

Figure 3.7: Control and state trajectory discretization for local collocation. [44]

There are several common collocation methods observed in the literature. Looking at Table 3.1, Hermite-Simpson collocation, Legendre-Gauss Pseudospectral Method (LGPM) collocation, and Chebyshev Pseudospectral collocation is observed. Hermite-Simpson collocation is a simple form of local Lobatto collocation. It is characterized by a 2^{nd} order polynomial for the state trajectory. From the discussion above, it follows that this method makes use of 3 orthogonal roots (quadrature points/collocation points/interpolation points) on each segment, where 2 roots are located at both ends, overlapping the discretization nodes k.

Chebyshev Pseudospectral collocation is a different approach than discussed so far. Instead of Lagrange polynomials to be used for the state and control trajectory approximation, a Chebyshev polynomial is used. Such a function makes use of trigonometric functions, which will not be discussed further.

3.3.4. Objective Functions

Considering the TOP, different types of objective functions are observed in the literature. The objective functions are mainly focused on minimizing DOC by making a trade-off between fuel cost and time cost, and/or minimizing climate impact. This sub-section presents the considerations for each type of objective function.

Optimizing for Cost Index The setup of the objective function is rather straightforward. In order to obtain the trajectory that results in the fastest travel time, the objective function is simply set equal to 1, as shown in Equation 3.25. In order to obtain the trajectory that results in the lowest total trip fuel, the modeled fuel flow is included in the objective function, as shown in Equation 3.26.

$$J = \int_{t_0}^{t_f} 1 \, \mathrm{d}t \tag{3.25}$$

$$J = \int_{t_0}^{t_f} \mathrm{ff}(\cdot) \, \mathrm{d}t \tag{3.26}$$

By combining both time and fuel, the objective function can be written as a function of the cost index [65]:

$$J = \int_{t_0}^{t_f} \underbrace{\frac{\mathrm{CI}}{\mathrm{CI}_{\max}} C_{\text{time}}}_{\text{Time Cost}} + \underbrace{\left(1 - \frac{\mathrm{CI}}{\mathrm{CI}_{\max}}\right) \mathrm{ff}(\cdot) \, C_{\text{fuel}}}_{\text{Fuel Cost}} \, \mathrm{d}t \tag{3.27}$$

Here, the time cost is modeled by using the average time cost (C_{time}) expressed per unit flight time, and the fuel cost is modeled by using the fuel cost (C_{fuel}) expressed per kg fuel. When setting CI=0, Equation 3.27 reduces to Equation 3.26, and when setting CI=$\mathrm{CI}_{\max}$, it reduces to Equation 3.25.

Optimizing for Climate Impact In order to change the objective to minimize climate impact, the objective function can be adapted to include emission properties. Climate impact is generally captured by the Global Warming Potential (GWP) and/or Global Temperature Potential (GTP). GWP is a measure that expresses the amount of energy that is absorbed by different gases compared to the same amount of CO_2 emissions. By considering particle decay, different time horizons can be established. GTP is a measure that expresses the increase in temperature at different time horizons resulting from the emission of certain species.

An example of how this can be included in the objective function is shown in Equation 3.28 [65]. Here, the emissions of CO_2, H_2O, NO_X, SO_X, and soot are included in the objective function, which is translated to either GWP or GTP through emission coefficients obtained from the literature.

$$J = \int_{t_0}^{t_f} C_{CO_2}\, f_{CO_2}(t) + C_{H_2O}\, f_{H_2O}(t) + C_{NO_X}\, f_{NO_X}(t) + C_{SO_X}\, f_{SO_X}(t) + C_{soot}\, f_{soot}(t)\, \mathrm{d}t \tag{3.28}$$

The emission coefficients for GWP are shown in Table 3.2. Similar coefficients can be obtained for the GTP.

Table 3.2: Emission coefficients for GWP climate impact. [65]

Emission	**GWP_{20}**	**GWP_{50}**	**GWP_{100}**
C_{CO_2}	1	1	1
C_{H_2O}	0.22	0.1	0.06
C_{NO_X}	619	205	114
C_{SO_X}	-832	-392	-226
C_{soot}	4288	2018	1166

Different studies consider the effect of aviation-induced clouds (contrails) on the climate impact [69, 70]. In order to include this aspect in the TOP, the dynamics of contrail formation, dispersion, and dissipation have to be modeled. An example of such an aircraft-induced clouds model can be found in Vitali et al. [69]. While this aspect is found to certainly relate to aircraft-induced climate impact [46], it is generally not considered in airline operations. Therefore, aircraft-induced clouds will not be considered in this thesis.

3.3.5. Performance Modeling

Aircraft performance models are used to describe the motion of the aircraft. As observed from the OC problem formulation, the thrust, drag, and fuel flow of the aircraft are required to model the aircraft dynamics. Performance models make use of polynomial expressions to approximate these properties. Different functional relationships are used for these polynomials, which result in different levels of accuracy. Generally, each aircraft type is modeled by a specific polynomial that is described using aircraft type-specific coefficients determined from reference data [52].

This sub-section discusses the physics-based functional relationships for the thrust, fuel flow, and drag curve, and relates this to the approximations used in common performance models. The performance models used as references are BADA Family 3, BADA Family 4 [29, 52], and OpenAP [67]. As can be observed from Table 3.1, BADA is widely used in flight trajectory optimization research. The difference between the two families is that BADA 4 uses more sophisticated functional relationships and provides reliable performance over the entire flight envelope [52]. OpenAP is a similar performance model that has the major advantage of being open source.

Thrust and Fuel Flow The thrust and fuel flow of the aircraft are two complex parameters that mainly depend on the engine rotation speed expressed using either the fan/low-pressure spool rotation speed (N_1), core/high-pressure spool rotation speed (N_2), or the throttle/power setting (δ_T); flight parameters such as airspeed (v), air pressure (p), air temperature (T_h), and specific air constant (γ_a); and physical engine characteristics such as the bypass ratio (λ), Turbine Inlet Temperature (TIT), Engine Pressure Ratio (EPR), and/or

Exhaust Gas Temperature (EGT). A typical representation of thrust and fuel flow can be formulated as [5]:

$$\begin{aligned} T &= \mathrm{f}(N_1, v, p, T_h, \gamma_a, \lambda) \\ ff &= \mathrm{f}(N_1, v, p, T_h, \gamma_a, \lambda) \end{aligned} \tag{3.29}$$

This functional relationship is often reduced by normalizing the thrust and fuel flow to ISA sea-level conditions. This results in the *corrected thrust* (T_c) and *corrected fuel flow* (ff_c), which is defined as follows [5]:

$$T_c = \frac{T}{\delta} = \mathrm{f}(\frac{N_1}{\sqrt{\theta}}, M) \tag{3.30}$$

$$ff_c = \frac{ff}{\delta\sqrt{\theta}} = \mathrm{f}(\frac{N_1}{\sqrt{\theta}}, M) \tag{3.31}$$

where $\delta = \frac{p}{p_0}$ and $\theta = \frac{T_h}{T_0}$ represent the ambient pressure and temperature ratio to ISA sea-level conditions, respectively. It should be observed that the size of the functional relationship is reduced, which simplifies the determination of both functions.

Fuel flow can also be described as a function of thrust and TSFC (C_T):

$$ff = \frac{T}{C_T} \tag{3.32}$$

The TSFC dictates how much fuel is required to produce a certain amount of thrust. Similar to thrust and fuel flow, the TSFC differs with airspeed, atmospheric properties, and some measures of throttle setting (e.g. N_1). This latter component is generally captured by the thrust, which results in the following functional relationship [7]:

$$C_T = \mathrm{f}(v, p, T_h, \gamma_a, T) \tag{3.33}$$

Similar to the corrected thrust and fuel flow, this relation can be reduced to arrive at the *corrected TSFC* ($C_{T,c}$), being a function of the Mach number and the corrected thrust:

$$C_{T,c} = \mathrm{f}(M, T_c) \tag{3.34}$$

Once, the corrected thrust is determined (Equation 3.30), using Equation 3.32 and Equation 3.34, the corrected fuel flow can also be expressed as:

$$ff_c = \mathrm{f}(M, T_c) \cdot T_c \qquad \rightarrow \qquad ff_c = \mathrm{f}(M, T_c) \tag{3.35}$$

The functional relations are typically determined by the aircraft and engine manufacturers. During the development phase engine thrust measurement are obtained in a test cell. Isolated test cell experiments allow the thrust to be measured, which cannot be done when the engine is mounted on the wing [10]. An example of a test cell engine performance curve is shown in Figure 3.8. Here, the combined relation of thrust and TSFC (Equation 3.29) is shown for different throttle settings (N_1 or TIT) and free-stream engine speed. This graph considers a constant altitude and local atmospheric properties.

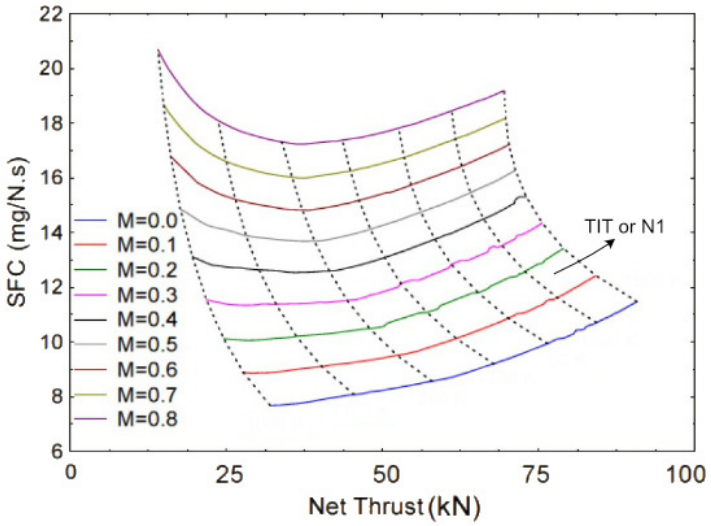

Figure 3.8: Engine thrust and TSFC performance characteristics obtained from test cell experiments. Modified from Bensel [7]

The engine performance characteristics are best captured by the engine models developed by the manufacturers. However, this data is considered confidential and not available for research. Simplified approximations have to be constructed that contain similar performance characteristics. BADA makes use of flight data to construct these functions. Their method is based on the total energy model:

$$(T - D)v = m\ g\ vs + m\ v\ a \tag{3.36}$$

Besides the values for thrust and drag, all other parameters are directly measured by the aircraft. By minimizing the Sum of Square Errors (SSE) using the least-square optimization technique, the type-specific coefficients ($a_1, a_2, ...$ and $b_1, b_2, ...$) are obtained that describe the thrust and drag:

$$SSE_{vs} = \sum_{i=1}^{n} \left[vs_i - (T_i - D_i)\ \frac{v_i}{m_i\ g}\ ESF_i \right] \tag{3.37}$$

$$\begin{aligned} \text{with:} \qquad ESF_i &= \left(1 + \frac{v_i}{g}\frac{\mathrm{d}v}{\mathrm{d}h}\right)^{-1} \\ T &= \mathrm{T}(a_1, a_2, ...) \\ D &= \mathrm{D}(b_1, b_2, ...) \end{aligned} \tag{3.38}$$

A similar method is used to model the fuel flow.

OpenAP is developed differently. Instead of using direct flight recordings, use is made of publicly available data sources, simplified physic-based models, and aircraft surveillance data. A further description of the type of functional relationships used to construct the performance models is provided next. The methods adopted for BADA 3 and BADA 4 are obtained from Nuic et al. [52], and the method for OpenAP from Sun et al. [67].

BADA 3 BADA 3 makes use of a thrust model that computes the maximum climb, maximum cruise, and idle descent thrust. Instead of computing the net thrust as a function of the power/throttle setting, it only calculates the thrust limits. Thrust is considered independent of airspeed and only modeled as a function of altitude:

$$T_{max,idle} = \mathrm{f}(h) \tag{3.39}$$

At different altitudes, ISA conditions are assumed for the atmospheric properties, and maximum thrust deviations are modeled for temperature difference w.r.t. ISA (ΔT_{ISA}).

Fuel flow is modeled as a function of thrust and airspeed, where the net thrust is obtained from evaluating the drag polar:

$$ff = \mathrm{f}(T, v) \tag{3.40}$$

BADA 4 BADA 4 uses a more sophisticated thrust model. Instead of only computing the maximum or idle thrust, the corrected thrust is modeled through a new dimensionless thrust coefficient (C_{Th}) and the maximum take-off weight (W_{MTOW}):

$$T_c = \frac{T}{\delta} = W_{MTOW}\ C_{Th} \tag{3.41}$$

The thrust coefficient is modeled as a function of Mach number and throttle parameter (δ_T):

$$C_{Th} = \mathrm{f}(M, \delta_T) \tag{3.42}$$

To account for non-ISA conditions, corrections are provided for the throttle parameter.

Fuel consumption is modified in a similar manner, where a new dimensionless fuel coefficient (C_F) is defined:

$$ff = LHV^{-1}\ W_{MTOW}\ a_0\ \delta\ \theta^{1/2}\ C_F \tag{3.43}$$

where LHV is the lower heating value, a_0 the speed of sound at Mean sea level (MSL), and δ and θ the pressure and temperature ratio w.r.t. ISA sea-level, respectively. The fuel coefficient is then modeled as a function of the Mach number and thrust coefficient:

$$C_F = \mathrm{f}(M, C_{Th}) \tag{3.44}$$

OpenAP OpenAP makes use of a simplified empirical thrust model proposed by Bartel and Young [6]. This model computes maximum thrust ratios relative to available thrust ratings at cruise level and/or MSL. Different empirical expressions are established for the take-off, climb, cruise, and descent thrust. The maximum thrust is then modeled as a function of altitude (h), airspeed (v), and vertical speed (vs):

$$T_{max} = \mathrm{f}(h, v, vs) \tag{3.45}$$

In order to obtain thrust values as a function of throttle setting (δ_T), the maximum thrust is multiplied by a scalar value:

$$T = \delta_T\ \mathrm{f}(h, v, vs) \tag{3.46}$$

The fuel flow model in OpenAP is based on public data from the ICAO aircraft engine emissions databank [36]. The fuel flow is modeled as a function of the net thrust ratio relative to maximum thrust at sea level ($T_{max,0}$). The net thrust is obtained from the drag polar and $T_{max,0}$ is obtained from the performance model. Subsequently, altitude effects are captured by a simplified linear correction factor $C_{ff,ch}$:

$$ff = \mathrm{f}(\frac{T}{T_{max,0}}) + C_{ff,ch}\ T\ h \qquad \rightarrow \qquad ff = \mathrm{f}(\frac{T}{T_{max,0}}, h) \tag{3.47}$$

Drag Polar Aircraft drag can be divided into two main components: *zero-lift drag* and *lift-induced drag*. Zero-lift drag (also known as parasitic drag) is the air resistance as a consequence of a body moving through the air. Lift-induced drag is the drag that results from a lift force being generated on the aircraft. A third component is related to compressibility effects: *wave drag*. Wave drag affects both zero-lift and lift-induced drag and is only observed in the transonic and supersonic operating regions.

The aircraft lift and drag that includes all these characteristics are computed as:

$$\begin{aligned} L &= \frac{1}{2}\ \rho\ v^2\ S\ C_L \\ D &= \frac{1}{2}\ \rho\ v^2\ S\ C_D \end{aligned} \tag{3.48}$$

where ρ, v, and S are the air density, airspeed, and lifting surface area, and C_L, and C_D are the non-dimensional lift and drag coefficient, respectively. The lift and drag coefficients are used to capture the aerodynamic characteristics. In general, these coefficients are modeled as a function of Angle of Attack (AoA) (α), Mach number, and flap deflection (δ_f) [66]:

$$\begin{aligned} C_L &= \mathrm{f}(\alpha, M, \delta_f) \\ C_D &= \mathrm{f}(\alpha, M, \delta_f) \end{aligned} \tag{3.49}$$

In point-mass models, the AoA is not directly modeled. Instead, the lift and drag coefficients are related to one another through the drag polar, which implicitly assumes AoA values. A typical drag polar is shown in Figure 3.9. This plot contains $C_L - C_D$ measurements obtained from Computational Fluid Dynamics (CFD) simulations for different values of AoA (circles). A common assumption made is to approximate the drag polar by a quadratic function, expressed by the zero-lift drag coefficient (C_{D_0}), lift-induced drag coefficient (C_{D_i}), and lift coefficient (C_L):

$$C_D = C_{D_0} + C_{D_i}\, C_L^2 \tag{3.50}$$

This approximated curve is also shown in Figure 3.9, where the parameter k is used for C_{D_i}. Often, the lift-induced drag coefficient is expressed by:

$$C_{D_i} = \frac{1}{\pi\, A\, e} \tag{3.51}$$

where A and e are the wing aspect ratio, and Oswald factor, respectively.

When considering compressibility effects for higher Mach numbers, the drag polar is seen to shift. This is caused by the wave drag, and should not be ignored for commercial aircraft. The shift in drag polar is shown in Figure 3.10.

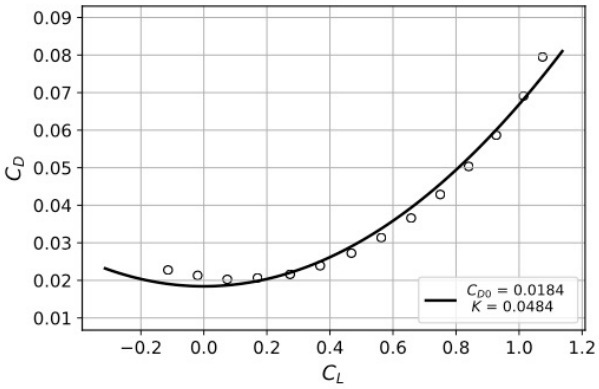

Figure 3.9: Drag polar comparison of CFD simulations and the quadratic approximation. [66]

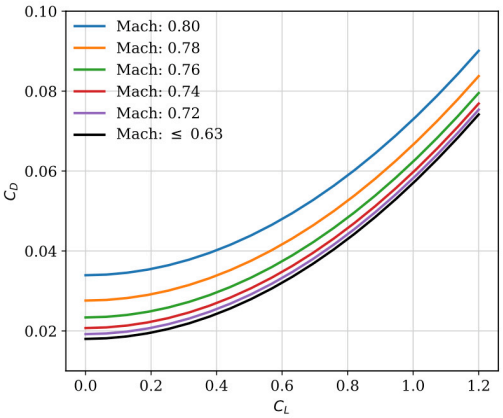

Figure 3.10: Influence of compressibility effects (wave drag) on the drag polar. [67]

The drag polar is also modified by the extension of High Lift Devices (HLD), landing gear, and/or speed brakes. The drag coefficient is affected by such changes in geometry which causes the drag polar to shift.

From the above discussion it can be concluded that the clean drag coefficient can be modeled as a function of the Mach number and lift coefficient:

$$C_D = \mathrm{f}(M, C_L) \tag{3.52}$$

When the effects of HLD, landing gear, and/or speed break deflections are required to be modeled, additional relations will have to be developed.

BADA 3, BADA 4, and OpenAP make use of different methods to model the drag coefficient. Similar to the thrust, polynomial expressions are constructed that approximate the functional relationships. Based on reference data, type-specific coefficients are obtained for the polynomials.

BADA 3 BADA 3 makes use of a drag model that relates the drag coefficient to the lift coefficient (C_L), high lift devices position (δ_{HL}), and landing gear position (δ_{LG}):

$$\begin{aligned} C_D &= \mathrm{f}(C_L, \delta_{HL}, \delta_{LG}) \\ D &= \frac{1}{2}\, \rho\, v^2\, S\, C_D \end{aligned} \tag{3.53}$$

It should be noted that no compressibility effects are included in BADA 3 [52]. Different aerodynamic configurations are assumed for take-off, initial climb, climb, cruise, descent, approach, and landing, which results in different drag polars.

BADA 4 BADA 4 uses a drag model that relates the drag coefficient to the lift coefficient (C_L), Mach number, high lift devices position (δ_{HL}), landing gear position (δ_{LG}), and speed brakes position (δ_{SB}):

$$\begin{aligned} C_D &= \mathrm{f}(C_L, M, \delta_{HL}, \delta_{LG}, \delta_{SB}) \\ D &= \frac{1}{2}\,\gamma_a\,p_0\,\delta\,M^2\,S\,C_D \end{aligned} \tag{3.54}$$

where γ_a, δ, and p_0 are the ratio of specific heat for air, pressure ratio related to MSL, and standard pressure at MSL, respectively. Different from BADA 3 compressibility effects are included. For both BADA 3 and BADA 4, no information is provided on the type of functions used to approximate the drag polar.

OpenAP Given that OpenAP is an open-source model, the expressions used for the drag model are clearly explained. OpenAP makes the assumption of the drag polar being quadratic (see Equation 3.50). For every aircraft type that is included in the model, a value of C_{D_0} and C_{D_i} is obtained for the clean configuration using the methodology explained in Sun et al. [66].

Furthermore, the drag coefficient is modeled as a function of lift coefficient (C_L), flap deflection ($\Delta C_{D,flap}$), landing gear position ($\Delta C_{D,gear}$), and compressibility effects (ΔC_{D_w}), which results in:

$$C_{D_0} = C_{D_0,clean} + \Delta C_{D,flap} + \Delta C_{D,gear} + \Delta C_{D_w} \tag{3.55}$$

The change in the drag coefficient of the flap, gear, and wave drag are computed using reference data and physical parameters, which are further described in Sun et al. [66] and Sun et al. [67]:

$$\begin{aligned} \Delta C_{D,flap} &= 0.9\left(\frac{c_{fp}}{c}\right)^{1.38}\left(\frac{S_{fp}}{S}\right)\sin^2(\delta_f) \\ \Delta C_{D,gear} &= \frac{W}{S}\,K_{uc}\,m_{max}^{-0.215} \\ \Delta C_{D_w} &= \begin{cases} 0 & M \le M_{crit} \\ 20(M - M_{crit})^4 & M > M_{crit} \end{cases} \end{aligned} \tag{3.56}$$

Emissions Emissions follow directly from the fuel flow. The combustion of jet fuel results in multiple emission types: H_2O, CO_2, SO_X, soot particles, NO_X, CO, and HC. The emissions of H_2O, CO_2, SO_X, and soot are considered to be proportional to the fuel flow [65]:

$$\begin{aligned} f_{CO_2} &= 3.149 \cdot ff \\ f_{H_2O} &= 1.230 \cdot ff \\ f_{SO_X} &= 0.00084 \cdot ff \\ f_{soot} &= 0.00003 \cdot ff \end{aligned} \tag{3.57}$$

The emissions of NO_X, CO, and HC are dependent on the temperature in the combustion chamber, which may be modeled as a function of the thrust setting. OpenAP makes use of published values from the ICAO engine emission databank at MSL, which are subsequently corrected for thrust using a linear model. Altitude corrections are considered using the Fuel Flow Method 2 developed by Boeing [23]. This results in these emission rates being modeled as:

$$\begin{aligned} f_{NO_X} &= \mathrm{f}(T, h, ff) \\ f_{CO} &= \mathrm{f}(T, h, ff) \\ f_{HC} &= \mathrm{f}(T, h, ff) \end{aligned} \tag{3.58}$$

Table 3.3: Selection of data fields recorded by the QAR.

Variable name	Symbol	Unit
Flight path	γ	deg
Angle of attack	α	deg
True airspeed	v	m/s
Mach number	M	–
Altitude	h	m
Lateral acceleration	a	m/s^2
Mass	m	kg
Air pressure	p	Pa
Air temperature	T_h	K
Air density	ρ	kg/m^3
Wind speed	w	m/s
Fuel flow	ff	kg/s
Fan rotation speed	N_1	–
Core rotation speed	N_2	–
Exhaust Gas Temperature	EGT	K
Flap deflection	δ_f	deg
Speed brake deflection	δ_{SB}	deg

Tail-Specific Performance Characteristics The performance models introduced so far are all based on aircraft type-specific relations. In order to increase accuracy, aircraft performance can be modeled for a single aircraft (tail). Tail-specific performance models can be constructed using high-resolution flight data obtained from the Quick Access Recorder (QAR). This device records many performance parameters with a resolution of 1 second. A selection of parameters that are recorded is given in Table 3.3.

As can be observed from this sub-section, there are multiple ways to capture performance characteristics. Flight performance can be estimated directly from the total energy model (Equation 3.36); using manufacturer data (Figure 3.8); employing physical relations (Equation 3.50); using simplified performance models [6]; and different forms of polynomials can be used. In order to obtain an accurate and resilient tail-specific performance model, different techniques will have to be investigated.

4

Research Gap

The previous chapter presented a literature review of the scientific research related to the cost index. Two different areas of research are identified: delay management and flight trajectory optimization. The main focus points and scope of the studied problems, including the different types of modeling methodologies, are identified. By extending the findings from the reviewed literature with the practical difficulties that aircraft operators have with cost index practices, as discussed in chapter 2, several observations can be made on research gaps that exist within the field of cost index research

This chapter presents three main research gaps identified from the evaluation of cost index practices, delay management, and flight trajectory optimization.

Cost Index Practices

The cost index was initially introduced to aid aircraft operators in developing more efficient flight operations. By being a simple constant, it could easily be implemented, understood, and managed by airlines. The intended cost index practices were based on the idea of airline-specific cost analysis. The cost of time expressed as an average value per unit flight time, had to be constructed, preferably on each specific flight route, and had to be monitored over time to correct for changes in the cost structure.

Over the years, airlines have struggled to integrate these cost-based cost index practices [1, 2, 9]. The concept of the cost index is said to be misunderstood by decision-makers, resulting in limited resources being placed on conducting the required cost analysis. The basic definition of the average time cost is also seen to not reflect the operational complexity that exists in airline operations. Furthermore, flight-specific schedule constraints are not included. This has resulted in airlines deviating from the intended cost-based cost index practice [11] and adopting the cost index as a simple performance setting intended to manage flight time, arrival time, and fuel consumption.

The management of arrival delays is a well-researched area in the scientific literature. Delay management is proven to be a valuable strategy to limit total network costs for airlines [58]. In order to construct recommendations on a single-flight basis, flight- and passenger-specific delay costs have to be considered. Such delay costs have successfully been introduced in Evler et al. [25, 27], Rosenow et al. [58], however, these studies do not address the relation to cost index practices. The studies of Aktürk et al. [4], Cook et al. [14], Delgado et al. [21] do investigate in-flight DCI practices by considering flight-specific arrival delay costs, however, these studies only focus on arrival management, instead of considering the entire flight process. Achenbach and Spinler [1] do attempt to include arrival delays into the pre-flight cost index optimization problem, but consider delay costs as a very generic average value, similar to the conventional cost index time cost. This results in the first research gap:

> *To the author's knowledge, flight- and passenger-specific delay costs have not been considered in conventional cost index practices.*

Because the cost index is directly related to the flown trajectory, a flight trajectory optimization problem is required to be set up to analyze and develop new cost index practices.

Flight Trajectory Optimization

The problem of flight trajectory optimization is extensively researched. Within this research field, the cost index is generally adopted as a performance metric to construct a trajectory that balances total fuel cost and time cost. The same basic definitions of fuel cost and time cost are used as defined before. Although aircraft operators are seen to not be able to effectively operate using this cost index practice, most research on the TOP problem is based on this principle.

Furthermore, research in the TOP is seen to not consider the matter of arrival delays. Although arrival times can be managed by increasing the cost index in the objective function, similar to how airlines operate, this matter is generally not covered. The research of Förster et al. [28] does focus on constructing a multi-criteria aircraft trajectory optimization tool (TOMATO), that considers airline-specific operations and evaluates different trajectories on fuel, operating, delay, and external environmental costs. Although much research is performed using this tool [56, 57, 59–61], no clear description is provided of how this tool is constructed. Furthermore, the optimization methodology used is based on a hybrid control approach, which is less efficient that the OC approach. This results in the second research gap:

> *To the author's knowledge, there is no research that extends the optimal control-based trajectory optimization problem to airline-specific cost index practices.*

Performance Modeling

Cost index practices by airlines are based on performance tables from the FMC. These performance tables allow the aircraft to quickly obtain performance characteristics corresponding to aircraft and atmospheric properties. These performance tables are constructed in the aircraft development phase and are never updated. Over time aircraft performance is seen to reduce, which results in an erroneous airspeed to follow from the FMC cost index calculation.

In more recent years, the OC approach is characterized as being one of the most reliable dynamic optimization techniques. By working in continuous time, considering the aircraft's dynamical behavior, and adopting numerical methods, it allows for increasingly accurate flight trajectory optimization. Being able to use more sophisticated aircraft performance models enables such optimization problems to capture accurate performance characteristics. Although much research is observed on the TOP problem using the OC approach [32, 64, 65, 68, 69], generic aircraft type-specific performance models are used in the optimization. In order to capture accurate tail-specific performance characteristics and relate it to the standard FMC performance tables, the OC approach can be used in combination with a tail-specific performance model. This results in the third and final research gap:

> *To the author's knowledge, there is no research that performs the optimal control-based trajectory optimization problem using a tail-specific performance model.*

5

Research Proposal

With the theory, practical limitations, research areas, methodologies, and research gap, covered on the cost index, this chapter serves to present the research proposal of this thesis. section 5.1 starts by stating the problem definition. section 5.2 presents the main research question, sub-questions, and research objective that will be used. section 5.3 finally presents a breakdown of the work to be performed.

5.1. Problem Definition

The cost index is a powerful tool introduced to aid aircraft operators in managing their operational flight efficiency. In essence, it can easily be understood: lowering the cost index saves fuel and adds flight time, increasing the cost index increases fuel consumption but lowers flight time. However, developing efficient cost index practices turns out to be quite challenging. It has become clear that this simple constant combines the aspects of flight trajectory optimization, operating cost minimization, aircraft performance modeling, and flight execution. For aircraft operators to maximize the benefits in operational efficiency from cost index practices, all these components will have to be combined.

An overview of the problem definition is provided in Figure 5.1. This figure distinguishes between the flight trajectory optimization problem (orange) and the flight trajectory evaluation problem (blue). Within the flight trajectory optimization problem, the cost index is used to manage time cost and performance costs. The performance cost is generally considered to be fuel cost but is sometimes seen to be extended to carbon, emissions, and/or climate impact costs. Following the flight trajectories constructed from different cost index values, delay costs can be evaluated based on the calculated arrival time. When considering airline or flight-specific operations, additional restrictions may be applied to the flight time, related to crew agreements, schedule, airport, and/or (night) slots.

The goal is to evaluate different trajectories on total time cost, performance cost, and delay cost, and to find the optimal cost index that results in the lowest total operating cost. The trajectory obtained for this optimal cost index is then provided to the FMC, together with the corrected FMC cost index that results in the airspeed profile obtained from the flight trajectory optimization. This latter parameter is a valuable result that describes the tail-specific error in the FMC performance model.

5.2. Research Question and Objective

The following main research question is established:

Research Question

How can tail-specific performance characteristics, flight trajectory optimization, and flight-specific costs be included in a comprehensive cost index model that resembles true airline operations?

This question is divided into four sub-questions, each consisting of multiple sub-questions:

1. **How should flight-specific cost components be quantified?**

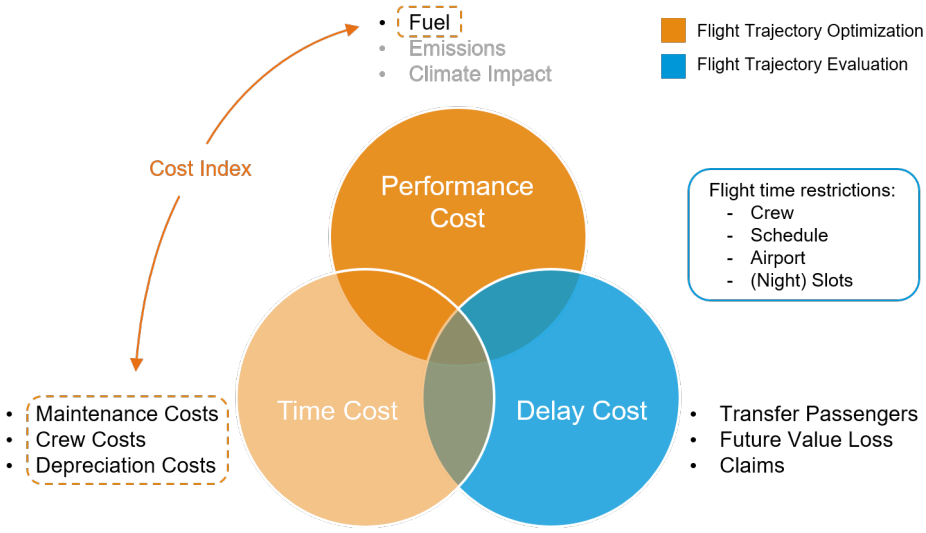

Figure 5.1: Problem definition of airline-specific cost index practices with the goal to minimize total flight-specific operating costs.

(a) What cost components are directly related to a single flight operation?

(b) To what level of detail should cost components be quantified?

2. **How can altitude and speed profiles be optimized from a cost index input?**

   (a) What approach is best suitable to model a flight trajectory?

   (b) What type of optimization method is best suitable?

   (c) What factors should be included in the objective function?

3. **How can tail-specific performance characteristics be included in the flight trajectory optimization problem?**

   (a) What approach is best suitable for tail-specific performance modeling?

   (b) How should flight data be used to create such a model?

   (c) How should the model handle missing or faulty data?

4. **How does the optimal cost index change with a new more comprehensive cost index model?**

   (a) How do flight-specific operating cost estimations change the conventional ECON cost index?

   (b) How effective is the cost index model in strategically accepting flight delays?

   (c) What is the error in the FMC cost index performance model?

   (d) What are the practical savings and difficulties observed from the cost index model experiments?

This results in the final research objective defined below:

Research Objective

To develop an airline-centered cost index practice built around a trajectory optimization model that incorporates tail-specific performance characteristics, time and fuel costs, and flight-specific delay costs, such that each flight operates at its true optimal speed and altitude.

5.3. Work Breakdown

Finally, the work to be performed can be divided into 5 phases. These phases are shown in Figure 5.2. The first three phases are focused on developing the flight-specific cost index model that includes all components mentioned in Figure 5.1. The mid-term meeting follows once a preliminary version of this model is

developed. After the mid-term meeting, case studies are developed and experiments are performed. The green-light meeting follows once the results have been processed.

In order to construct such a flight-specific cost index model, three sub-models have to be created: a flight trajectory optimization model, a tail-specific performance model, and a flight- and passenger-specific delay cost model. The creation of three such models from scratch is considered not feasible for this master thesis. Luckily, for the first two models, open-source models exist that can be taken as a baseline. No such open-source model exists to evaluate flight-specific delay cost, however, KLM has developed its own flight- and passenger-specif delay cost model (MIDAS) which can be used for this. The three phases are further described below.

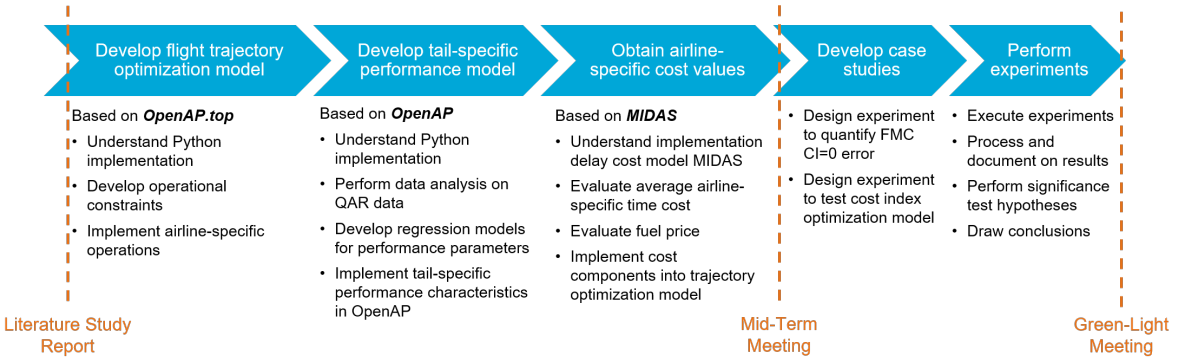

Figure 5.2: Work breakdown to be performed during the thesis.

Develop flight trajectory optimization model For the development of the flight trajectory optimization model, the open-source OC-based model of Sun [65] is taken as the basis (OpenAP.top). The mathematical formulation of the problem and optimization method is seen to follow the description presented in section 3.3. As mentioned before, no operational constraints are considered, which have to be added. More specifically, constraints have to be developed that restrict the optimization problem to pre-defined waypoints and that limit the aircraft to fly certain calibrated airspeed values. Furthermore, airline-specific requirements may be added to the model, to ensure that the optimized trajectory can actually be flown.

Develop tail-specific performance model For the development of the tail-specific performance model, the open-source type-specific performance model of Sun et al. [67] is considered as a basis (OpenAP). This model is already used as the basis for the trajectory optimization model (OpenAP.top), which makes implementing both models straightforward. A new performance model will be developed that uses a similar structure as OpenAP. This new performance model is based on high-resolution flight data and will be developed for single aircraft tails within the fleet of KLM, making the model more accurate and resembling actual flight measurements.

Obtain airline-specific cost values The required cost values for the flight-specific cost index model consist of average flight or airline-specific cost values as presented in subsection 2.1.2, a local fuel price as presented in subsection 2.1.3, and flight- and passenger-specific delay costs as presented in subsection 3.2.2. Regarding the first two values, no attempt will be made to construct airline- and route-specific cost values from a cost analysis. Rather, a standard value is taken from literature, or a very simplified relation is established for the specific airline. The flight-specific aspect of the proposed cost index practice follows from the delay cost model (MIDAS), which is extensive enough for this purpose and considers flight-specific passenger characteristics, including transfer passengers and travel classes.

Bibliography

[1] Anna Achenbach and Stefan Spinler. Prescriptive analytics in airline operations: Arrival time prediction and cost index optimization for short-haul flights. *Operations Research Perspectives*, 5:265–279, 2018.

[2] Airbus. *Getting to grips with the cost index, Issue II*. Flight Operations Support & Line Assistance (STL), Blagnac, 1998.

[3] Airbus. *Getting to grips with Aircraft Performance*. Flight Operations Support & Line Assistance (STL), Blagnac, 2002.

[4] M Selim Aktürk, Alper Atamtürk, and Sinan Gürel. Aircraft rescheduling with cruise speed control. *Operations Research*, 62(4):829–845, 2014.

[5] Rojo Princy Andrianantara, Georges Ghazi, and Ruxandra M Botez. Aircraft engine performance model identification using artificial neural networks. In *AIAA Propulsion and Energy 2021 Forum*, page 3247, 2021.

[6] Matthias Bartel and Trevor M Young. Simplified thrust and fuel consumption models for modern two-shaft turbofan engines. *Journal of Aircraft*, 45(4):1450–1456, 2008.

[7] Artur Bensel. *Characteristics of the Specific Fuel Consumption for Jet Engines*. Hamburg: Aircraft Design and Systems Group (AERO), Department of Automotive , 2018.

[8] Boeing. FMC supplementary data document for model 777-300ER with GE90-115BL engines. Seattle, 2005.

[9] Boeing. *Fuel conservation strategies: cost index explained*. AERO Quarterly (Quarter 2), Seattle, 2007.

[10] Boeing Flight Operations Engineering. Propulsion: Jet engines basics. https://www.smartcockpit.com/docs/Jet_Engines_Basics.pdf, 2010. Accessed: 202210-12.

[11] Geoff Burrows, Christine A Brown, Trevor W Thom, John MC King, and John Frearson. Real-time cost management of aircraft operations. *Management Accounting Research*, 12(3):281–298, 2001.

[12] P. Calders. G.A.M.E aircraft performance model description; DIS/ATD unit. In *DOC.CoE-TP-02002*. Eurocontrol: Brussels, 2002.

[13] Abhijit Chakravarty. Selection of an optimal cost index for airline hub operation. *Journal of Guidance, Control, and Dynamics*, 8(6):777–781, 1985.

[14] Andrew Cook, Graham Tanner, Victoria Williams, and Gerhard Meise. Dynamic cost indexing–managing airline delay costs. *Journal of air transport management*, 15(1):26–35, 2009.

[15] Andrew J Cook and Graham Tanner. European airline delay cost reference values - updated and extended values. Technical report, University of Westminster, 2015.

[16] Ramon Dalmau, Xavier Prats, and Brian Baxley. Sensitivity-based non-linear model predictive control for aircraft descent operations subject to time constraints. *Aerospace*, 8(12):377, 2021.

[17] R Dancila and R Botez. Vertical flight profile optimization for a cruise segment with rta constraints. *The Aeronautical Journal*, 123(1265):970–992, 2019.

[18] MK DeJonge and WH Syblon. Application of cost index to fleet hub operation. In *1984 American Control Conference*, pages 179–183. IEEE, 1984.

[19] Daniel Delahaye, Stéphane Puechmorel, Panagiotis Tsiotras, and Eric Féron. Mathematical models for aircraft trajectory design: A survey. In *Air Traffic Management and Systems*, pages 205–247. Springer, 2014.

[20] Luis Delgado, Jorge Martin, Alberto Blanch, and Samuel Cristóbal. Hub operations delay recovery based on cost optimisation-dynamic cost indexing and waiting for passengers strategies. *Sixth SESAR Innovation Days*, 2016.

[21] Luis Delgado, Jorge Martín, Alberto Blanch, and Samuel Cristóbal. Agent based model for hub operations cost reduction. In *International Conference on Practical Applications of Agents and Multi-Agent Systems*, pages 3–15. Springer, 2017.

[22] D.Simos. *PIANO: PIANO user's guide version 4.0*. Lissys Limited, London, UK, 2002.

[23] Doug DuBois and Gerald C Paynter. " fuel flow method2" for estimating aircraft emissions. *SAE Transactions*, pages 1–14, 2006.

[24] Holly A Edwards, Darron Dixon-Hardy, and Zia Wadud. Aircraft cost index and the future of carbon emissions from air travel. *Applied energy*, 164:553–562, 2016.

[25] Jan Evler, Michael Schultz, Hartmut Fricke, and AJ Cook. Development of stochastic delay cost functions. *10th SESAR Innovation Days*, 2020.

[26] Jan Evler, Michael Schultz, Hartmut Fricke, and Andrew Cook. Development of stochastic delay cost functions. https://www.youtube.com/watch?v=QXf_61J1Xog, September 2020. URL https://www.youtube.com/watch?v=QXf_61J1Xog. Accessed on Sep 22, 2022.

[27] Jan Evler, Michael Schultz, Hartmut Fricke, and Andrew Cook. Stochastic delay cost functions to estimate delay propagation under uncertainty. *IEEE Access*, 10:21424–21442, 2022.

[28] Stanley Förster, Judith Rosenow, Martin Lindner, and Hartmut Fricke. A toolchain for optimizing trajectories under real weather conditions and realistic flight performance. *Greener Aviation, Brussels*, 2016.

[29] Eduardo Gallo, Francisco A Navarro, Angela Nuic, and Mihai Iagaru. Advanced aircraft performance modeling for atm: Bada 4.0 results. In *2006 ieee/aiaa 25TH Digital Avionics Systems Conference*, pages 1–12. IEEE, 2006.

[30] Alessandro Gardi, Roberto Sabatini, and Subramanian Ramasamy. Multi-objective optimisation of aircraft flight trajectories in the atm and avionics context. *Progress in Aerospace Sciences*, 83:1–36, 2016.

[31] Georges Ghazi and Ruxandra Mihaela Botez. Identification and validation of an engine performance database model for the flight management system. *Journal of Aerospace Information Systems*, 16(8): 307–326, 2019.

[32] Daniel González-Arribas, Manuel Soler, and Manuel Sanjurjo-Rivo. Robust aircraft trajectory planning under wind uncertainty using optimal control. *Journal of Guidance, Control, and Dynamics*, 41(3):673–688, 2018.

[33] S Hartjes. *An optimal control approach to helicopter noise and emissions abatement terminal procedures*. PhD thesis, Delft University of Technology, 2015.

[34] Albert A Herndon. Flight management computer (FMC) navigation database capacity. In *2012 Integrated Communications, Navigation and Surveillance Conference*, pages M6–1. IEEE, 2012.

[35] Geoffrey Todd Huntington. *Advancement and analysis of a Gauss pseudospectral transcription for optimal control problems*. PhD thesis, MIT, 2007.

[36] ICAO. Aircraft engine emissions databank, 2018. International Civil Aviation Organization: Montreal, QC, Canada.

[37] ICAO. States adopt net-zero 2050 global aspirational goal for international flight operations, October 2022. URL https://www.icao.int/Newsroom/Pages/States-adopts-netzero-2050-aspirational-goal-for-international-flight-operations.aspx. Accessed on Oct 16, 2022.

[38] IEA. Aviation. https://www.iea.org/reports/aviation, September 2022. URL https://www.iea.org/reports/aviation. Accessed on Sep 28, 2022.

[39] IVAO. Cost index. https://mediawiki.ivao.aero/index.php?title=Cost_Index, August 2022. URL https://mediawiki.ivao.aero/index.php?title=Cost_Index. Accessed on Aug 15, 2022.

[40] Luke Jensen, R John Hansman, Joseph C Venuti, and Tom Reynolds. Commercial airline speed optimization strategies for reduced cruise fuel consumption. In *2013 Aviation Technology, Integration, and Operations Conference*, page 4289, 2013.

[41] Shumpei Kamo, Judith Rosenow, Hartmut Fricke, and Manuel Soler. Robust cdo trajectory planning under uncertainties in weather prediction. In *Proceedings of the 14th USA/Europe Air Traffic Management Research and Development Seminar (ATM Seminar), Virtual Event*, pages 20–23, 2021.

[42] Taehak Kang and Jaiyoung Ryu. Determination of aircraft cruise altitude with minimum fuel consumption and time-to-climb: An approach with terminal residual analysis. *Mathematics*, 9(2):147, 2021.

[43] Matthew Kelly. An introduction to trajectory optimization: How to do your own direct collocation. *SIAM Review*, 59(4):849–904, 2017.

[44] Matthew P Kelly. Transcription methods for trajectory optimization: a beginners tutorial. *arXiv preprint arXiv:1707.00284*, 2017.

[45] Donald E Kirk. *Optimal control theory: an introduction*. Courier Corporation, 2004.

[46] David S Lee, DW Fahey, Agnieszka Skowron, MR Allen, Ulrike Burkhardt, Q Chen, SJ Doherty, S Freeman, PM Forster, J Fuglestvedt, et al. The contribution of global aviation to anthropogenic climate forcing for 2000 to 2018. *Atmospheric Environment*, 244:117834, 2021.

[47] Sam Liden. Practical considerations in optimal flight management computations. *Journal of Guidance, Control, and Dynamics*, 9(4):427–432, 1986.

[48] Sam Liden. Optimum 4d guidance for long flights. In *[1992] Proceedings IEEE/AIAA 11th Digital Avionics Systems Conference*, pages 262–267. IEEE, 1992.

[49] Ryota Mori. In-flight profile updates by appropriate cost index selectionoperational perspective. *transactions of the Japan society for aeronatical and space sciences*, 65(2):56–65, 2022.

[50] Alejandro Murrieta-Mendoza and Ruxandra Botez. Lateral navigation optimization considering winds and temperatures for fixed altitude cruise using dijsktras algorithm. In *ASME International Mechanical Engineering Congress and Exposition*, volume 46421, page V001T01A054. American Society of Mechanical Engineers, 2014.

[51] Alejandro Murrieta-Mendoza and Ruxandra Botez. Aircraft vertical route optimization deterministic algorithm for a flight management system. In *SAE 2015 AeroTech Congress & Exhibition*, volume 13, 2015.

[52] Angela Nuic, Damir Poles, and Vincent Mouillet. Bada: An advanced aircraft performance model for present and future atm systems. *International journal of adaptive control and signal processing*, 24(10): 850–866, 2010.

[53] Matteo Prussi, Uisung Lee, Michael Wang, Robert Malina, Hugo Valin, Farzad Taheripour, César Velarde, Mark D Staples, Laura Lonza, and James I Hileman. Corsia: The first internationally adopted approach to calculate life-cycle ghg emissions for aviation fuels. *Renewable and Sustainable Energy Reviews*, 150: 111398, 2021.

[54] Anil V Rao. A survey of numerical methods for optimal control. *Advances in the Astronautical Sciences*, 135(1):497–528, 2009.

[55] Damián Rivas and Alfonso Valenzuela. Compressibility effects on maximum range cruise at constant altitude. *Journal of guidance, control, and dynamics*, 32(5):1654–1658, 2009.

[56] Judith Rosenow and Michael Schultz. Coupling of turnaround and trajectory optimization based on delay cost. In *2018 Winter Simulation Conference (WSC)*, pages 2273–2284. IEEE, 2018.

[57] Judith Rosenow, Stanley Förster, Martin Lindner, and Hartmut Fricke. Impact of multi-critica optimized trajectories on european air traffic density, efficiency and the environment. In *Proceedings of the Twelfth USA/Europe Air Traffic Management Research and Development Seminar, Seattle, DC, USA*, pages 26–30, 2017.

[58] Judith Rosenow, Philipp Michling, Michael Schultz, and Jörn Schönberger. Evaluation of strategies to reduce the cost impacts of flight delays on total network costs. *Aerospace*, 7(11):165, 2020.

[59] Judith Rosenow, David Strunck, and Hartmut Fricke. Trajectory optimization in daily operations. *CEAS Aeronautical Journal*, 11(2):333–343, 2020.

[60] Judith Rosenow, Martin Lindner, and Joachim Scheiderer. Advanced flight planning and the benefit of in-flight aircraft trajectory optimization. *Sustainability*, 13(3):1383, 2021.

[61] Judith Rosenow, Ehsan Asadi, Daniel Lubig, Michael Schultz, and Hartmut Fricke. Long range air traffic flow management with flight-specific flight performance. *Future Transportation*, 2(2):310–327, 2022.

[62] Ger J.J. Ruijgrok. *Elements of airplane performance*. Delft Academic Press (VSSD), second edition, 2009.

[63] Abolfazl Simorgh, Manuel Soler, Daniel González-Arribas, Sigrun Matthes, Volker Grewe, Simone Dietmüller, Sabine Baumann, Hiroshi Yamashita, Feijia Yin, Federica Castino, et al. A comprehensive survey on climate optimal aircraft trajectory planning. *Aerospace*, 9(3):146, 2022.

[64] Manuel Soler, Alberto Olivares, and Ernesto Staffetti. Multiphase optimal control framework for commercial aircraft four-dimensional flight-planning problems. *Journal of Aircraft*, 52(1):274–286, 2015.

[65] Junzi Sun. Openap. top: Open flight trajectory optimization for air transport and sustainability research. *Aerospace*, 9(7):383, 2022.

[66] Junzi Sun, Jacco M Hoekstra, and Joost Ellerbroek. Aircraft drag polar estimation based on a stochastic hierarchical model. *Eighth SESAR Innovation Days*, 2018.

[67] Junzi Sun, Jacco M Hoekstra, and Joost Ellerbroek. Openap: An open-source aircraft performance model for air transportation studies and simulations. *Aerospace*, 7(8):104, 2020.

[68] Santi Vilardaga and Xavier Prats. Operating cost sensitivity to required time of arrival commands to ensure separation in optimal aircraft 4d trajectories. *Transportation Research Part C: Emerging Technologies*, 61:75–86, 2015.

[69] Alessio Vitali, Manuela Battipede, and Angelo Lerro. Multi-objective and multi-phase 4d trajectory optimization for climate mitigation-oriented flight planning. *Aerospace*, 8(12):395, 2021.

[70] Hiroshi Yamashita, Feijia Yin, Volker Grewe, Patrick Jöckel, Sigrun Matthes, Bastian Kern, Katrin Dahlmann, and Christine Frömming. Newly developed aircraft routing options for air traffic simulation in the chemistry–climate model emac 2.53: Airtraf 2.0. *Geoscientific Model Development*, 13(10): 4869–4890, 2020.